DESIGN OF PORPHYRIN SOLIDS

ZN···NO_2 RECOGNITION, MULTI-STEP SINGLE CRYSTAL TO SINGLE CRYSTAL TRANSFORMATIONS AND COFACIAL DIMERS

By
SALIMGEREY ADILOV

A Dissertation Submitted to the Faculty of the

WORCESTER POLYTECHNIC INSTITUTE

In partial fulfillment of the requirements for the
Degree of Doctor of Philosophy
in Chemistry
by

July 2008

APPROVED:

Dr. Venkat R. Thalladi Advisor	Dr. Dhandapani Venkataraman External Reviewer; UMass Amherst
Dr. James P. Dittami Committee Member	Dr. Weiyong Yu Committee Member
Dr. Kristin N. Wobbe Head of Department	

ACKNOWLEDGEMENTS

I would like to thank my research advisor Professor Venkat R. Thalladi for his scientific supervision as well as moral support during my stay at WPI. He has always been inspiring and his scientific discussions have been highly encouraging. I learnt a lot from him about science and about life.

I would like to thank all the faculty and staff of the Department of Chemistry and Biochemistry at WPI. Thanks to my graduate committee Professors James P. Dittami, Weiyong Yu and Dhandapani Venkataraman. I would like to thank Professor John MacDonald for his discussions throughout my Ph.D. career.

Special thanks to Dr. Richard Staples and Dr. Jingwei Huang of Harvard University and Dr. Hans-Christoph Weiss of Bayer, Germany and Professor Roland Bose of University Duisburg-Essen for collecting single crystal X-ray data on some of the structures reported in this thesis.

I would like to thank my friendly and supportive labmates. In particular, I thank Marta Dabros, Jason R. Cox, Taner Gokcen and Paul Emery for their help, critical reading and valuable discussions that helped my thesis look better. Marta is one of the nicest people I have ever met. She gave me moral and also material support. Jason has been a close friend from the beginning when I first came to WPI. His advice and full support helped me to fit into American society. It has been a great pleasure to work with them. Additionally, I would like to thank all the undergraduate students who have worked in our lab during the last five years. I thank Eftim Milkani for his discussions on social and political issues.

I thank Backlin Fund for the financial support they gave me for the last semester.

I would like to thank all my Kazak friends in the US, especially Kazak community in New York and a special friend in particular.

I wish to thank my parents, brothers and sisters for their continuous support, encouragement and for making me what I am.

TABLE OF CONTENTS

1 INTRODUCTION

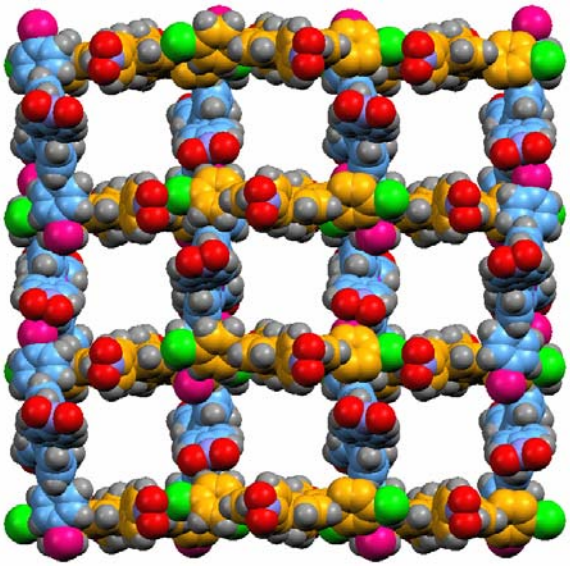

1.1 PORPHYRINS AND PORPHYRIN DERIVATIVES

The chemistry of porphyrins and related compounds dates back to eighteenth century. The porphyrin molecules and their derivatives in different forms are currently utilized in a variety of applications that span medicine (photodynamic therapy),[1] optoelectronics (nonlinear optics),[2-3] nanofabrication (two-photon absorption),[4-6] organic chemistry (catalysis),[7] photovoltaics (light harvesting)[8] and so on. Much of the excitement in porphyrin research lies in their modular and facile synthesis, large size, ready dissolution in organic solvents, characteristic colors, rigidity, thermal stability, and affinity for metallation.[9]

The name porphyrin comes from the Greek word for purple as a result of their intense purple color. The simplest porphyrin, called porphine, consists of four pyrrolic units connected by methyne bridges. This bridging of the pyrrole units ensures continuous conjugation of unsaturated atomic centers and results in a large, planar macrocycle with twenty two electrons. This highly conjugated aromatic macrocycle is the core of the substituted porphyrins studied in this chapter. Different positions on the porphyrin periphery are referred by specific names (Figure 1.1a). In this symmetric molecule, there are eight α, eight β, and four *meso* positions; the β and *meso* positions are susceptible for substitution by functional groups. In this thesis, we use *meso* substituted tetra-aryl porphyrins (Figure 1.1b) towards the exploration of weak coordination synthons,[10] porous materials,[11-13] single crystal to single crystal transformations,[14-16] second harmonic generation,[17-19] and other applications.

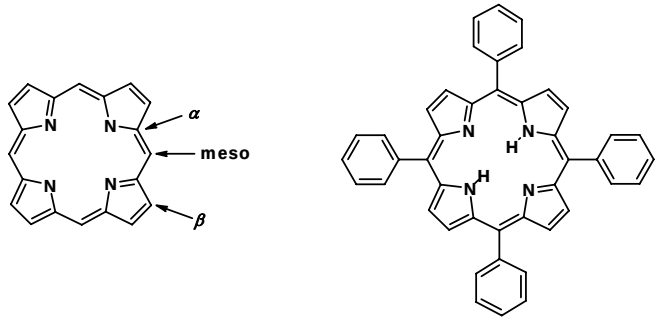

Figure 1.1 (a) Molecular structure of porphine and its nomenclature. **(b)** Free-base tetraphenylporphyrin after *meso* substitution.

In addition to substitution on the periphery of the core, porphyrins can be metallated at the center of the core to give another dimension of modularity.[20] Different metal atoms can be inserted into core of the macrocycle yielding different electronic and binding properties than the free-base form. In nature, both free-base and metallated porphyrins are present.[21]

1.2 PORPHYRINS IN NATURE

Interest in porphyrin chemistry is largely influenced by the utility of naturally occurring porphyrin compounds.[22] Some of the research in the area of porphyrin systems (such as artificial light harvesting) is a direct imitation of naturally occurring events.[23-25] Here we give two examples from nature that are related to this thesis, hemoglobin and chlorophyll.

Hemoglobin is an iron substituted porphyrin derivative found in mammalian blood. It is used in the transportation of oxygen. The reversible iron-oxygen binding occurs by changing the oxidation state of iron. In this thesis we employ $Zn\cdots NO_2$ recognition, where Zn^{2+} ion inserted into a porphyrin core loosely binds to the oxygen atom of a nitro group.

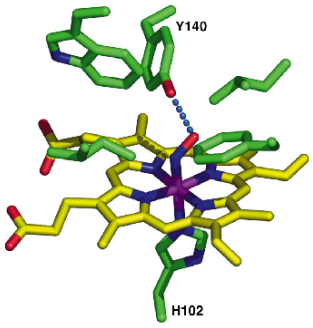

Figure 1.2 Stick model of heme in a nitric oxide sensing protein. Notice that the iron inserted into the porphyrin core is central to the function of heme. Image is taken from esrf.eu.

Chlorophyll plays an important role in photosynthesis. Chlorophyll molecules enable transfer of photonic energy to a reaction center. The highly conjugated structure of individual chlorophyll unit in conjunction with the close packing of multiple chlorophyll molecules facilitates a very high-yield energy transfer. In the photosynthesis both free-base and metallated porphyrins are employed among other chromophores.

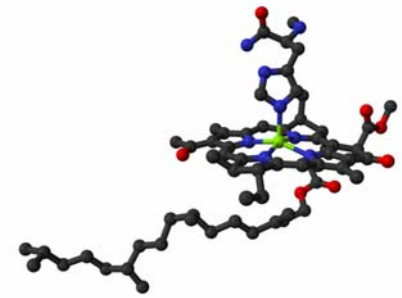

Figure 1.3 Ball-and-stick model of chlorophyll molecule within a protein. An Mg^{2+} ion is bound at the center of the macrocyclic core. Image is taken from wikimedia.org.

1.3 PROPERTIES OF PORPHYRINS

As mentioned at the outset of this chapter, porphyrin systems are used in numerous applications owing to the structural diversity they can achieve based on the substituents or metal species.[9] We do not delve here into myriad porphyrin based compounds and their applications; rather, we provide a snapshot of certain porphyrin properties that make them attractive candidates for the applications in this work. In terms of the substituents, porphyrins offer greater separation between functional groups while providing constant communication through continuous conjugation across the molecular framework.[26-28] This attribute makes them excellent candidates for electrooptic applications. Porphyrins display remarkable thermal and photochemical stability; they are thus useful in studying heat induced phase transitions. Apart from these innate properties, addition of other functional groups allows the tailoring of porphyrin derivatives towards functions that are otherwise not easily achievable. We exploit all these features of porphyrins in the current work towards applications weak supramolecular synthons, porous materials, multi-step phase transitions and synthesis of large molecules with cubic topologies.

1.4 POROUS MATERIALS

In Chapters 2 and 3, we describe a series of porous materials based on a weak coordination synthon. Here we refer to some of the previous work in the area of porous materials to provide context for our work. Porous materials have garnered much attention in applications such as molecular storage, explosive detection, and chiral separation.[11-13] Inorganic zeolites are extremely stable and inexpensive; they have been the standard bearer of porous materials for a long time. The need for increased functionality within the solid state in order to develop porous catalysts and better electronic materials has made organic solids and metal organic frameworks (MOFs) a rapidly growing area of research.

Hydrogen bonding is the key structural element used in the crystal packing of porous organic solids.[29] Indeed, the interest in the area of organic-based porous materials evolved after a seminal paper on diamondoid networks in the crystal structure of adamantane-tetracarboxylic acid has appeared in the literature.[30] Several strategies have been developed in the early to late nineties to prepare porous organic solids.[31] Though there has been considerable progress in the design, most of these solids are stable only in the presence of guests and typically collapse into nonporous materials once the guest is removed. Concurrent with the work on porous solids, crystal engineering has flourished at this time and several guiding principles and different intermolecular interactions have been identified.[32] In this context, the current work brings together the concepts of porous materials and weaker coordination synthons to create materials that have the flexibility of organics and robustness of MOFs.

MOFs are newly emerging systems for construction of extended solids. Structurally, MOFs can be regarded as systems between inorganic and organic solids. Although the stability of these networks is inferior to zeolites, MOFs have much stronger binding and stability than hydrogen bonded organic solids. One of the advantages of MOFs over zeolites is that pore size and shape can be modified at the molecular scale by changing

the organic linkers. MOFs are involved in a number of applications, especially as hydrogen storage systems.

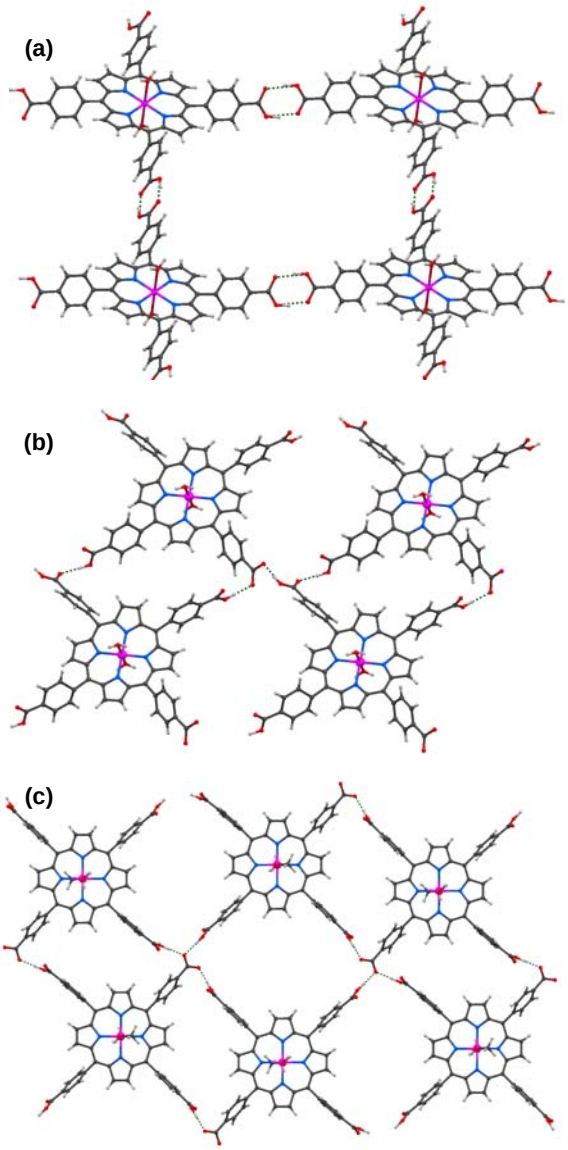

Figure 1.4 (a) Crystal packing of a 4-carboxyphenyl substituted porphyrin. **(b)** Same molecule as in **(a)** but packing in a catemeric array with smaller void space. **(c)** Combination of dimers and catemers to generate a layered structure. The H-bonds are marked by dotted lines. Images in this figure and the following two figures are drawn based *Chem. Commun.*, 2005, 1243.

1.5 EXTENDED PORPHYRIN SYSTEMS

The physical and optical properties of porphyrins make them an attractive choice for use as templates for porous systems. The square planar geometry combined with their ability to decorate the periphery with hydrogen bond donating and accepting groups generates a variety of extended networks. Extended systems can be two or three-dimensional and are characterized by interporphyrin hydrogen bonds, metal-ligand coordination, organic bridging ligands or a combination of some or all these approaches. In the following sections we will discuss each of these approaches.

1.5.1 Hydrogen Bond Networks in Porphyrin Solids. Hydrogen bonds are primarily electrostatic interactions and typically occur between -OH or -NH groups and other electronegative atoms. Nature uses hydrogen bonds elegantly in almost all of the biological functions because of their collective strength and the short time scale in which these bonds can be formed and broken. In synthetic supramolecular chemistry hydrogen bonds offer the greatest diversity in the types of molecules that can be used and ranges of networks that can be generated. Not surprisingly, the early work in porphyrin extended systems has generated several porphyrin networks with complex and aesthetic topologies.[33] In a typical crystal design experiment, porphyrin molecules are modified with hydrogen bond donating and accepting groups at their *meso* positions. A number of hydrogen bonding synthons have been investigated in this context, but the most common and perhaps the most robust of these are carboxylic acid dimers, amide dimers or dimers of aminopyridyl units.[34-36] In addition, synthons based on hydroxy group or multi-point binding are also employed in the synthesis of networks. In most cases, this approach generates 2-D grids due to the square planar geometry of the porphyrin molecule. The advantages of this approach are that hydrogen bond synthons are well characterized and yield predictable geometries. This approach can be applied to metallated or free-base porphyrins with little difference in the packing of the molecules. Figure 1.4 illustrates some examples of this approach.[37]

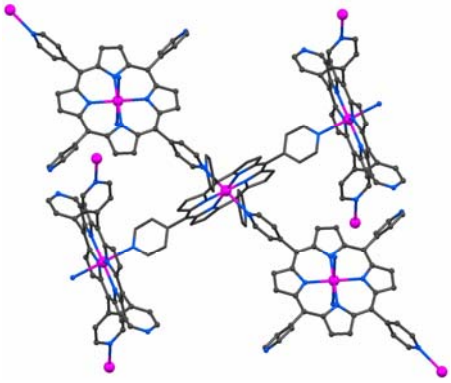

Figure 1.5 4-pyridyl substituted porphyrins chelating with the metallated core of neighboring molecules resulting in a 2-D framework.

1.5.2 Coordination Polymers of Porphyrin Systems. Metal-ligand coordination may be employed in porphyrin derivatives through either exocyclic ligands or through axial chelation of metal ion at the core. In the case of porphyrins metallated with octahedrally coordinating metal atoms, functional groups from adjacent porphyrins can bind and create 2-D or 3-D networks. Carboxy functional groups are particularly useful for this approach as well as pyridyl groups. An example is given in Figure 1.5.

In the case of metals that do not have a propensity to coordinate octahedrally, exocyclic cations can be used to facilitate the formation of a network. This approach is illustrated in Figure 1.6.

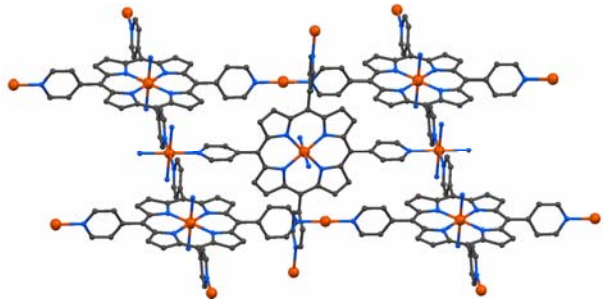

Figure 1.6 Portion of a 3-D network formed by the tetrapyridyl substituted porphyrin binding to exocyclic metal atoms.

The advantage to this approach is that different metals can facilitate different geometries without the need to modify the porphyrin building block. In addition, mixed-metal frameworks have been constructed which are particularly important in light-harvesting systems.

1.5.3 Organic Bridging Ligands. In addition to the self-complementary systems described above, separate organic ligands have also been used to bind the metallated core of adjacent metal atoms. In the absence of hydrogen bond forming functional groups on the porphyrin molecule, organic bridging ligands can axially coordinate with the metal centers and create an extended porphyrin system.[33] When used in conjunction with hydrogen bond forming moieties, bridging ligands can aid in the formation of robust 3-D networks. The advantage to all of these approaches is that they generate open lattice networks that contain large void volumes and their formation is reversible. More importantly, they form layered structures that can act like reversible sponges for sensing or catalytic applications. In addition to the extended systems, the bridging ligand approach has also been used in the templated synthesis of giant molecules that have sizes in the nanometer scale (Figure 1.7).[34]

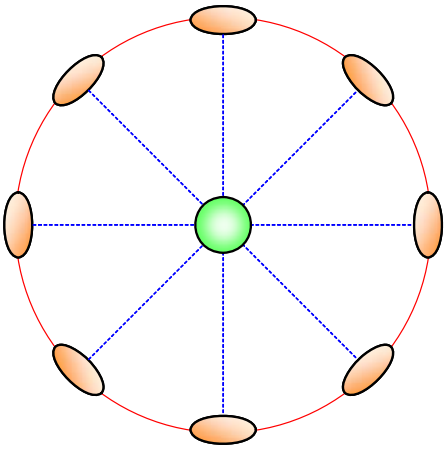

Figure 1.7 Molecular nanoring synthesized based on the templating of Zn^{2+} ion at the porphyrin core (orange ellipses) and an octapyridyl porphyrin derivative (green circle). Red solid lines indicate covalent cross-links and blue dashed lines indicate noncovalent bonds. This image is a schematic drawing of a nanoring published in *Angew. Chem. Int. Ed.* **2007**, *46*, 3122.

1.6 LAYERED STRUCTURES

As mentioned in the previous section, the approximate square planar geometry of porphyrins and functionalized porphyrins yields 2-D grids. Axial coordination of the metal center can add a third dimension to these networks yielding a layered structure. Layered structures are particularly well suited for molecular storage, catalysis, separation and sensing applications. Recent work has focused on developing organic and hybrid organic-inorganic layered structures with increased functionality and variable pore sizes.

A familiar example of a layered structure is graphite (Figure 1.8). The carbon atoms form covalently bonded flat sheets that are attached to adjacent sheets through π-stacking interactions. The weak interaction between sheets allows slippage and contributes to graphite's utility as a lubricant.

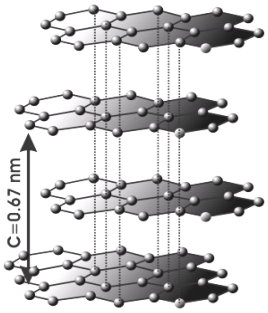

Figure 1.8 Crystal structure of graphite illustrating the weak interaction between covalently-bound carbon sheets. Image is taken from wikimedia.org.

In addition to use as lubricants, layered structures are being investigated for their use as storage frameworks. One growing area of interest is in clay mimics. The major advantage of organic and hybrid organic-inorganic clay mimics is that the pores can be anisotropic unlike zeolites. By tuning the functionalities present, a predictable network can be built towards specific applications like second harmonic generation and molecular sensing. One of the well-known early examples of clay mimicry was conducted using guanidinium sulfonates.[35] In this work, a variety of layered structures could be easily prepared simply by varying alkyl or aryl group attached to the sulfonate. Examples studied included monoaryl and diaryl sulfonates and in this system it is possible to tune the pore size by adjusting the functional groups attached to the sulfonates in a predictable manner. The attached aryl groups serve as adjustable pillars between sheets; Figure 1.9 shows an example from this work.

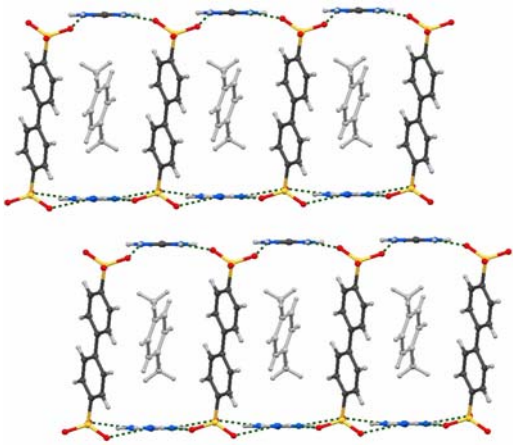

Figure 1.9 Crystal structure of a guanidinium biphenyldisulfonate clay mimic. Notice the inclusion of ordered solvent molecules between the pillars. Image is drawn based on *Chem. Mater* **2000**, *10*, 4159.

Another approach for the design of layered materials is shown in Figure 1.10.[36] In this approach, sheets of dicarboxylic acids are linked by flexible diamine pillars. The flexibility of the pillars is expected to allow the reversible intercalation of guest molecules without destroying the host network. In this case, the weak interactions between the pillars and sheets mimic the shape of a clay but not the function. In order to fully mimic the function of clay material, a more robust approach to linking the adjacent sheets is necessary.

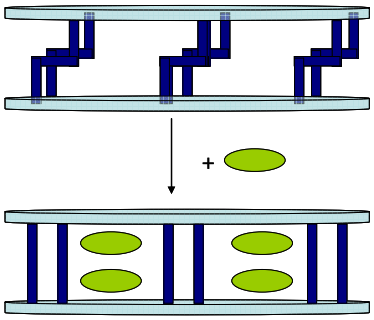

Figure 1.10 Proposed scheme for the reversible intercalation of guest species in a host network. Blue rods represent the diamine pillars and red circles represent guest molecules. Image is drawn based on *Chem. Eur. J.* **2002**, *8*, 3254.

1.7 POROUS PORPHYRIN MATERIALS

To construct porphyrin porous solids with a predictable topology different kinds of interactions have been investigated. Robson showed construction of a 3-D porous solid using copper tetrakis-4-cyanophenylporphyrin (Figure 1.11).[37] Although the materials lose crystallinity very quickly upon exposure to the air, this work is one of the first examples of a porphyrin network. Later, others used similar interactions with improved physical properties. Porphyrin chemistry is enhanced through metal-ligand interactions. The metal core of porphyrins has a high binding affinity for a variety of ligands. Amine based ligands are prominent along with hydroxyl and carbonyl based functional groups. Due to the size and symmetry of the porphyrin molecules, porous materials with large pore dimensions and with defined shapes can be synthesized.

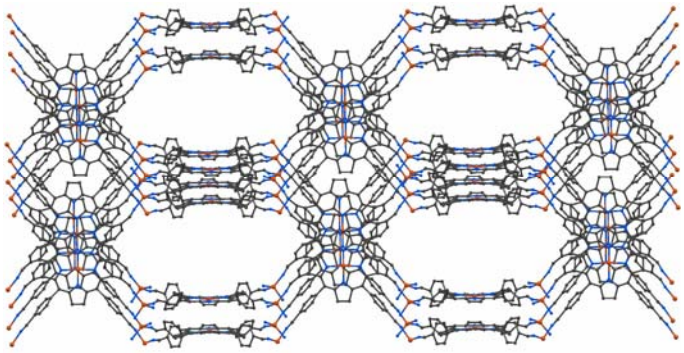

Figure 1.11 Construction of a 3-D network structure using copper-metallated tetrakis-4-cyanophenylporphyrin and exocyclic copper ions. The porphyrin ligand has a square planar geometry and the copper ion has the tetrahedral geometry. Combination of these two geometries leads to the exquisite PtS networks shown here. Notice the large cavities which are stable in the absence of a guest molecule for a short period of time. Image is drawn based on *Nature*, **1994**, *369*, 727.

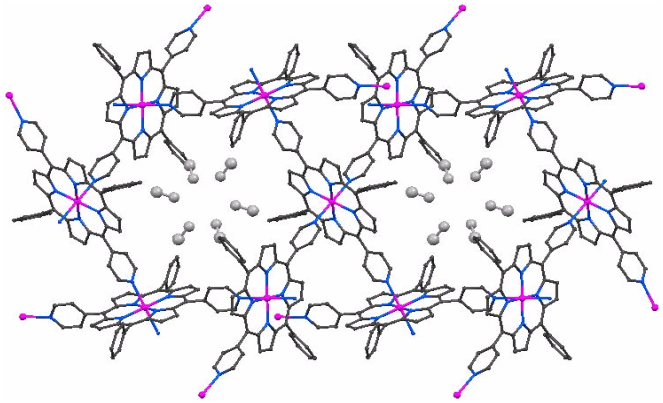

Figure 1.12 3-D layered structure built using Zn-metallated bispyridyl porphyrin building blocks. Notice the large cavities which permit guest removal and exchange. Image is drawn based on *Chem. Commun.*, **2005**, 3906.

Another example of a three dimensional porphyrin coordination polymer that is of interest in the context of our work is given in Figure 1.12.[38] Zinc-metallated bispyridyl-porphyrin forms a 3-D honeycomb network with voids large enough to fit six small guest molecules. This particular network is highly robust – it is based on strong coordination bonds between Zn^{2+} ion and pyridyl N-atoms – and does not collapse after the removal of the guest. Indeed, within this 3-D host it is possible to exchange one set of solvent molecules with another set of solvent molecules without changing the host architecture. The important lesson to be learned from Figures 1.11 and 1.12 is that a 3-D network must be based on highly robust interactions between the molecules in order to sustain the empty pores that remain when the guest is removed. The network shown in Figure 1.11 is based on weaker interactions between copper ion and neutral cyano groups. In our work, we use 2-D networks that stack on each other in order to evaluate the efficacy of a new coordination synthon called $Zn\cdots NO_2$ recognition.

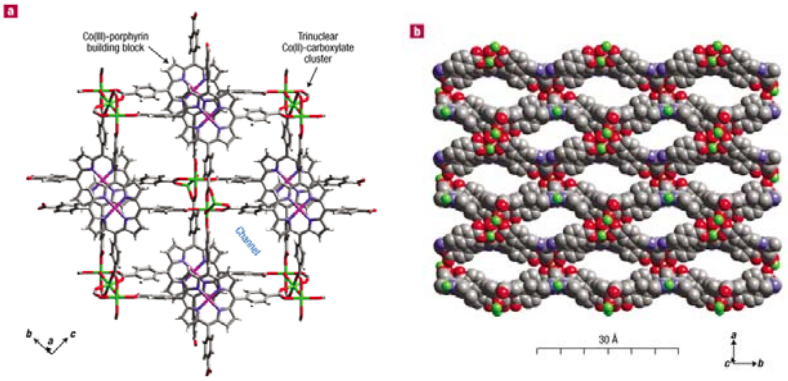

Figure 1.13 A 3-D MOF assembled from trinuclear metal carboxylate clusters and metallated tetracarboxy porphyrin. The clusters act as bridging nodes and the porphyrin molecule as the linkers. Images are taken from http://www.scs.uiuc.edu/suslick/

Yet another way of building 3-D architectures is to use the MOF methodology. In this method, metal-carboxylyate clusters are used as nodes between the organic linkers. Indeed, the carboxylate group is an integral covalent part of the ligand and in essence the total framework is sustained by very strong bonds and hence withstands guest removal.[39] Figure 13 shows an example of 3-D MOF based on cobalt metallated tetrakis-4-carboxyphenylporphyrin and a cobalt carboxylate cluster.[40] This MOF exhibited several zeolitic properties in terms of range of compounds it can adsorb and the level of selectivity when exposed to a combination of guests.

1.8 USE OF WEAK INTERACTIONS IN THE DESIGN OF POROUS SOLIDS

We conclude this introductory chapter with some thoughts on the use of stronger versus weaker interactions in the preparation of porous materials or more generally solid state structures. We have discussed the utility of interactions such hydrogen bonds, coordination bonds, and metal-carboxylate clusters in the design of porous materials. The major reason for the use of these interactions is that they are strong and directional. In the same vein, it is common to discard interactions that are weaker with the notion that weaker interactions can be non-directional or easily perturbed by other interactions in the solid state. We believe that weaker interactions, when used with proper care, can be attractive targets in the design of materials with predictable network topologies and tunable porosities. Weaker interactions are malleable – they can continue to operate even under slightly misaligned geometries – and adaptable. Consideration of weaker interactions also extends the range of materials that can be synthesized and improve our understanding of their role in solids that are 'governed' by stronger interactions. We show in the next two chapters the utility of $Zn\cdots NO_2$ recognition, a weak coordination synthon in the production of layered porphyrin solids with several interesting properties.

1.9 REFERENCES

1. Banfi, S.; Caruso, E.; Caprioli, S.; Mazzagatti, L.; Canti, G.; Ravizza, R.; Gariboldi, M.; Monti, E., Photodynamic effects of porphyrin and chlorin photosensitizers in human colon adenocarcinoma cells. *Bioorganic & Medicinal Chemistry* **2004,** *12*, 4853-4860.
2. Screen, T. E. O.; Thorne, J. R. G.; Denning, R. G.; Bucknall, D. G.; Anderson, H. L., Amplified Optical Nonlinearity in a Self-Assembled Double-Strand Conjugated Porphyrin Polymer Ladder. *J. Am. Chem. Soc.* **2002,** *124*, 9712-9713.
3. Screen, T. E. O.; Thorne, J. R. G.; Denning, R. G.; Bucknall, D. G.; Anderson, H. L., Two methods for amplifying the optical nonlinearity of a conjugated porphyrin polymer: transmetallation and self-assembly. *J. Mat. Chem.* **2003,** *13*, 2796-2808.
4. Ogawa, K.; Ohashi, A.; Kobuke, Y.; Kamada, K.; Ohta, K., Strong Two-Photon Absorption of Self-Assembled Butadiyne-Linked Bisporphyrin. *J. Am. Chem. Soc.* **2003,** *125*, 13356-13357.
5. Drobizhev, M.; Stepanenko, Y.; Dzenis, Y.; Karotki, A.; Rebane, A.; Taylor, P. N.; Anderson, H. L., Understanding Strong Two-Photon Absorption in p-Conjugated Porphyrin Dimers via Double-Resonance Enhancement in a Three-Level Model. *J. Am. Chem. Soc.* **2004,** *126*, 15352-15353.

6. Humphrey, J. L.; Kuciauskas, D., Charge Transfer Enhances Two-Photon Absorption in Transition Metal Porphyrins. *J. Am. Chem. Soc.* **2006,** *128*, 3902-3903.
7. Chen, J.; Zhang, W.; Officer, D.; Swiegers, G. F.; Wallace, G. G., A readily-prepared, convergent, oxygen reduction electrocatalyst. *Chem. Comm.* **2007**, 3353-3355.
8. Choi, M.-S.; Yamazaki, T.; Yamazaki, I.; Aida, T., Bioinspired molecular design of light-harvesting multiporphyrin arrays. *Angew. Chem. Int. Ed.* **2003,** *43*, 150-158.
9. Kadish, K. M.; Smith, K. M.; Guilard, R.; Editors, *The Porphyrin Handbook; Volumes 1-20*. 2000-2003.
10. Desiraju, G. R., Supramolecular synthons in crystal engineering - a new organic synthesis. *Angew. Chem. Int. Ed.* **1995,** *34*, 2311-2327.
11. Yaghi, O. M.; O'Keeffe, M.; Ockwig, N. W.; Chae, H. K.; Eddaoudi, M.; Kim, J., Reticular synthesis and the design of new materials. *Nature* **2003,** *423*, 705-714.
12. Kitagawa, S.; Kitaura, R.; Noro, S.-I., Functional porous coordination polymers. *Angew. Chem. Int. Ed.* **2004,** *43*, 2334-2375.
13. Ferey, G., Hybrid porous solids: past, present, future. *Chem. Soc. Rev.* **2008,** *37*, 191-214.
14. Halder, G. J.; Kepert, C. J., Single Crystal to Single Crystal Structural Transformations in Molecular Framework Materials. *Aust. J. Chem.* **2006,** *59*, 597-604.
15. Suh, M. P.; Cheon, Y. E., Recent Advances in the Dynamics of Single Crystal to Single Crystal Transformations in Metal-Organic Open Frameworks. *Aust. J. Chem.* **2006,** *59*, 605-612.
16. Chandler, B. D.; Enright, G. D.; Udachin, K. A.; Pawsey, S.; Ripmeester, J. A.; Cramb, D. T.; Shimizu, G. K. H., Mechanical gas capture and release in a network solid via multiple single-crystalline transformations. *Nature Mater.* **2008,** *7*, 229-235.
17. Chemla, D. S.; Zyss, J.; Editors, *Nonlinear Optical Properties of Organic Molecules and Crystals, Vol. 2*. 1987.
18. Chemla, D. S.; Zyss, J.; Editors, *Nonlinear Optical Properties of Organic Molecules and Crystals, Vol. 1*. 1987.
19. Kanis, D. R.; Ratner, M. A.; Marks, T. J., Design and construction of molecular assemblies with large second-order optical nonlinearities. Quantum chemical aspects. *Chem. Rev.* **1994,** *94*, 195-242.
20. Sanders, J. K. M.; Bampos, N.; Clyde-Watson, Z.; Darling, S. L.; Hawley, J. C.; Kim, H.-J.; Mak, C. C.; Webb, S. J., Axial coordination chemistry of metalloporphyrins. *Porphyrin Handbook* **2000,** *3*, 1-48.
21. Kadish, K. M.; Smith, K. M.; Guilard, R.; Editors, *The Porphyrin Handbook: Volume 13 / Chlorophylls and Bilins: Biosynthesis, Synthesis, and Degradation*. 2003.
22. Kadish, K. M.; Smith, K. M.; Guilard, R.; Editors, *The Porphyrin Handbook: Volume 11 / Bioinorganic and Bioorganic Chemistry*. 2003.
23. Gust, D.; Moore, T. A.; Moore, A. L., Mimicking Photosynthetic Solar Energy Transduction. *Acc. Chem. Res.* **2001,** *34*, 40-48.

24. Kobuke, Y.; Ogawa, K., Porphyrin supramolecules for artificial photosynthesis and molecular photonic/electronic materials. *Bull. Chem. Soc. Jpn.* **2003,** *76*, 689-708.
25. Balaban, T. S., Tailoring Porphyrins and Chlorins for Self-Assembly in Biomimetic Artificial Antenna Systems. *Acc. Chem. Res.* **2005,** *38*, 612-623.
26. Sen, A.; Ray, P. C.; Das, P. K.; Krishnan, V., Metalloporphyrins for Quadratic Nonlinear Optics. *Journal of Physical Chemistry* **1996,** *100*, 19611-19613.
27. Verbiest, T.; Houbrechts, S.; Kauranen, M.; Clays, K.; Persoons, A., Second-order nonlinear optical materials: recent advances in chromophore design. *J. Mat. Chem.* **1997,** *7*, 2175-2189.
28. Albota, M.; Beljonne, D.; Bredas, J.-L.; Ehrlich, J. E.; Fu, J.-Y.; Heikal, A. A.; Hess, S. E.; Kogej, T.; Levin, M. D.; Marder, S. R.; McCord-Maughon, D.; Perry, J. W.; Rockel, H.; Rumi, M.; Subramaniam, G.; Webb, W. W.; Wu, X.-L.; Xu, C., Design of organic molecules with large two-photon absorption cross sections. *Science* **1998,** *281*, 1653-1656.
29. Su, D.; Wang, X.; Simard, M.; Wuest, J. D., Molecular tectonics. *Supramolecular Chemistry* **1995,** *6*, 171-178.
30. Ermer, O., Five-fold diamond structure of adamantane-1,3,5,7-tetracarboxylic acid. *J. Am. Chem. Soc.* **1988,** *110*, 3747-54.
31. Hollingsworth, M. D., Crystal engineering: from structure to function. *Science* **2002,** *295*, 2410-2413.
32. Desiraju, G. R., Crystal engineering: a holistic view. *Angew. Chem. Int. Ed.* **2007,** *46*, 8342-8356.
33. Diskin-Posner, Y.; Patra, G. K.; Goldberg, I., Crystal engineering of metalloporphyrin assemblies. New supramolecular architectures mediated by bipyridyl ligands. *Chem. Comm.* **2002**, 1420-1421.
34. Hoffmann, M.; Wilson, C. J.; Odell, B.; Anderson, H. L., Template-directed synthesis of a p-conjugated porphyrin nanoring. *Angew. Chem. Int. Ed.* **2007,** *46*, 3122-3125.
35. Holman, K. T.; Pivovar, A. M.; Swift, J. A.; Ward, M. D., Metric Engineering of Soft Molecular Host Frameworks. *Acc. Chem. Res.* **2001,** *34*, 107-118.
36. Beatty, A. M.; Granger, K. E.; Simpson, A. E., Crystal engineering of organic clay mimics from 3,5-pyrazoledicarboxylic acid and amines. *Chem. Eur. J.* **2002,** *8*, 3254-3259.
37. Abrahams, B. F.; Hoskins, B. F.; Michall, D. M.; Robson, R., Assembly of porphyrin building blocks into network structures with large channels. *Nature* **1994,** *369*, 727-9.
38. Deiters, E.; Bulach, V.; Hosseini, M. W., Reversible single-crystal-to-single-crystal guest exchange in a 3-D coordination network based on a zinc porphyrin. *Chem. Comm.* **2005**, 3906-3908.
39. Suslick, K. S.; Chen, C. T.; Meredith, G. R.; Cheng, L. T., Push-pull porphyrins as nonlinear optical materials. *Journal of the American Chemical Society* **1992,** *114*, 6928-30.
40. Smithenry, D. W.; Wilson, S. R.; Suslick, K. S., A Robust Microporous Zinc Porphyrin Framework Solid. *Inorg. Chem.* **2003,** *42*, 7719-7721.

2 ZINC···NITRO RECOGNITION – A NEW COORDINATION SYNTHON FOR LAYERED PORPHYRIN MATERIALS

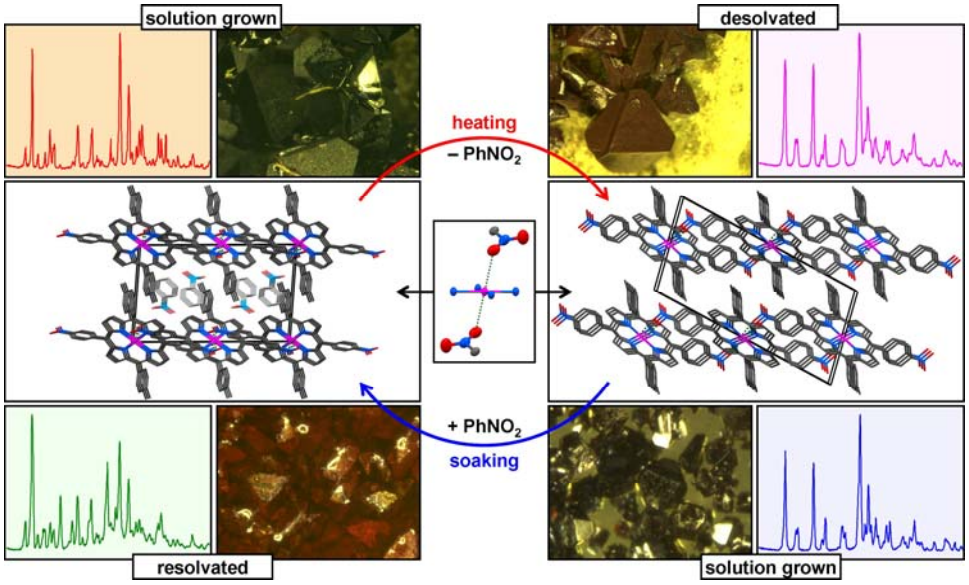

2.1 INTRODUCTION

Coordination polymers containing porphyrin moieties are important targets in crystal engineering because they exhibit unique optical, photochemical, and catalytic properties.[1-13] Previously, a variety of two- and three-dimensional porphyrin coordination polymers have been created; most of these networks are built by carboxy,[14-18] hydroxy,[19] aza,[20-31] cyano,[32] and other well-known ligands. Porphyrin moieties in these solids are connected by strong and directional metal-ligand coordination bonds. These strong bonds often lead to insoluble products that are difficult to characterize and develop into processable materials. A number of porous porphyrin solids, referred to as porphyrin sponges, have also been made using van der Waals interactions.[33] Crystal packing of these sponges is guest dependent and often unpredictable. In this chapter we discuss the use of Zn···NO_2 recognition as a coordination synthon[34] in the design and preparation of a porphyrin-based layered coordination polymer that possesses predictable topology and that can selectively intercalate guest molecules between the layers. We discuss the extension of Zn···NO_2 type of recognition patterns to other metal ions and ligands and rationalize the effectiveness of metal···NO_2 recognition in the context of different cations.

2.2 ZINC···NITRO RECOGNITION

We define Zn···NO_2 recognition as the coordination of Zn^{2+} ion, embedded inside the porphyrin core, with two nitro groups, one approaching above and the other below the plane of the porphyrin (Figure 2.1a). Each nitro group is bonded to the Zn^{2+} ion through one of its O-atoms. The Zn^{2+} ion adopts a tetragonal geometry, with four pyrrolic N-atoms lying in the square plane and the nitro O-atoms forming the axial coordination bonds. There are at least eight known porphyrin derivatives that show short intermolecular contacts between O-atoms of the nitro groups and Zn^{2+} ions embedded in the porphyrin core. There is only one known porphyrin derivative (Figure 2.1b) that contains the Zn···NO_2 recognition as defined above. In this system, Zn···NO_2 recognition occurs between the nitro groups of the nitrobenzene guest molecules and the Zn^{2+} ion of porphyrin host.[33] Noting the recurrence of Zn···O contacts in different porphyrin derivatives, we wished to explore its use of Zn···NO_2 recognition as a synthon in the preparation of layered porous coordination polymers.

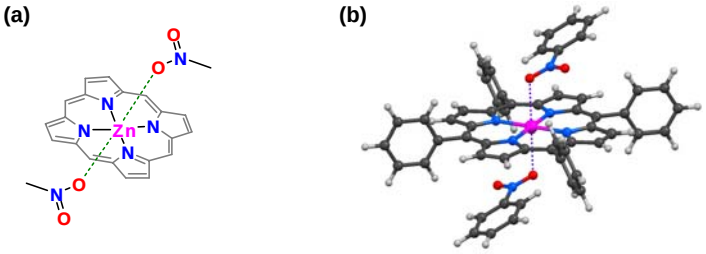

Figure 2.1 (a) Schematic representation of Zn···NO_2 recognition showing the porphyrin core and axial bonding of nitro groups. **(b)** Zn···NO_2 Recognition observed in the nitrobenzene solvate of zinc-*meso*-tetraphenylporphyrin. Notice the tetragonal coordination geometry adopted by the Zn^{2+} ion. Color scheme: Zn-magenta; O-red; N-blue; and C-grey.

The primary goal in the development of organic porous materials, beginning with the early work on hydrogen bonded systems[35-37] followed by the metal-ligand coordination polymers[38] and all the way to the current day metal-organic frameworks,[6] has been to prepare analogues of zeolites that offer greater control over pore size, guest selection, and chemistry inside the pores. Though there has been great success in this research, some fundamental limitations still remain to be resolved. For example, while the hydrogen bonded networks collapse after the removal of guests, the metal-organic frameworks are highly rigid, often insoluble, and difficult to process for use in different applications. We envisaged that (a) the tetragonal geometry of Zn···NO_2 recognition enables the design of predictable networks and (b) the inherent weakness of coordination bonds formed by the nitro groups leads to solids that are easily soluble in organic solvents and processable into materials such as thin films. We set out to create layered coordination polymers that contain two-dimensional networks, with the goal of testing the viability of Zn···NO_2 recognition and exploring the guest selection, intercalation and deintercalation between the layers.

2.3 DESIGN AND SYNTHESIS OF 1-ZN

In order to test the efficacy of Zn···NO_2 recognition in forming two-dimensional networks, we began our work with **1-Zn** (Figure 2.2a), the zinc metallated derivative of porphyrin **1**, 5,15-di(4-nitrophenyl)-10,20-di(*p*-tolyl)porphyrin. Compound **1-Zn** contains two *p*-nitrophenyl groups at alternate *meso* positions on the porphyrin ring; it is designed to have two nitro groups in *trans* geometry and no other functional groups that can potentially form coordination bonds. Groups such as hydroxy, amino, and carboxy form stronger coordination bonds and they can negatively interfere with the realization of Zn···NO_2 recognition. Thus, in the early stages of this work (Chapters 2 and 3) we used groups such as methyl, chloro and bromo on the remaining two phenyl rings; these groups do not compete with the nitro groups to form coordination bonds with the Zn^{2+} ion. In later chapters we describe the effect of competing ligands on the molecular and crystal structures and the overall properties of the derived materials.

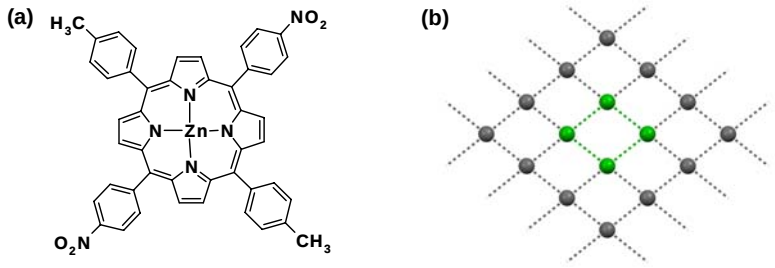

Figure 2.2 (a) Molecular structure of **1-Zn**. **(b)** Schematic representation the 4^4 network that **1-Zn** can adopt in its crystal structure. Each node in this network represents a molecule of **1-Zn**. Note that each node is connected to four other nodes and the smallest cycle, highlighted in green, contains four nodes.

We designed **1-Zn** to create 4^4 networks using the Zn···NO_2 recognition. A 4^4 network refers to a two-dimensional grid in which each node is connected to *four* other nodes and the smallest loop in the grid consists of *four* nodes (Figure 2.2b). The definition of a network using this terminology is elegant because it eases the restriction on the internodal distances and angles, and allows the comparison of patterns that otherwise may appear different. In our design, the porphyrin molecule acts as the node and the Zn···NO_2 recognition acts as the node connector. The following attributes are considered in the design of **1-Zn** towards the synthesis of 4^4 networks.

1. *Substitution of nitro groups at the para positions.* At this position the nitro groups are least hindered and most accessible for interaction with the Zn^{2+} ions.
2. *The trans-disposition of the p-nitrophenyl groups.* In this orientation, the *p*-nitrophenyl groups can form extended networks. For comparison, the *cis*-disposition may result in discrete assemblies.
3. *Choice of Zn^{2+} as the metal cation.* The Zn^{2+} has the right size to fit well inside the porphyrin core and to keep the core in a planar conformation. It is known to form weak coordination bonds with the nitro groups. The Zn^{2+} ion is inert to oxidation; its axial binding sites do not get saturated by counter ions. In the context of current work, the axial positions are available for bonding with nitro or other ligands. Finally, in terms of hard-soft acid-base concept, Zn^{2+} is a borderline acid and the nitro ligand is a borderline base. The matching softness of Zn^{2+} ion and nitro groups can facilitate the realization of Zn···NO_2 recognition under different conditions.
4. *Tetragonal geometry of Zn^{2+}.* Each **1-Zn** molecule can participate in four Zn···O bonds, two at the central Zn^{2+} ion and two at the peripheral nitro groups, leading to a 4^4 network.

We synthesized **1-Zn** in a modular procedure (Figure 2.3) starting from pyrrole and the corresponding aldehydes. The first step in this process is the preparation of the intermediate 5-(4-nitrophenyl)dipyrromethane.[39] This intermediate is used in the synthesis of several porphyrins discussed later in this thesis.[40] Full synthetic details are given in the experimental section at the end of the chapter.

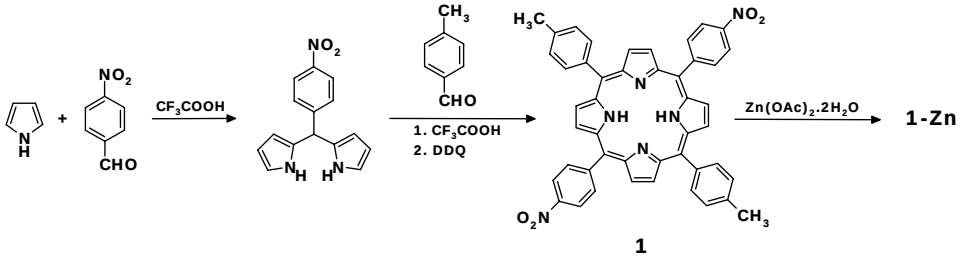

Figure 2.3 Modular synthesis of metalloporphyrin **1-Zn** starting from pyrrole, *p*-nitrobenzaldehyde and *p*-tolualdehyde.

2.4 CRYSTAL STRUCTURE OF 1-ZN

Single crystals of **1-Zn** suitable for X-ray diffraction are grown by slowly evaporating a chloroform solution containing **1-Zn**. Once grown, these crystals can be dissolved back into solution by adding more solvent and gentle heating. Crystals of **1-Zn** belong to the space group $P2_1/n$ with the molecules located on inversion centers. Within the structure, the nitro groups interact with the Zn^{2+} ions through one of the oxygen atoms. It is well-known that tetracoordinated Zn^{2+} ions enclosed in the porphyrin core frequently form one or two additional bonds with axial ligands. Figure 2.4 shows the tetragonal coordination around Zn^{2+} in **1-Zn**. The four pyrrolic N-atoms form Zn–N bonds of nearly equal length (2.032-2.052 Å); two nitro groups form longer Zn···O bonds (2.521 Å) above and below the plane of the porphyrin ring. These longer contacts constitute weaker coordination bonds and allow the free dissolution of the compound in organic solvents.

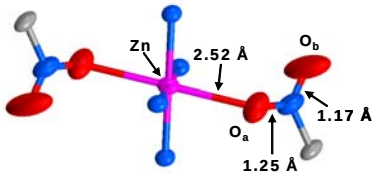

Figure 2.4 Zn···NO_2 Recognition in **1-Zn**. Notice tetragonal coordination around Zn^{2+} and differences in thermal ellipsoids of metal bound and free O-atoms.

2.4.1 Structural Evidence of Zn···NO_2 Recognition. The following observations demonstrate the bonding nature of Zn···O contacts of **1-Zn**. (a) The Zn···O distance is significantly shorter than the sum of the corresponding van der Waals radii (2.521 vs 2.910 Å). (b) The metal bound N–O_a bond in –NO_2 group is longer than the free N–O_b bond (1.246 vs 1.171 Å). (c) The geometry at Zn^{2+} ion is tetragonal. (d) Thermal motion of the metal bound O_a-atom (U_{eq} = 0.070 Å^2) is lower than that of the free O_b-atom (U_{eq} = 0.128 Å^2).[41-42] If the O_a-atom is not involved in bonding with Zn^{2+} ion, we would expect it to have higher thermal motion because N–O_a bond is longer than N–O_b bond. (e) Finally, the Zn···NO_2 recognition is reproducible; we show in later sections of this chapter and the next chapter several coordination polymers that are sustained by Zn···NO_2 recognition.

2.4.2 Layered 4^4 Networks in 1-Zn. Figure 2.5b shows the layered structure of **1-Zn**. Within the layer, each molecule donates two Zn···O bonds through two nitro groups and accepts two bonds through Zn^{2+} ion leading to a two-dimensional network with 4^4 topology. The cores of the porphyrin rings are inclined at an angle of 42.3° with respect to the mean plane of the layer and partially project the *p*-tolyl groups into the interlayer space (Figure 2.5a). Adjacent layers are stacked on each other such that they adopt an interdigitated packing, which maximizes the close packing between the layers. A separation of 9.806 Å and an offset of 2.784 Å between adjacent layers accommodate such interdigitated packing. The overall structure has a packing efficiency of 69.0%.

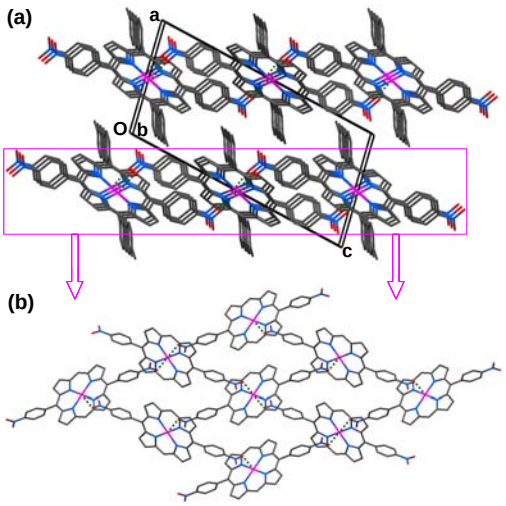

Figure 2.5 Crystal structure of **1-Zn**. **(a)** Interlayer stacking. Notice interdigitated packing and offset of layers. H-atoms are omitted. **(b)** 4^4 Networks formed by Zn···NO_2 recognition. *p*-Tolyl groups and H-atoms are omitted.

2.5 DESIGN AND STRUCTURE OF 1-ZN-PHNO$_2$

Noting the lamellar structure of **1-Zn** and the potential space between *p*-tolyl groups in the interlayer region, we explored the guest inclusion properties of **1-Zn**. Slow evaporation of a chloroform solution of **1-Zn** and nitrobenzene yielded solvated crystals containing **1-Zn** and nitrobenzene in 1:2 ratio; we refer to this solvate as **1-Zn-PhNO$_2$**. Crystallization of **1-Zn** from varying molar ratios of chloroform and nitrobenzene (100:1 to 0:100) also led to the exclusive crystallization of **1-Zn-PhNO$_2$**.

In the crystal structure of **1-Zn-PhNO$_2$** (space group $P2_1/c$) the key structural features of **1-Zn** are retained. These features include the Zn···NO_2 recognition, layered structure with 4^4 topology (Figure 2.6b), and stacking of the layers (Figure 2.6a). The inclusion of nitrobenzene molecules between the layers, however, imposes certain changes in intra- and interlayer parameters. In **1-Zn-PhNO$_2$**, porphyrin molecules are tilted at a steeper angle (48.2°) with respect to the mean plane of the layer to project *p*-tolyl groups into interlayer space to a greater extent. Layers are stacked at longer separation (11.289 Å) and shifted by shorter offset (0.851 Å) to create rectangular channels along the *b*-axis; solvated nitrobenzene molecules are located in these channels. Guest inclusion is further facilitated by the near perpendicular alignment of the tolyl rings with respect to the central porphyrin ring in **1-Zn-PhNO$_2$** (interplanar angle: 89.1°). In **1-Zn**, this angle is 68.1°. The interplanar angles between the porphyrin ring and nitrophenyl rings in **1-Zn** (77.2°) and **1-Zn-PhNO$_2$** (65.3°) also differ significantly. The Zn···O bonds are longer (2.722 Å); concurrently the differences in the N–O bond lengths (1.231 *vs* 1.216 Å) and thermal motions (U_{eq}: 0.068 vs 0.090) between metal-bound and free O-atoms are

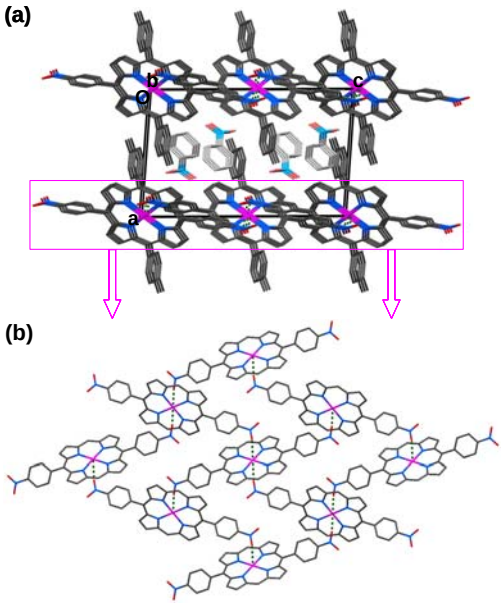

Figure 2.6 Crystal structure of **1-Zn-PhNO$_2$**. **(a)** Interlayer stacking showing the intercalation of nitrobenzene between the layers. Notice longer interlayer separation and shorter layer offset compared to **1-Zn** (Figure 2.5a). Nitrobenzene molecules are plotted in lighter colors. H-atoms are omitted. **(b)** 4^4 Networks formed by Zn···NO$_2$ recognition. *p*-Tolyl groups and H-atoms are omitted.

smaller. Despite these differences, the Zn···O contacts in **1-Zn-PhNO$_2$** show all the bonding characteristics outlined in Section 2.4.1.

The packing efficiency of **1-Zn-PhNO$_2$** with and without the nitrobenzene molecules is 69.7 and 52.7%.[43] Considering that the overall network structure in both solvated and unsolvated crystals is similar, a difference of 16.3% (69.0-52.7%) between the packing efficiency of **1-Zn** and guest free **1-Zn-PhNO$_2$** is fairly significant, and this fact demonstrates the reliability of Zn···NO$_2$ recognition as a coordination synthon.

Significant intermolecular interactions are not found among nitrobenzene molecules though they are confined to the interlayer region. These guest molecules do, however, form C–H···O and C–H···π interactions with *p*-nitrophenyl and *p*-tolyl rings of the host molecules. Two symmetry-independent C–H···O interactions (H···O (Å), C···O (Å), C–H···O (°): 2.25, 3.293, 161; 2.71, 3.576, 137) and one C–H···π interaction (H···X (Å), C···X (Å), C–H···X (°): 2.97, 3.784, 132; X refers to the centroid of aromatic rings) are seen in the crystals. The presence of solvated nitrobenzene in the bulk sample is confirmed, as shown below, by powder X-ray diffraction (PXRD) analysis, differential scanning calorimetry (DSC), and thermal gravimetric analysis (TGA).

2.6 HEAT INDUCED DESOLVATION OF 1-ZN-PHNO$_2$

Figure 2.7 shows that metalloporphyrin **1-Zn** is stable to thermal treatment at least up to 350 °C. High thermal stability is a desirable feature in porous materials that can be used in the fabrication of potential storage or sensor devices. The DSC thermogram of **1-Zn-PhNO$_2$** shows an endotherm with double minima between 145-170 °C corresponding to the loss of two solvated nitrobenzene molecules. No other phase transitions are observed on further heating of the sample. The molecular weight (246 amu) of the two solvent molecules is 23.6% of the total molecular weight of **1-Zn-PhNO$_2$** (796 + 246 = 1042 amu); the TGA shows that compound **1-Zn-PhNO$_2$** loses both solvent molecules in the temperature range 100-150 °C. The apparent difference in the temperatures at which solvent loss occurs in DSC and TGA is related to the experimental conditions; closed pans are used in the DSC whereas the TGA is performed in open pans. The TGA of **1-Zn-PhNO$_2$** also shows that no further loss of mass occurs beyond 150 °C.

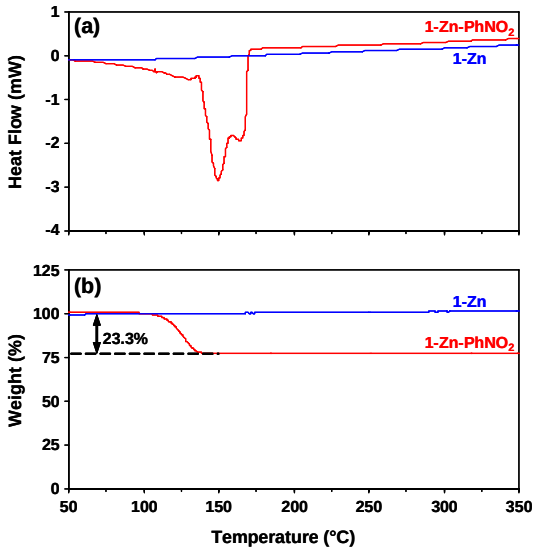

Figure 2.7 Thermal analysis of **1-Zn** (blue) and **1-Zn-PhNO$_2$** (red). **(a)** DSC thermograms. Notice the endotherm (with double minima) corresponding to the desolvation of nitrobenzene molecules in **1-Zn-PhNO$_2$**. **(b)** TGA plots showing the solvent loss in **1-Zn-PhNO$_2$** and the stability of **1-Zn** when subjected to heating up to 350 ºC.

2.7 FLEXIBILITY AND ROBUSTNESS OF 4^4 NETWORKS

Crystals of **1-Zn-PhNO$_2$** subjected to guest removal appear shiny and crystalline; ^{1}H-NMR analysis (not shown) indicated that these desolvated crystals contained only **1-Zn**. We monitored the removal of guest molecules by TGA (Figure 2.7b), which showed that complete loss of nitrobenzene molecules occurred in the range 100-150 °C. The desolvated crystals were cooled to room temperature in the TGA chamber and used for PXRD analysis immediately. Interestingly, removal of the guest species led to the reverse transition of solvate structure to that of the unsolvated form of **1-Zn**. Both solvate and

nonsolvate experimental powder patterns are compared in Figure 2.8 with the calculated powder patterns from single crystal data. It should be noted that compounds **1-Zn** and **1-Zn-PhNO$_2$** melt above 400 °C; the desolvated crystals are formed by solid-to-solid phase transition, not by cooling of the melt. We have not established the mechanism of this phase transition. We also observed the desolvation of **1-Zn-PhNO$_2$** optically on a Fisher-Jones melting point apparatus. The crystals remained intact with no apparent change in morphology during the whole heating cycle (25 – 300 °C and back to 25 °C) suggesting the possibility that the desolvation might be a single crystal to single crystal transformation.

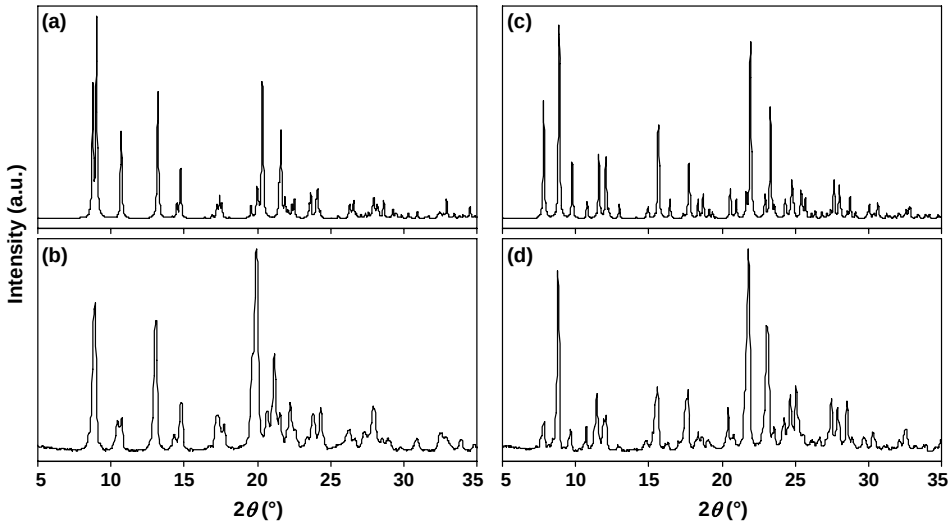

Figure 2.8 Calculated (top) and experimental (bottom) PXRD patterns of **1-Zn** (left) and **1-Zn-PhNO2** (right). These patterns indicate that the crystals in bulk samples have the same structures as those reported above (Figures 2.5 and 2.6).

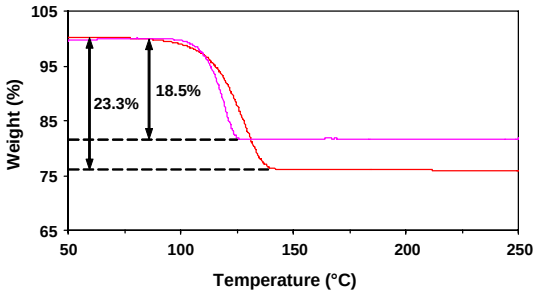

Figure 2.9 TGA plots of the solution grown crystals of **1-Zn-PhNO$_2$** (red) and the mixture of **1-Zn** and **1-Zn-PhNO$_2$** obtained by soaking the crystals of **1-Zn** in nitrobenzene for 2 h. The 23.3% weight loss (in red plot) corresponds to the complete desolvation of nitrobenzene from **1-Zn-PhNO$_2$** (calculated weight loss: 23.6%). The 18.5% weight loss (in magenta plot) indicates that the mixture contains 74.4% of **1-Zn-PhNO$_2$** and 25.6% of **1-Zn**.

2.8 RESOLVATION OF 1-ZN TO 1-ZN-PHNO$_2$

The results from desolvation experiment and the structural similarities between solvate and nonsolvate, encouraged us to test the resolvation properties of **1-Zn**. We soaked the desolvated crystals (~ 30 mg) obtained by heating **1-Zn-PhNO$_2$** in a small amount (0.2 mL) of nitrobenzene for 2 hours and monitored the crystals under an optical microscope.

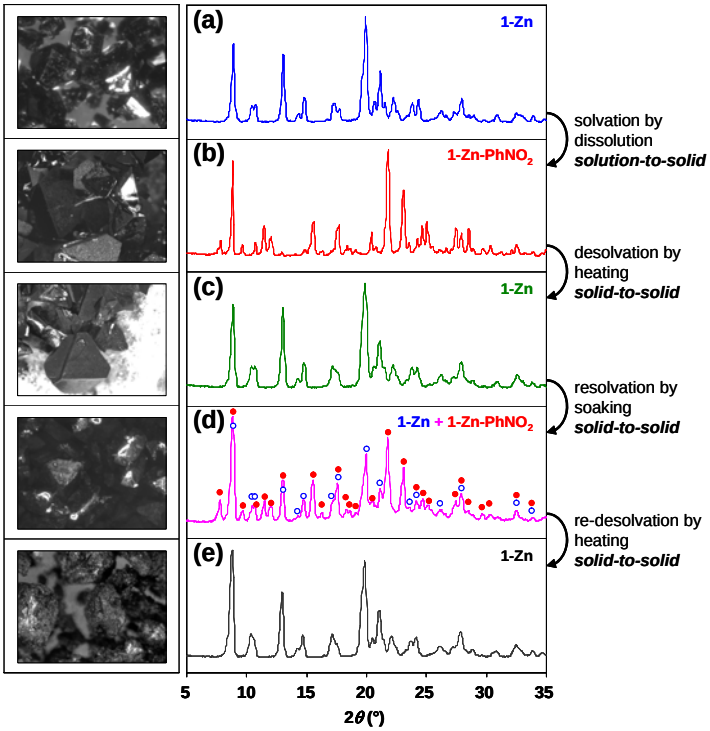

Figure 2.10 PXRD patterns of **(a**) **1-Zn** grown in $CHCl_3$ solution, **(b) 1-Zn-PhNO$_2$** grown in $CHCl_3$/$PhNO_2$ solution, **(c) 1-Zn** obtained by heating the **1-Zn-PhNO$_2$** to 350 °C, **(d)** mixture of **1-Zn** and **1-Zn-PhNO$_2$** obtained by soaking the crystals of **1-Zn** in **(c)**, and **(e) 1-Zn** obtained by heating of the mixture in **(d)** to 350 °C. Note in **(c)** and **(e)** that the diffraction patterns of desolvated and re-desolvated crystals correspond to that of **1-Zn**. Note in **(d)** the peaks corresponding to **1-Zn** (open, blue circles) and **1-Zn-PhNO$_2$** (filled, red circles). This pattern indicates the formation of **1-Zn-PhNO$_2$** through the process of solid-to-solid intercalation of nitrobenzene molecules into **1-Zn**. Microscopic images of the crystals corresponding to the diffraction patterns are shown on the left. The image next to **(d)** is taken while the crystals are soaking in nitrobenzene. The crystals in **(e)** do not seem to have well-developed faces. This is due to the crushing and aggregation of crystals that occur when the soaked crystals are transferred onto the filter paper for drying. Morphology of the crystals remains unchanged during the heating in TGA chamber. For PXRD patterns, the *y*-axis refers to diffraction intensity in arbitrary units.

We dried the soaked crystals on a filter paper for 30 min (to remove any physisorbed nitrobenzene) and analyzed them with TGA (Figure 2.9) and PXRD (Figure 2.10). We can deduce from the TGA that at least ~74% of the **1-Zn** crystals are resolvated with nitrobenzene during the 2 hours of soaking.

Powder X-ray analysis (Figure 2.10d) provided the unequivocal proof for the formation of **1-Zn-PhNO$_2$** during the resolvation with nitrobenzene. Optical microscopy showed that the crystals remained intact for the duration of soaking; we did not witness dissolution and re-growth of the crystals. These observations suggest that resolvation of **1-Zn** with nitrobenzene to form **1-Zn-PhNO$_2$** is also a solid-to-solid transformation. We subjected these resolvated crystals to another cycle of heating in the TGA chamber; remarkably, desolvation occurred again as a solid-to-solid transformation to yield the crystals of **1-Zn** (Figure 2.10e).

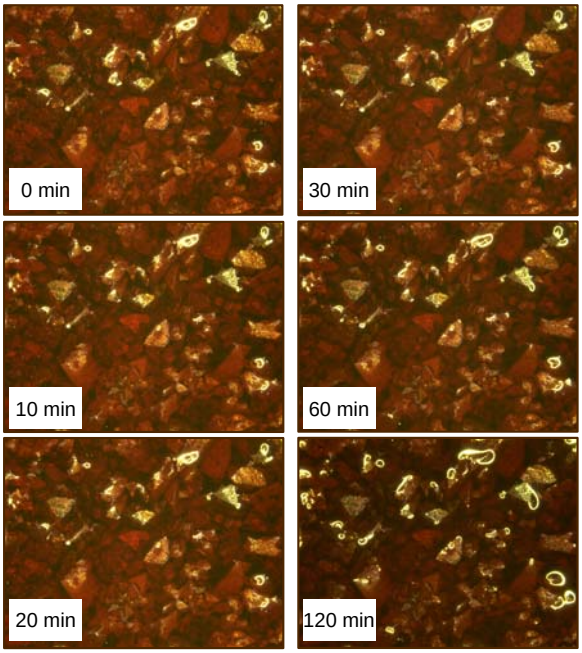

Figure 2.11 Optical microscopic images of desolvated **1-Zn** crystals subjected to resolvation with nitrobenzene. Note that the sizes and morphologies of the crystals remain unchanged with time.

A description of the terms such as desolvation and resolvation we used above will be useful. We refer to the removal of nitrobenzene molecules from **1-Zn-PhNO$_2$** as *desolvation*. This process can also be called *deintercalation* because (a) the materials described in this work have layered structures and (b) solvent molecules are located between layers. *Resolvation* refers to the incorporation of nitrobenzene molecules into **1-Zn** that is obtained by desolvation of **1-Zn-PhNO$_2$**. This process can also be called

reintercalation for the reasons given above. *Re-desolvation* refers to the removal of nitrobenzene molecules from **1-Zn-PhNO$_2$** that is obtained from resolvation of **1-Zn**.

As mentioned above, we monitored the resolvation of **1-Zn** crystals with nitrobenzene under an optical microscope. Pictures are taken at regular intervals for the duration of soaking. Figure 2.11 shows the microscopic images at various stages of the resolvation. It can be seen that the sizes and shapes of different crystals remain unchanged for at least two hours. These observations suggest that the formation of **1-Zn-PhNO$_2$** in the resolvation experiments is not a result of dissolution followed by re-growth of the crystals. After resolvation, the remaining solid was transferred on to the filter paper to remove excess nitrobenzene, and then transferred to another filter paper where crystals dried for 10 minutes. Transferring solvated crystals to filter paper requires mechanical manipulation of crystals. During this process crystals that were intact during the resolvation get pulverized to some extent. These crystals were then characterized by TGA, DSC and PXRD analysis.

2.9 GUEST DISCRIMINATION BASED ON STERIC AND ELECTRONIC PROPERTIES

We explored the inclusion properties of **1-Zn** to determine if this compound exhibits any selectivity towards different guest species. The interlayer spaces in **1-Zn** are walled by *p*-tolyl rings that are expected to be electron rich, and this is the reason our initial studies included electron deficient nitrobenzene as the guest. We began further guest inclusion studies with toluene, chlorobenzene, and bromobenzene; these molecules have nearly the same size as nitrobenzene but have different electronic character. Repeated attempts to crystallize solvates of **1-Zn** with these guest species resulted in the crystallization of unsolvated **1-Zn**.

Figures 2.12 and 2.13 show thermal and diffraction analysis of the materials obtained from solutions containing toluene, chlorobenzene, and bromobenzene; in all the cases it can be seen that solvent inclusion does not occur when these guests are used. To take further advantage of this observation, we attempted competitive guest inclusion experiments between these three guests and nitrobenzene. In these experiments, chloroform solutions containing **1-Zn**, toluene (or chlorobenzene or bromobenzene) and nitrobenzene are allowed to evaporate and the obtained materials are characterized. We varied the relative ratios of the guests (from 1:1 to 20:1, with nitrobenzene in smaller quantity) and also the overall concentrations of the solutions. In separate experiments, we crystallized **1-Zn** from a chloroform solution containing all four of the guest species. In each of these experiments, we obtained crystals of only the nitrobenzene solvate. This level of selectivity is unusual for a compound that is not specifically designed for selective inclusion of a particular guest. We surmised that the observed selectivity is related to the size and electronic character of nitrobenzene.

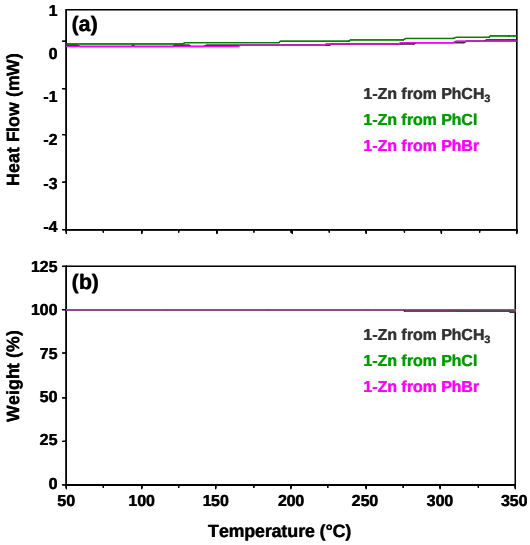

Figure 2.12 Thermal analysis, **(a)** DSC and **(b)** TGA, of **1-Zn** obtained from toluene (dark grey), chlorobenzene (green) and bromobenzene (magenta). In DSC and TGA the thermograms from different samples are superimposed on each other.

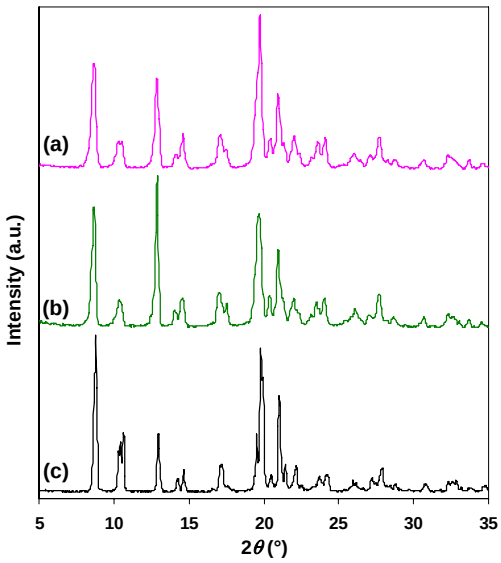

Figure 2.13 PXRD patterns of **1-Zn** samples obtained from **(a)** bromobenzene, **(b)** chlorobenzene, and **(c)** toluene solvents. Note that all powder patterns are similar to the one obtained from the nonsolvate **1-Zn** shown in Figure 2.8b.

To evaluate the effect of size, shape and electronic features of the guests, we attempted the preparation of nitromethane, acetonitrile, benzonitrile, and *o*-nitrotoluene solvates of **1-Zn**. The first two guests are electron deficient akin to nitrobenzene; they are, however, smaller and non-aromatic. Several crystallization trials using these two guests led to pure **1-Zn**, with no solvent inclusion. Attempts to prepare the *o*-nitrotoluene solvate of **1-Zn** also resulted in the crystallization of pure **1-Zn**. This guest is still electron deficient but it is slightly bigger in size than nitrobenzene. We note that crystals of pure **1-Zn** are also routinely obtained from organic solvents such as chloroform. The non-inclusion findings in all these cases are ascertained by DSC, TGA, and PXRD analyses. In contrast to the results above, intercalation of **1-Zn** with benzonitrile led to the quantitative crystallization of 1:1 solvate **1-Zn-PhCN**. These observations suggest that **1-Zn** is capable of discriminating between electron rich guest species from electron deficient ones and within the latter category **1-Zn** shows greater selectivity towards aromatic guests of specific size(s).

2.10 THERMAL AND STRUCTURAL ANALYSIS OF 1-ZN-PHCN

Small, needle like single crystals of **1-Zn-PhCN** are readily obtained when a chloroform solution containing **1-Zn** and an excess of benzonitrile is slowly evaporated. The first signs of intercalation of benzonitrile by **1-Zn** are noticed in a DSC experiment (Figure 2.14a). The uneven endotherm between 110-145 ºC indicated the possibility of guest uptake by **1-Zn**. Analysis by TGA revealed that the crystals lose 11.3% mass by weight between 110-145 ºC; this mass loss corresponds to a 1:1 complex between **1-Zn** and benzonitrile.

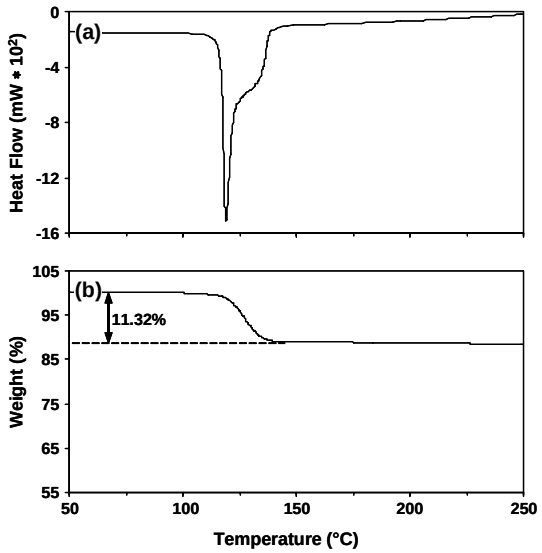

Figure 2.14 (a) DSC and **(b)** TGA plots of **1-Zn-PhCN**. The endotherm in **(a)** and weight loss in **(b)** correspond to the desolvation of benzonitrile from the crystals.

Encouraged by these results we attempted the single crystal X-ray diffraction analysis of **1-Zn-PhCN**. Recall that crystals of **1-Zn-PhNO$_2$** contain the porphyrin and the guest in 1:2 proportions. Given that **1-Zn** and benzonitrile exist in 1:1 stoichiometry in **1-Zn-PhCN** it is imperative to analyze the crystal structure of this complex. We sought to address the following questions with this structure determination. (a) Can Zn···NO$_2$ recognition persist with a different guest and in a different host-guest stoichiometry? (b) Does this structure contain a 4^4 network? (c) Finally, is this an intercalated structure (that has guest inclusion between the layers)? Figure 2.15 reveals that the answer to all these questions is affirmative. Indeed the crystal structure of **1-Zn-PhCN** contains continuously stacked layers of **1-Zn** (Figure 2.15a); benzonitrile molecules are located between the layers. Within each layer, adjacent **1-Zn** molecules are connected to each other through Zn···NO$_2$ recognition to form 4^4 networks, similar to those seen in pure **1-Zn** (Figure 2.5b) and **1-Zn-PhNO$_2$** (Figure 2.6b). These similarities occur despite the differences between the overall structures of **1-Zn** (space group $P2_1/n$) and **1-Zn-PhNO$_2$** (space group $P2_1/c$) and **1-Zn-PhCN** (space group $C2/c$). We argue that the recurrence of important similarities, notwithstanding the inconsequential differences, is a testament to both the flexibility and the robustness of the new coordination synthon we have developed. The differences and similarities between different structures are further discussed in Chapter 3 using various intra- and interlayer parameters.

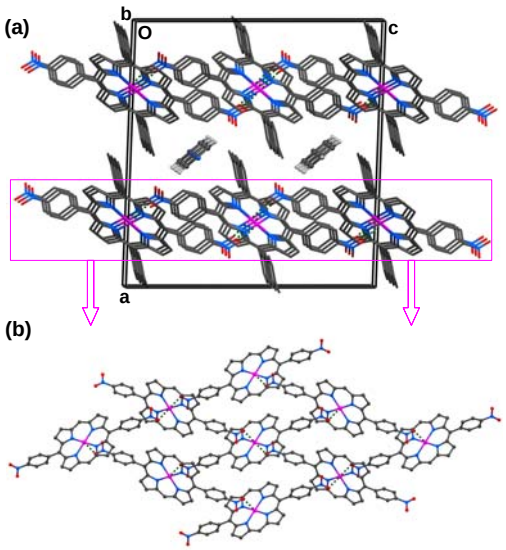

Figure 2.15 Crystal structure of **1-Zn-PhCN**. **(a)** Interlayer stacking showing the intercalation of benzonitrile between the layers. Notice the collinear arrangement of guest molecules along the *b*-axis. H-atoms of **1-Zn** are omitted. **(b)** 4^4 Networks formed by Zn···NO$_2$ recognition. *p*-Tolyl groups and H-atoms are omitted. Compare and contrast this figure with Figures 2.5 and 2.6.

One particularly striking aspect of the structure of **1-Zn-PhCN** is the collinear assembly of benzonitrile molecules. Short, linear C–H···N interactions (H···N: 2.24 Å; C···N: 3.33 Å; C–H···N: 180°) connect the adjacent guest molecules to form a linear hydrogen bonded chain. The benzonitrile molecules lie on special positions such that the -C≡N and *para*-C–H groups are arranged on crystallographic 2-fold axes. Incidentally, a similar linear assembly made of C–H···N interactions also exists in the crystal structures of pure benzonitrile (H···N: 2.59 Å; C···N: 3.68 Å; C–H···N: 180°)[44] and 4-ethynylpyridine (H···N: 2.19 Å; C···N: 3.28 Å; C–H···N: 180°)[45] In general, it is rare to find linear assemblies made of weak C–H···Y (Y = O, N, F etc) interactions,[46] and in Chapter 3 we further explore the inclusion of benzonitrile in other porphyrin analogues of **1-Zn**.

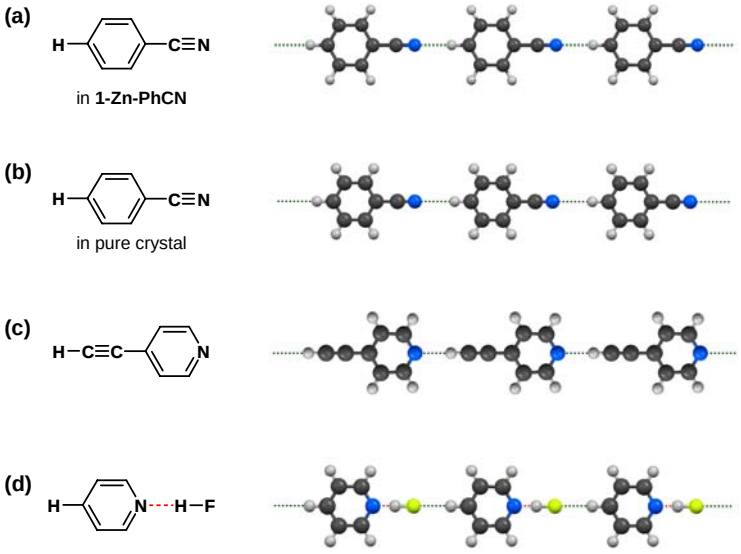

Figure 2.16 (a) Linear arrays of benzonitrile molecules (in **1-Zn-PhCN**) sustained by C–H···N hydrogen bonds. These linear chains fit within the voids that run along the *b*-axis in **1-Zn-PhCN** (Figure 2.15). For comparison, linear chains made of weak hydrogen bonds in other systems are also shown: **(b)** pure benzonitirle, **(c)** 4-ethynylpyridine, and **(d)** pyridine hydrofluoride. The last complex contains chains of molecules that are held together by strong (F–H···N) and weak (C–H···F) hydrogen bonds.

In future work, it will also be of interest to test the intercalation of guests such as 4-ethynylpyridine and 4-cyano-4′-ethynylbiphenyl that show similar linear hydrogen bonded chains within their solid state structures.[47] Unfortunately, however, molecules such as 4-ethynylpyridine compete with the nitro groups and disrupt Zn···NO_2 recognition; inclusion of these or other guests with competing donor atoms may not therefore be used for intercalation. In Chapters 4 and 5 we describe the structures of aniline and pyridine complexes of **1-Zn** and its analogues, and discuss the effects of competing ligands. One important lesson that we can learn from the structure of **1-Zn-**

PhCN is that the cyano group, a well explored ligand in the crystal engineering of coordination polymers, fails to compete with the nitro group. If it were successful in this competition, we would see the formation of Zn···N≡C–Ph bonds in the structure of **1-Zn-PhCN**.

2.11 FURTHER CONSIDERATIONS IN THE USE OF ZN···NO_2 RECOGNITION

The discussion above clearly showed that Zn···NO_2 recognition is a useful and reliable synthon to prepare coordination polymers with predictable topology. In this section, we discuss a few ideas on the possible extension of this new coordination synthon. Within this thesis, some of these ideas are fully explored, some are tested with a small number of preliminary experiments, and some are not yet investigated but only discussed as foundations for future work in this area. These ideas include changing the location of ligand on the phenyl rings, changing the nitro ligand to other neutral ligands, changing the metal cation, and finally changing the tolyl groups with other non-competing groups.

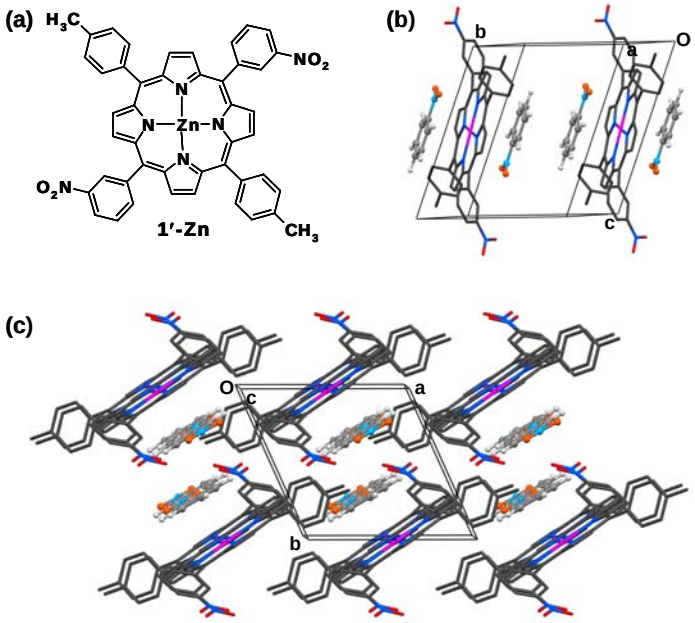

Figure 2.17 (a) Molecular structure of **1′-Zn**. **(b)** Crystal structure of **1′-Zn-PhNO$_2$** showing the stacked arrays of porphyrin rings and nitrobenzene molecules. **(c)** View down *c*-axis showing the overall arrangement of host (**1′-Zn**) and guest (nitrobenzene) molecules. In **(b)** and **(c)** H-atoms on **1′-Zn** are omitted and guest molecules are shaded with lighter colors.

2.11.1 Position of Nitro Ligands on Phenyl Rings. In Section 2.3 we discussed several factors that are considered in the design of **1-Zn**. One of the factors is the location of

nitro group on the phenyl ring. We argued that nitro groups at the *para* positions are easily accessible for binding to the Zn^{2+} ion. To evaluate this argument we synthesized **1′-Zn**, Zn-5,15-di(3-nitrophenyl)-10,20-di(*p*-tolyl)porphyrin (Figure 2.17a). This is an isomer of **1-Zn** (Figure 2.2a); the difference between these two zinc metallated porphyrins is that **1′-Zn** contains the nitro groups on the *meta* positions of phenyl rings whereas **1-Zn** has nitro groups on the *para* positions.

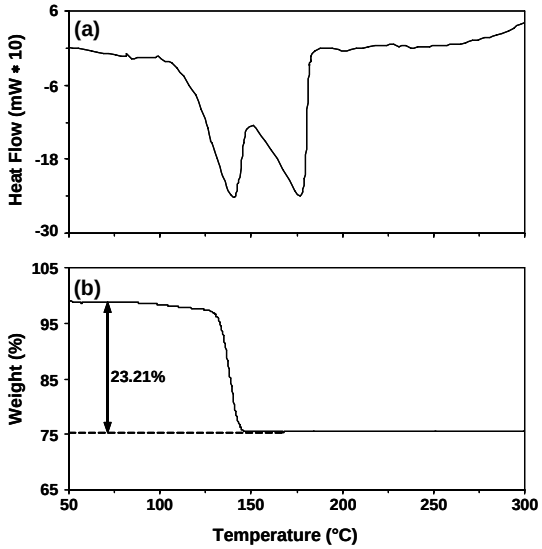

Figure 2.18 (a) DSC and **(b)** TGA plots of **1′-Zn-PhNO$_2$**. The endotherms in **(a)** and weight loss in **(b)** correspond to the desolvation of nitrobenzene from the crystals. The close match between the experimental (23.21%) and theoretical weight loss (23.62%) suggest the high purity of the solvated crystals.

We attempted the crystallization of **1′-Zn** from different solvents; the best crystals suitable for single crystal X-ray diffraction are obtained from a solution made of chloroform and nitrobenzene. These crystals are nitrobenzene solvates wherein the host and guest are in 1:2 stoichiometry as revealed by TGA (Figure 2.18b). As with **1-Zn-PhNO$_2$** (Figure 2.7), the loss of nitrobenzene occurred in two stages when the samples are heated in a sealed pan in the DSC (Figure 2.18a). Though **1-Zn-PhNO$_2$** and **1′-Zn-PhNO$_2$** have similar host-guest stoichiometry, structural analysis revealed that **1′-Zn-PhNO$_2$** contains neither Zn···NO$_2$ recognition nor 4^4 networks. Instead, **1′-Zn** adopts a structure in which nitrobenzene molecules stack above and below the plane of the porphyrin core. Figures 2.17b-c show that the planes of porphyrin rings and guest molecules are nearly parallel (inter planar angle 4.65º) and are at short separation (3.26 Å). Stacking of guest molecules on porphyrin rings is a common feature observed in porphyrin sponges.[33] The nitro groups of **1′-Zn** as well as the guest molecules in **1′-Zn-PhNO$_2$** are involved in several short C–H···O interactions. It appears that positioning the nitro groups at *meta* positions on the phenyl rings is unfavorable to form Zn···O contacts. The lack of Zn···NO$_2$ recognition in **1′-Zn-PhNO$_2$**, however, is compensated by stacking

of aromatic rings on the Zn^{2+} ion and C–H···O hydrogen bonds around the nitro groups. More work needs to be done and more structures need to be determined before we can assert that *m*-nitrophenyl rings are not suitable for the design of 4^4 networks using Zn···NO_2 recognition.

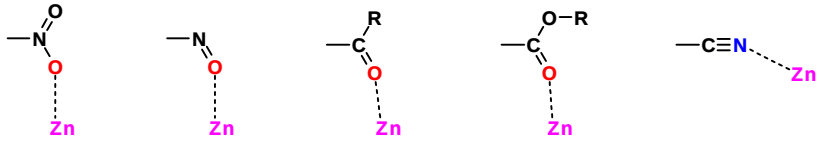

Figure 2.19 Possible ligands that can be used in the preparation of 4^4 networks. Binding atoms are drawn in color and approximate binding geometry is indicated by the dashed bonds to the Zn^{2+} ion.

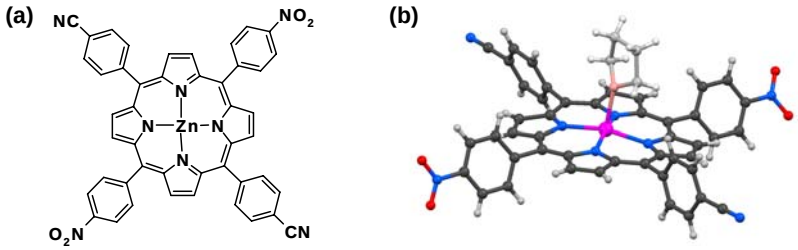

Figure 2.20 (a) Molecular structure of an analogue of **1-Zn** containing nitro and cyano ligands. **(b)** Crystal structure of porphyrin in **(a)** showing the binding of THF to the Zn^{2+} ion.

2.11.2 Substitution of Nitro Groups by Other Ligands. One important reason we chose nitro groups as the ligands is that they form *weak* coordination bonds with the Zn^{2+} ion. Figure 2.19 shows other possible ligands that can potentially form similar 4^4 networks when substituted at the *para* positions on phenyl rings. Of these groups, the nitroso, acyl, and ester functionalities possess the same geometry as the nitro group and project the ligand O-atom (roughly) perpendicular to the phenyl ring. The cyano group, however, projects the ligand N-atom within the plane of the phenyl ring. We did not explore these ligands in the current work. A survey of the Cambridge Structural Database (CSD)[48] suggests that all these ligands are capable of forming coordination bonds with the metal cations embedded in the porphyrin cores. In the context of these different ligands, we prepared a dicyano-dinitro-analogue of **1-Zn** (Figure 2.20a) to test which of the two functional groups, $–NO_2$ or –C≡N, would form the coordination bonds with the Zn^{2+} ions. Unfortunately this compound has poor solubility and to date we have not been able to grow diffraction quality single crystals from non-competing solvents. When crystallized from a chloroform solution containing trace amount THF (tetrahydrofuran), this compound yields a coordination complex in which THF binds to the Zn^{2+} ion (Figure 2.20b).

2.11.3 Substitution of Zinc by Other Metals. Porphyrins are known to embed a range of cations (transition metals, rare earth metals, and Group II metals) within the

tetrapyrrole core. Only some metal cations, however, fit well within this core; many other cations, due to their inappropriate (smaller or larger) size, are known to pucker or skew the planar geometry of the central porphyrin ring. The planarity of the central porphyrin ring is essential to sustain the M···NO_2 recognition (M = metal) because nitro groups need to bind to both axial positions of the embedded cation. We performed some preliminary experiments to explore M···NO_2 recognition using Co^{2+} and Mg^{2+} ions. Reaction of porphyrin **1** with $Co(OAc)_2$ in dimethylformamide (DMF) (Section 2.12) readily produced the metalloporphyrin **1-Co**, an analogue of **1-Zn**. Slow evaporation of a chloroform solution containing **1-Co** and nitrobenzene yielded prismatic crystals of **1-Co-PhNO$_2$** in quantitative yields. Thermal analysis of these crystals showed that the host (**1-Co**) and the guest (nitrobenzene) are in 1:2 stoichiometry (Figure 2.21b) and that the desolvation endotherms (Figure 2.21a) are similar to those of **1-Zn-PhNO$_2$**.

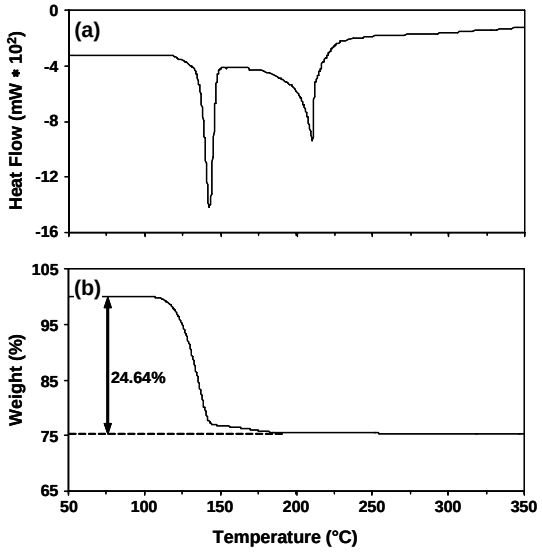

Figure 2.21 (a) DSC and **(b)** TGA plots of **1-Co-PhNO$_2$**. The endotherm in **(a)** and weight loss in **(b)** correspond to the desolvation of nitrobenzene from the crystals.

2.11.3.1 Co···NO$_2$ Recognition in 1-Co-PhNO$_2$. Persuaded by the results from DSC and TGA (Figure 2.21), we determined the crystal structure of **1-Co-PhNO$_2$** at -80 °C. The overall structure of **1-Co-PhNO$_2$** (Figure 2.22) is similar to that of **1-Zn-PhNO$_2$** (Figure 2.6). They both belong to the same space group ($P2_1/c$); their *a*- and *c*-axes have nearly similar lengths (11.40, 18.43 and 11.32, 18.15 Å) and the values of their β-angles (95.33 and 94.31°) are also almost similar. The major difference between the two structures is that the *b*-axis of **1-Co-PhNO$_2$** (35.40 Å) is about three times longer than that of the **1-Zn-PhNO$_2$** (11.92 Å). The asymmetric unit (Z') of **1-Co-PhNO$_2$** contains one-and-half molecules of porphyrins (one located on an inversion center, orange in Figure 2.22, and the other on a general position, blue in Figure 2.22) and three molecules of nitrobenzene (all located on general positions). In contrast, the asymmetric unit of **1-Zn-PhNO$_2$** contains half a molecule of porphyrin and one molecule of nitrobenzene. In essence, the

unit cell of **1-Co-PhNO$_2$** (7406.7 Å^3) is about three times larger than that of the **1-Zn-PhNO$_2$** (2443.0 Å^3).

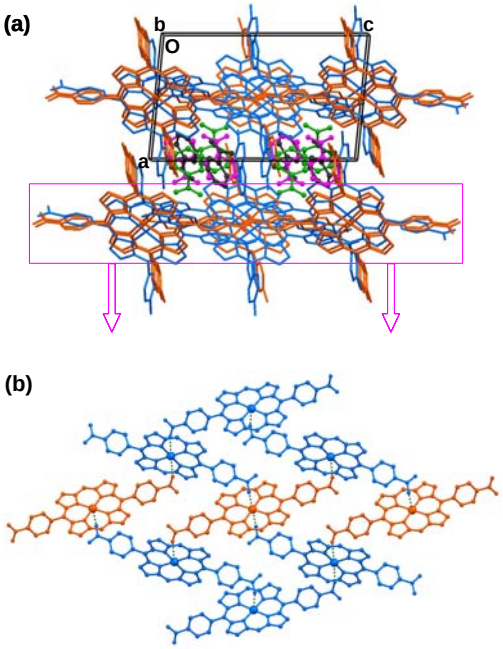

Figure 2.22 Crystal structure of **1-Co-PhNO$_2$** determined at -80 °C. **(a)** Interlayer stacking showing the intercalation of nitrobenzene between the layers. Symmetry independent host (orange and blue) and guest (black, magenta, and green) are colored differently. One of the three nitrobenzene molecules is disordered over two positions; only one position is shown. H-atoms are omitted. Compare and contrast this structure with that of **1-Zn-PhNO$_2$** (Figure 2.6). **(b)** 4^4 Networks formed by Co···NO$_2$ recognition. *p*-Tolyl groups and H-atoms are omitted. Note that each 4^4 network in the crystal contains both symmetry independent porphyrin molecules.

In the crystal structure of **1-Co-PhNO$_2$** the host molecules assemble into layers and the guest molecules are confined to the interlayer region. Within the layer, the two symmetry independent porphyrin molecules are joined together by Co···NO$_2$ recognition to form 4^4 networks (Figure 2.22b). Each 4^4 network contains the orange ($Z' = 0.5$) and blue ($Z' = 1$) porphyrin molecules in 1:2 ratio. Each orange molecule is connected to four blue molecules, whereas each blue molecule is connected to two orange and two blue molecules. There are a total of three independent Co···O contacts (2.62, 2.59, and 2.66 Å); all are shorter than the sum of van der Waals radii (3.52 Å) of Co and O-atoms. The Co bound N–O bonds (1.240, 1.234 and 1.241 Å) are longer than the free N–O bonds (1.220, 1.230 and 1.220 Å), and the thermal parameters of metal bound O-atoms (U_{eq} = 0.040; 0.034; 0.032 Å^2) are smaller than the free O-atoms (U_{eq} = 0.051; 0.036; 0.038 Å^2). Both symmetry independent Co^{2+} ions display tetragonal geometry. All these

observations indicate that Co···NO_2 recognition has the same bonding characteristics as the Zn···NO_2 recognition (see Section 2.4.1).

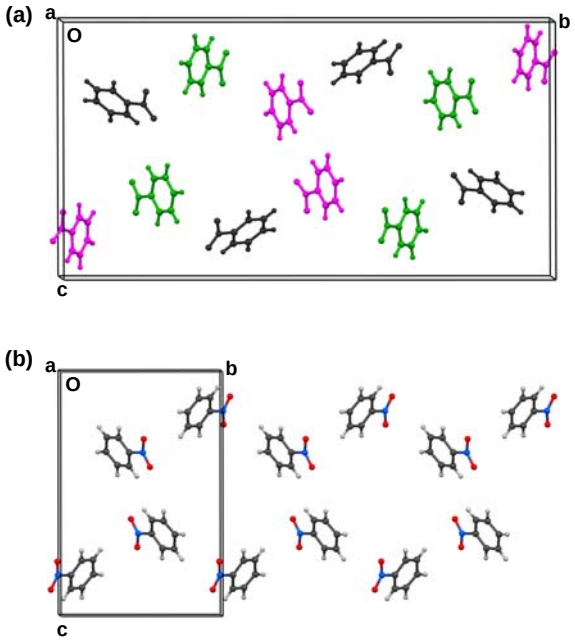

Figure 2.23 Arrangements of nitrobenzene molecules in the crystal structures of **(a) 1-Co-PhNO$_2$** and **(b) 1-Zn-PhNO$_2$**. In **(a)**, symmetry independent molecules are drawn in different colors. Notice the striking similarity between the two structures.

The interlayer packing in **1-Co-PhNO$_2$** (Figure 2.22a) closely resembles the stacking in **1-Zn-PhNO$_2$** (Figure 2.6a). The porphyrin molecules are titled (49.42 and 50.79°) with respect to the mean plane of the layer to project *p*-tolyl groups into interlayer space. The tolyl rings are nearly perpendicular to the porphyrin rings (interplanar angles: 83.72 and 88.52°). The layers are separated by 11.14 Å and offset by 1.13 Å to create rectangular channels along the *b*-axis. Solvated nitrobenzene molecules occupy these channels. The only apparent difference between **1-Zn-PhNO$_2$** and **1-Co-PhNO$_2$** is the slight misalignment of stacked porphyrin molecules along the *b*-axis in the latter structure. Despite this misalignment and despite the differences in the number of molecules in the asymmetric unit and the overall unit cell volume, both crystals are nearly isostructural. The structural similarity can be clearly illustrated by considering the packing of nitrobenzene molecules confined to the interlayer region (Figure 2.23). Though there are three symmetry independent nitrobenzene molecules in **1-Co-PhNO$_2$**, their overall packing is the same as the packing of nitrobenzene molecules in **1-Zn-PhNO$_2$**.

2.11.3.2 Higher-Z′ to Lower-Z′ Phase Transition in 1-Co-PhNO$_2$. Why do **1-Co-PhNO$_2$** and **1-Zn-PhNO$_2$** adopt different crystal structures and yet display similarity at many levels? Is it possible that each of these compounds has an as yet undiscovered polymorph

that crystallizes in the other structure? Does the structure of **1-Co-PhNO$_2$** represent the 'fossil relic' of **1-Zn-PhNO$_2$**? In other words, does the structure of **1-Co-PhNO$_2$** (with higher *Z*′) represent kinetically locked-in *arrested crystallization* that is yet to transform to a potentially more stable structure with lower Z′?[49-51] It is important to note here that crystals of both compounds, **1-Co-PhNO$_2$** and **1-Zn-PhNO$_2$**, are grown at the same temperature (20 °C) and that their structures are determined at the same temperature (-80 °C). If **1-Co-PhNO$_2$** is indeed a kinetically trapped structure, one way of inducing its transformation to the more stable structure would be to heat the sample from -80 °C to a higher temperature and determine its structure at this elevated temperature. Indeed, the unit cell parameters of **1-Co-PhNO$_2$** determined at 0 °C are practically similar to those of **1-Zn-PhNO$_2$**. At higher temperature (0 °C) **1-Co-PhNO$_2$** (Figure 2.24) is fully isostructural with **1-Zn-PhNO$_2$**.

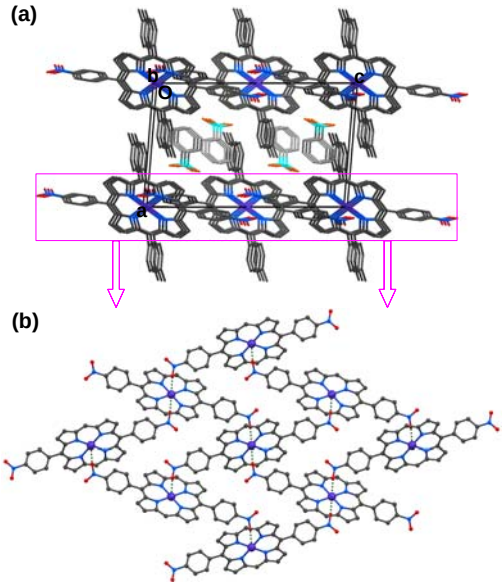

Figure 2.24 Crystal structure of **1-Co-PhNO$_2$** determined at 0 °C. **(a)** Interlayer stacking showing the intercalation of nitrobenzene between the layers. Nitrobenzene molecules are plotted in lighter colors. Nitrobenzene is disordered over two positions; only one position is shown. H-atoms are omitted. Notice the isostructural relationship between this structure and **1-Zn-PhNO$_2$** (Figure 2.6). **(b)** 4^4 Networks formed by Co···NO$_2$ recognition. *p*-Tolyl groups and H-atoms are omitted. Contrast **(a)** and **(b)** in this figure with Figure 2.22; symmetry independent molecules in Figure 2.22 became symmetry equivalent at higher temperature.

We have monitored the higher-*Z*′ to lower-*Z*′ phase transition of **1-Co-PhNO$_2$** on the single crystal X-ray diffractometer. A crystal of **1-Co-PhNO$_2$** is taken out of crystallization solution and immediately placed into a drop of mineral oil. The crystal is then mounted on a Bruker APEX II single crystal X-ray diffractometer such that it is immersed into a cold stream of nitrogen. We collected the X-ray data on this crystal at -173, -80, -40, 0, 50, and 100 °C and determined unit cell parameters at all these

temperatures and deduced the full structure at -173, -80, and 0 °C. These data confirm that **1-Co-PhNO$_2$** adopts higher-*Z*′ structure (Figure 2.22) at -173 and -80 °C, and lower-*Z*′ structure from -40 °C to 100 °C. Beyond 100 °C desolvation ensued and **1-Co-PhNO$_2$** lost the crystallinity by 150 °C. The transition between higher-*Z*′ to lower-*Z*′ polymorphs of **1-Co-PhNO$_2$** occurred between -80 and -40 °C; we did not determine the exact temperature of phase transition. Figure 2.25 gives the visual evidence of phase transition monitored by the single crystal X-ray diffraction.

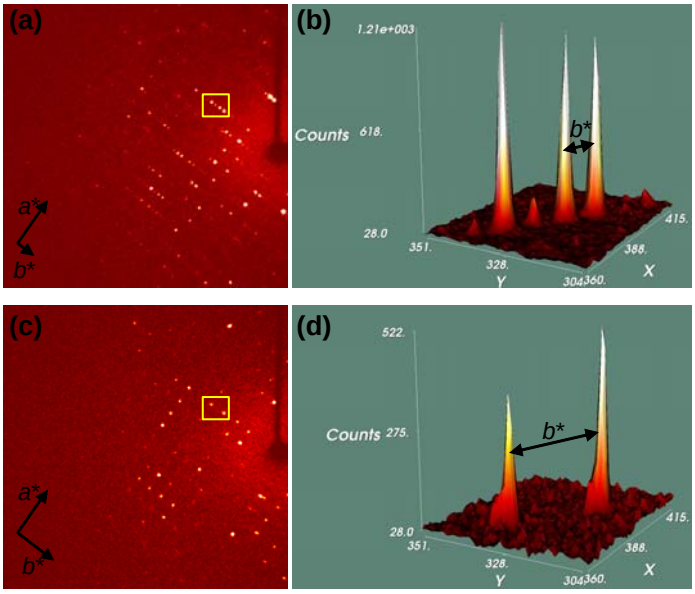

Figure 2.25 Monitoring of phase transition in **1-Co-PhNO$_2$** by single crystal X-ray diffraction. X-ray diffraction images of **(a)** higher-*Z*′ and **(c)** lower-*Z*′ polymorphs. The crystal is kept in the same orientation during the data collection in these two images. Notice the closely spaced diffraction spots along *b** in **(a)** compared to **(c)**. The closer the spots in the reciprocal space the longer are the diffraction planes in crystals. The images in **(b)** and **(d)** are three-dimensional views of diffraction intensities in the boxed regions in **(a)** and **(c)**. Notice the disappearance of two intervening spots in **(d)**; the *b**-axis in **(d)** is three times longer than the *b**-axis in **(b)**. The X-ray data in **(a)** and **(b)** were collected at -173 °C, and **(c)** and **(d)** at -40 °C.

The advent of the four circle diffractometers in the 1970s and the area detectors in the 1990s have resulted in the discovery of an increased number of crystal structures with multiple molecules in the asymmetric unit ($Z' > 1$). It has been suggested that some of these structures with higher Z' may be metastable phases – they represent 'crystals on the way' – that can transform to more stable phases with a smaller Z'. The lower and higher temperature structures of **1-Co-PhNO$_2$** (say at -80 and 0 °C) effectively illustrate this phenomenon of higher-Z' to lower-Z' phase transition. They also suggest that if the multiple molecules in the asymmetric unit of a crystal are related by some pseudo-symmetry (Figure 2.26), there is a possibility that this crystalline phase can be

transformed to a more stable polymorph in which the molecules are related by real crystallographic symmetry.

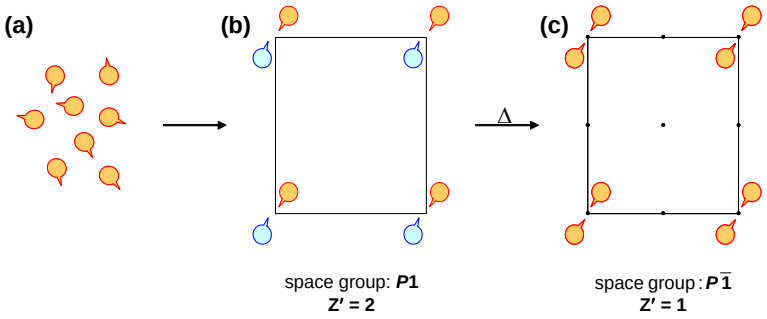

Figure 2.26 Schematic depiction of phase transition from a higher-*Z*′ to a lower-*Z*′ structure. Molecules in solution **(a)** crystallize into a metastable polymorph **(b)** with higher-*Z*′. Two symmetry independent molecules in **(b)** are shaded in different colors. Notice the pseudo-inversion symmetry between the orange and blue molecules in **(b)**. On heating, **(b)** transforms to the stable polymorph **(c)** with lower-*Z*′. In **(c)** centers of symmetry are indicated by black dots.

2.11.3.3 Desolvation and Resolvation of 1-Co-PhNO$_2$. Heating of the crystals of **1-Co-PhNO$_2$** to 200 °C in a TGA chamber (Figure 2.21b) led to the complete loss of the guest molecules. It can be seen from Figures 2.27a-b that the crystals retained their morphology after this heat induced desolvation. Powder X-ray analysis showed that the crystals also retained crystallinity to some extent (Figures 2.27d-e). From morphology it appeared that the desolvation of **1-Co-PhNO$_2$** to **1-Co** is a single crystal to single crystal phase transition. Yet, when subjected to single crystal X-ray diffraction these desolvated crystals resulted in powder rings as opposed to discrete spots. Thus we concluded that the prismatic blocks in Figure 2.25b (obtained after desolvation) are not single crystals; they are polycrystalline solids. When we attempted the resolvation of these desolvated crystals (by soaking the crystals with a very small volume, 0.2 mL, of nitrobenzene) we noticed significant dissolution of the crystals followed by the growth of new solvated crystals (Figure 2.27c). This result is in stark contrast to the resolvation of **1-Zn** crystals with nitrobenzene (Section 2.7). It appears that **1-Co** has far greater solubility in nitrobenzene than **1-Zn**. In the case of **1-Co** the rate of dissolution is faster than the rate of diffusion of nitrobenzene into the solid, leading to a greater amount of re-grown **1-Co-PhNO$_2$** (needles in Figure 2.27c) than resolvated **1-Co-PhNO$_2$** (dark blocks). TGA analysis (Figure 2.28) of these re-grown and resolvated crystals showed near complete inclusion of guest molecules into the crystals. Analysis of these nitrobenzene soaked samples by PXRD (Figure 2.27f) confirmed that these crystals belong to **1-Co-PhNO$_2$**.

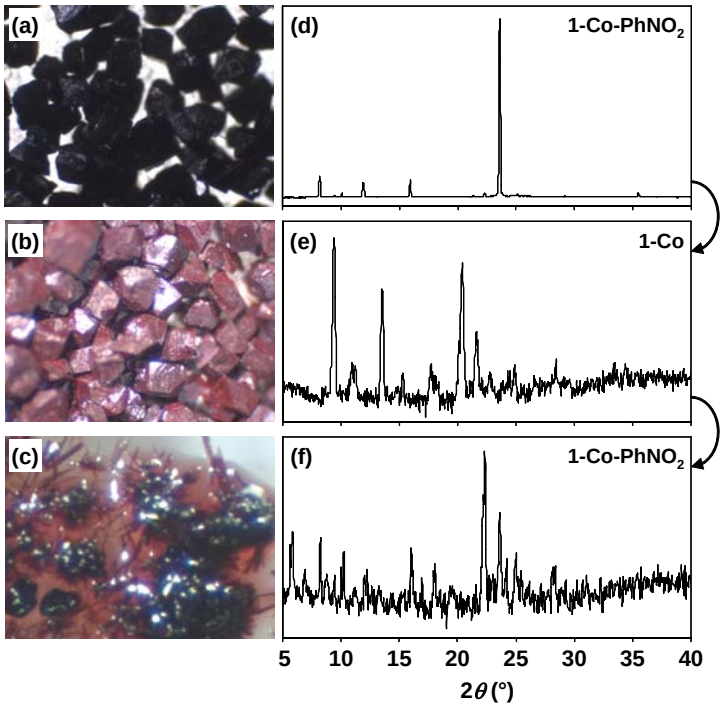

Figure 2.27 Desolvation and resolvation of **1-Co-PhNO$_2$** monitored by **(a-c)** optical microscopy and **(d-f)** PXRD analysis. The solution grown crystals of **1-Co-PhNO$_2$ (a)** show fewer peaks in the powder diffraction pattern **(d)** than expected. The crystals are not pulverized to avoid grinding induced desolvation; they adopt preferred orientation on sample holders and give fewer diffraction peaks. The desolvated crystals **(b)** show distinct color but retain the morphology of **1-Co-PhNO$_2$**. The powder diffraction pattern **(e)** of desolvated crystals confirm the phase transition of **1-Co-PhNO$_2$** to **1-Co**. **(c)** Microscopic image of the desolvated crystals soaked in nitrobenzene for 1.5 hours. Notice the growth of needle like crystals and some remnants of block shaped crystals. **(f)** Powder diffraction pattern of the needle and block shaped crystals shown in **(c)**. Notice the disappearance of peaks corresponding to **1-Co** and emergence of peaks corresponding to **1-Co-PhNO$_2$**. The crystals in **(c)** do not adopt preferred orientation on the sample holder; this is the reason for the difference in relative intensities in diffraction patterns shown in **(b)** and **(f)**. For PXRD patterns in **(d-f)**, the *y*-axis refers to diffraction intensity in arbitrary units.

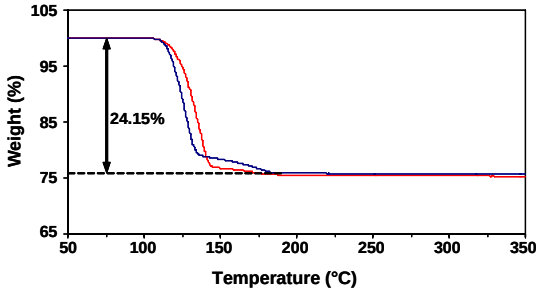

Figure 2.28 TGA plots of the solution grown crystals of **1-Co-PhNO$_2$** (red) and samples of **1-Co-PhNO$_2$** (blue) obtained by soaking desolvated crystals in nitrobenzene for 1.5 hours. Notice the close match of weight loss between red and blue plots (24.64 vs 24.15%). The resolvated material (that is subjected to the TGA experiment, blue plot) contained needles (grown after dissolution) and blocks (crystals that remained intact at the end of soaking) of **1-Co-PhNO$_2$**. This result shows that resolvation of **1-Co** involves two mechanisms: (a) dissolution of **1-Co** followed by the re-growth of **1-Co-PhNO$_2$** and (b) diffusion of nitrobenzene into the solid **1-Co**. The relative masses of needles and blocks have not been determined.

2.11.3.4 Lack of Co···NO$_2$ Recognition in Chloroform Solvate of 1-Co. Unlike **1-Zn**, **1-Co** forms a 1:1 solvate with chloroform, which we refer as **1-Co-CHCl$_3$**. Crystals of this solvate belong to the space group $P\bar{1}$. The porphyrin ring is puckered and the nitro groups do not form close contacts with Co^{2+} ions. Instead, the nitro groups form short C–H···O hydrogen bonds with H-atoms on the porphyrin and chloroform molecules. Porphyrin molecules form π-stacked offset dimers (*J*-aggregates) at an interplanar distance of 3.97 Å. Figure 2.29 shows the packing diagram of **1-Co-CHCl$_3$**.

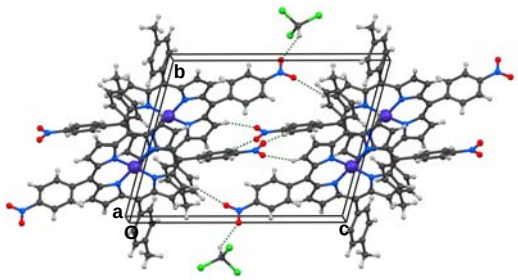

Figure 2.29 Crystal structure **1-Co-CHCl$_3$** viewed down *a*-axis. Notice offset stacked porphyrin dimers and the C–H···O contacts between adjacent dimers. Solvated chloroform molecules are ordered; they form short C–H···O hydrogen bonds with the nitro groups.

2.11.3.5 Oxidation of Co^{2+} to Co^{3+} in Chlorobenzene and Bromobenzene Solvates. When **1-Co** is crystallized from solutions containing chlorobenzene or bromobenzene, it readily formed the corresponding solvates. The crystals diffracted well and X-ray diffraction analysis showed that these two solvates are isostructural. Both of these structures, however, contain Co^{3+} at the porphyrin core instead of Co^{2+}. The axial sites of

the Co^{3+} are occupied by chloride ions and water molecules in both cases (Figure 2.30). It appears that **1-Co** undergoes oxidation in the presence of halogenated benzenes. The source of chloride ion in these structures is puzzling: the salt used in the synthesis of **1-Co** is $Co(OAc)_2$, and at no time in the synthesis the materials are treated with chloride containing compounds. We presume that Co^{2+} is oxidized by chloroform solvent or some other chlorine containing material (e.g., dichloromethane) that is abundant in the laboratory. In the context of current work, oxidation of Co^{2+} renders the axial positions unavailable for binding with nitro groups and hence these structures do not contain $Co\cdots NO_2$ recognition.

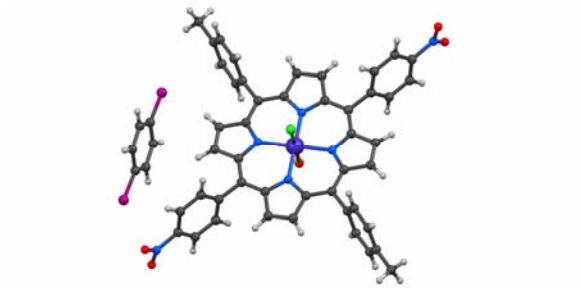

Figure 2.30 Structures of the host and guest molecules in **1-Co-PhBr**. Notice that Co^{3+} ion is bound to chloride ion and water molecule at the axial positions. Each axial site is occupied by 50% chloride ion and 50% water molecule. The bromobenzene molecule is disordered over two positions across an inversion center.

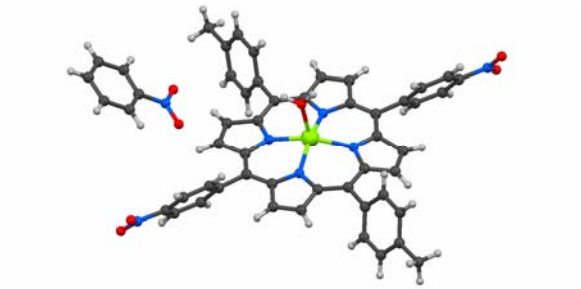

Figure 2.31 Structures of the host and guest molecules in **1-Mg-** ***$PhNO_2$***. Notice that Mg^{2+} ion is bound to water molecule on one of the two axial positions.

2.11.3.6 Axial Ligation by Water in 1-Mg-$PhNO_2$. Another metal cation that we tested for $M\cdots NO_2$ recognition is Mg^{2+}. This cation is small, it has the right charge (to produce neutral metalloporphyrin), and it can adopt octahedral coordination geometry to enable binding of nitro groups at axial positions. The contrasting character of Mg^{2+} is that it is a hard acid; Zn^{2+} and Co^{2+}, on the other hand, are borderline acids. The nitro ligand is a borderline base; we expected that it can interact favorably with Zn^{2+} or Co^{2+}. It is in this context we studied the solvates of **1-Mg** to test the applicability of hard-soft acid-base concept to the rationalization of $M\cdots NO_2$ recognition. To date, we have been able to

obtain the crystals of only nitrobenzene solvate, **1-Mg-PhNO$_2$**. In this solvate, the Mg^{2+} ion embedded in the porphyrin core is ligated at one of the axial positions by a water molecule (Figure 2.31). Water is a hard base, and Mg^{2+} is a hard acid, and the two species form a very strong coordination bond in **1-Mg-PhNO$_2$** as evidenced by short Mg···O separation (2.03 Å). For comparison the Zn···O distance is 2.52 Å in **1-Zn-PhNO$_2$** and the Co···O distance is 2.59 Å in **1-Co-PhNO$_2$**.

2.11.4 Substitution of *p*-Tolyl Groups by Other Non-Competing Groups. We have looked at the effects of position and types of ligands and the types of metal ions on the realization of M···NO_2 recognition. In the next chapter we describe the most useful method of creating layered solids in a reliable manner using Zn···NO_2 recognition. In this method, the *p*-tolyl groups on **1-Zn** are replaced by other groups that do not interfere with the binding of Zn^{2+} ions and nitro groups. We expect that that materials obtained by changing the steric and electronic properties of these side groups can have different sorption, dissolution and growth properties. Chapter 3 describes the structural and physical properties of layered coordination polymers based on chlorophenyl and bromophenyl substituted porphryins.

2.12 IMPORTANCE OF ZN···NO$_2$ RECOGNITION – 1-PHNO2 VERSUS 1-ZN-PHNO2

To evaluate the importance of Zn···NO_2 recognition in the formation of porous coordination polymers and their solvation and desolvation properties, we have studied the structural and guest inclusion properties of free-base analog of **1-Zn**. This dinitrophenyl and ditolyl substituted porphyrin (**1**, Figure 2.3) crystallizes as a nitrobenzene solvate, **1-PhNO$_2$**, from a solution of chloroform and nitrobenzene. The crystal structure of **1-PhNO$_2$** (space group $P\bar{1}$) shows certain similarities to that of **1-Zn-PhNO$_2$** (space group $P2_1/n$). Both crystals contain the host and guest species in 1:2 stoichiometry. Both structures contain host layers and the guest molecules are intercalated between the layers (Figures 2.6a and 2.32a). The free-base, however, lacks Zn^{2+} ion; the nitro groups of the host form C–H···O hydrogen bonds with neighboring molecules and result in continuous offset stacks along the *a*-axis (Figure 2.32b). Interdigitation of *p*-tolyl groups along the *c*-axis leaves rectangular channels in the structure; the guest molecules are located within these channels.

Crystal structure of **1-PhNO$_2$** is similar to one of the several structures of porphyrin sponges.[33] As with porphyrin sponges, the crystal structure of **1** can easily change depending on the guest species. It is difficult to predict the structure of **1** because there are no reliable patterns of interactions that provide directionality to the molecular assembly. In contrast, **1-Zn** adopts the 4^4 network structure as long as the Zn···NO_2 recognition is not interrupted. It is the reliability in the crystal design that separates **1-Zn** from **1**.

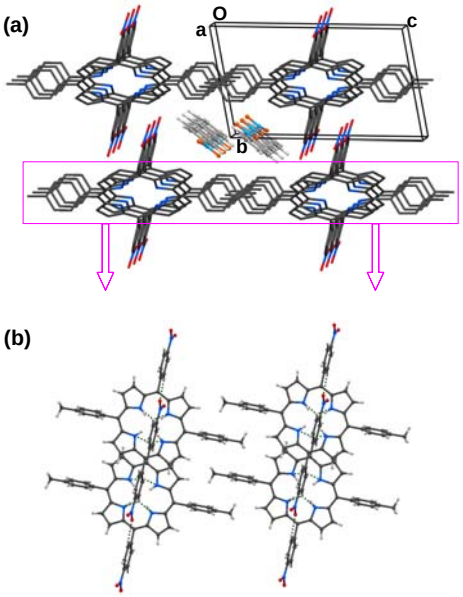

Figure 2.32 Crystal structure of **1-PhNO$_2$**. **(a)** Interlayer stacking showing the intercalation of nitrobenzene between the layers. Nitrobenzene molecules are plotted in lighter colors. H-atoms on the porphyrin are omitted. Notice that the nitrophenyl groups of the host are projected into the interlayer space. Contrast this structure with the interlayer stacking in **1-Zn-PhNO$_2$** (Figure 2.6a), where the tolyl groups wall the interlayer region. **(b)** Porphyrin packing within the layer. C–H···O and C–H···N interactions between neighboring molecules are drawn with dashed lines. Notice the interdigitated packing of tolyl groups. Two H-atoms in the porphyrin core are disordered over four pyrrolic N-atoms.

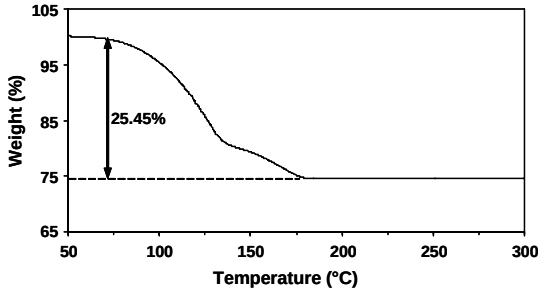

Figure 2.33 TGA plot of **1-PhNO$_2$**. Notice the onset of desolvation at 60 C. The close match between the experimental (25.45%) and theoretical weight loss (25.15%) suggest the high purity of the solvated crystals.

Although **1-PhNO$_2$** and **1-Zn-PhNO$_2$** possess 1:2 stoichiometry and layered structures, they have different host-guest properties. In **1-PhNO$_2$** desolvation of nitrobenzene begins at 60 °C (Figure 2.33), whereas the onset of desolvation occurs at 100 °C in metallated **1-Zn-PhNO$_2$** (Figure 2.7b). In addition, resolvation can be performed in **1-Zn** for multiple cycles; on the contrary, **1** undergoes complete dissolution when brought in contact with

nitrobenzene. The desolvated samples of **1-PhNO$_2$** show good crystallinity; the powder diffraction pattern of **1** obtained by desolvation is distinctly different from that of **1-PhNO$_2$** (Figure 2.34) indicating that the phase transition from solvate to non-solvate is completed.

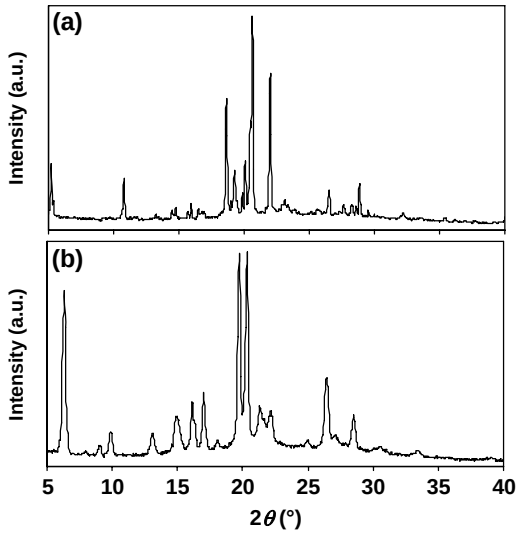

Figure 2.34 PXRD patterns of **(a) 1-PhNO$_2$** and **(b) 1** obtained by heat induced desolvation of **1-PhNO$_2$**.

2.13 EXPERIMENTAL

2.13.1 Synthesis. All the solvents were purchased from Pharmco and rest of the chemicals were purchased from Alfa Aesar and used as received in the synthesis (Figure 2.3) and crystallization. Dueterated solvents were purchased from Norell. The NMR spectra were recorded on a Bruker 400 MHz or a Bruker 500 MHz spectrometer. The IR spectra were recorded in the ATR (attenuated total reflection) mode on a Perkin Elmer Spectrum One spectrometer.

2.13.1.1 Synthesis of 5-(4-nitrophenyl)dipyrromethane. Pyrrole (1.14 mol, 100 mL) and 4-nitrobenzaldehyde (57.6 mmol, 8.92 g) were added to a dry round-bottomed flask and degassed with nitrogen for 10 min (Figure 2.3). After adding trifluoroacetic acid (TFA, 5.76 mmol, 0.43 mL) the solution was stirred at room temperature for 10 min. A solution (35 mL) of 0.1 M NaOH was added to quench the remaining acid. Ethyl acetate (~150mL) was added to this mixture and the organic phase was washed with water (3×100 mL) and dried over Na_2SO_4. Ethyl acetate was removed by rotary evaporation; pyrrole was removed under high vacuum to afford an oily product. This orange colored oil was crystallized from ethyl acetate-hexanes, and then recrystallized from ethanol giving 4.71 g (31%) of yellow crystals.

Synthesis at a Larger Scale. Pyrrole (71 mol, 481 mL) and 4-nitrobenzaldehyde (284 mmol, 42.9 gr) were added to a dry round-bottomed flask and degassed with nitrogen for 20 min. After adding trifluoroacetic acid (TFA, 2.84 mmol, 1.26 mL) the solution was stirred at room temperature for 10 min. A solution (200 mL) of 0.1 M NaOH was added to quench the remaining acid. Ethyl acetate (~350 mL) was added to this mixture and the organic phase was washed with water (3×200 mL) and dried over Na_2SO_4. Ethyl acetate was removed by rotary evaporation; pyrrole was removed under high vacuum to afford an oily product. This orange-black viscous crude product was solidified upon standing. Solid was crushed, treated with small amount of ethyl acetate and sonicated. Filtration gave 27 grams of yellow solid. The remaining black filtrate was evaporated, treated with small amount of ethyl acetate, sonicated and filtered again (19 g). Total yield was 46 g (70%). ^{1}H-NMR ($CDCl_3$): δ = 5.51 (s, 1 H); 5.79 (s, 2 H); 6.10 (q, 2 H); 6.67 (m, 2 H); 7.30 (d, 2 H); 8.00 (br s, 2 H); 8.10 (d, 2 H) ppm. ^{13}C-NMR ($CDCl_3$): δ = 42.8; 106.7; 107.7; 116.9; 122.7; 128.2; 129.8; 145.8; 148.7 ppm.

2.13.1.2 Synthesis of 5,15-di(4-nitrophenyl)-10,20-di(p-tolyl)porphyrin (1). A solution of 5-(4-nitrophenyl)dipyrromethane (4 mmol, 1.07 g) and 4-methylbenzaldehyde (4 mmol, 0.48 g) in CH_2Cl_2 (400 mL) was prepared in a 500 mL three-necked round-bottomed flask. After degassing the flask for 15 min with nitrogen, TFA (7.12 mmol, 0.55 mL) was added. The reaction mixture was stirred for 35 min at room temperature, 2,3-dichloro-5,6-dicyano-1,4-benzoquinone (DDQ) (4 mmol, 0.91 g) was added, and stirred for an additional hour. The solution with products and other contaminants was poured onto an alumina pad placed in a 1L separatory funnel, and eluted with CH_2Cl_2 (~ 1L). A dark solid with purple tinge was obtained after the removal of the solvent under vacuum; this solid was refluxed in toluene (150 mL) for 1 h after adding the oxidant DDQ (4 mmol, 0.91 g). A second elution of the concentrate through a pad of alumina (500 mL separatory funnel) with CH_2Cl_2 (~600 mL) followed by concentration under vacuum gave the product as a purple solid (0.33 g; 22.5%). ^{1}H-NMR ($CDCl_3$): δ = -2.80 (br. s, 2 H, NH); 2.72 (s, 6 H, CH_3); 7.58 (d, 4 H); 8.09 (d, 4 H); 8.41 (d, 4 H); 8.66 (d, 4 H); 8.76 (d, 4 H, β_1-pyrrole); 8.94 (d, 4 H, β_2-pyrrole) ppm.

2.13.1.3 Synthesis of Zn-5,15-di(4-nitrophenyl)-10,20-di(p-tolyl)porphyrin (1-Zn). A solution of free-base porphyrin **1** (0.4 mmol, 0.29 g) in $CHCl_3$ (90 mL) was combined with a solution of zinc acetate dihydrate (6 mmol, 1.5 g) in methanol (90 mL) and refluxed for 4 hours. After the reaction was completed, the contents were cooled to room temperature and excess methanol was added to the reaction mixture to precipitate the metalloporphyrin. The precipitate was filtered, washed with methanol, and air dried to yield 0.19 g (60%) of shiny purple solid. ^{1}H-NMR ($CDCl_3$): δ = 2.65 (s, 6 H, CH_3); 7.51 (d, 4 H); 8.02 (d, 4 H); 8.34 (d, 4 H); 8.57 (d, 4 H); 8.78 (d, 4 H, β_1-pyrrole); 8.96 (d, 4 H, β_2-pyrrole) ppm.

2.13.1.4 Synthesis of Co-5,15-di(4-nitrophenyl)-10,20-di(p-tolyl)porphyrin (1-Co). Free base porphyrin **1** (0.65 mmol, 0.48 gr) and cobalt acetate dihydrate (3.25 mmol, 0.58 g) was put in a 500 mL round-buttom flask with 150 mL DFM. The mixture was refluxed for 3 hours under nitrogen, and then solvent evaporated off. Crude solid was purified using column chromatography (0.32 g, 62.4 %).

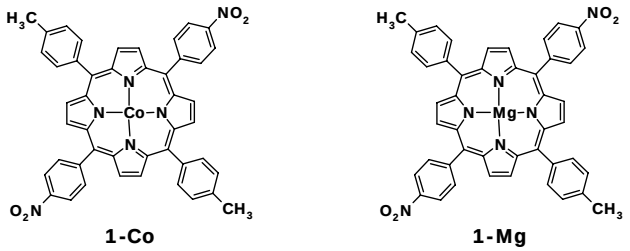

Figure 2.36 Synthesis of **1′-Zn** using pyrrole, *m*-nitrobenzaldehyde and *p*-tolualdehyde.

2.13.1.5 Synthesis of Mg-5,15-di(4-nitrophenyl)-10,20-di(p-tolyl)porphyrin (1-Mg). Free base porphyrin **1** (0.7 mmol, 0.514 g) and magnesium chloride (28 mmol, 5.69 g) was put in a 500 mL round-buttom flask with 150 mL DFM. The mixture was refluxed for 2.5 hours, and then solvent evaporated off. Crude solid was purified using column chromatography (0.34 g; 64.33 %). ^{1}H-NMR ($CDCl_3$): δ = 2.72 (s, 6 H, CH_3); 7.55 (d, 4 H); 8.10 (d, 4 H); 8.40 (d, 4 H); 8.62 (d, 4 H); 8.75 (d, 4 H, β_1-pyrrole); 8.93 (d, 4 H, β_2-pyrrole).

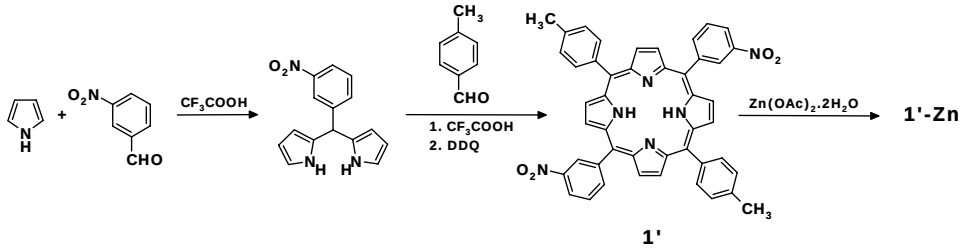

Figure 2.36 Synthesis of **1′-Zn** using pyrrole, *m*-nitrobenzaldehyde and *p*-tolualdehyde.

2.13.1.6 Synthesis of 5-(3-nitrophenyl)dipyrromethane. Pyrrole (250 mL) and 3-nitrobenzaldehyde (144 mmol, 21.76 g) were added to a dry round-bottomed flask and degassed with nitrogen for 20 min. After adding trifluoroacetic acid (0.65 mL) the solution was stirred at room temperature for 7 min. A solution (150 mL) of 0.1 M NaOH was added to quench the remaining acid. Ethyl acetate (~150mL) was added to this mixture and the organic phase was washed with water (3×150 mL) and dried over Na_2SO_4. Ethyl acetate was removed by rotary evaporation; pyrrole was removed under high vacuum to afford an oily product. This brown-colored oil was solidified upon standing. Formed solid was powderized treated with small amount of ethyl acetate and sonicated. Black-brown impurity dissolved, yellow solid was filtered out (21.87 g; 56.8 %). ^{1}H-NMR ($CDCl_3$): δ = 5.58 (s, 1 H); 5.87 (s, 2 H); 6.18 (m, 2 H); 6.75 (s, 2 H); 7.52 (m, 4 H); 8.00 (br s, 2 H); 8.12 (d, 2 H). ^{13}C-NMR ($CDCl_3$): 43.7; 107.8; 108.8; 118.0; 122.1; 123.3; 129.5; 130.9; 134.5.

2.13.1.7 Synthesis of 5,15-di(3-nitrophenyl)-10,20-di(p-tolyl)porphyrin (1′). Condensation of 5-(3-nitrophenyl)dipyrromethane (10 mmol, 2.675 g) and 4-methylbenzaldehyde (10 mmol; 1.18 mL) in CH_2Cl_2 (1L) with TFA (1.4 mL) gave a purple solid (0.78 g; 10.64 %). ^{1}H-NMR ($CDCl_3$): δ = -2.81 (s, 2 H, NH); 2.72 (s, 6 H, CH_3); 7.58 (d, 4 H); 7.96 (t, 2 H); 8.15 (d, 4 H); 8.55 (d, 2 H); 8.69 (d, 2 H); 8.72 (d, 4 H, β_1-pyrrole); 8.94 (d, 4 H, β_2-pyrrole); 9.09 (s, 2 H).

2.13.1.8 Synthesis of Zn-5,15-di(3-nitrophenyl)-10,20-di(p-tolyl)porphyrin (1′-Zn). A solution of free-base porphyrin **1′** (0.4 mmol, 0.29 g) in $CHCl_3$ (90 mL) was combined with a solution of zinc acetate dihydrate (6 mmol, 1.5 g) in methanol (90 mL) and refluxed for 4 hours. After the reaction was completed, the contents were cooled to room temperature and excess methanol was added to the reaction mixture to precipitate the metalloporphyrin. The precipitate was filtered, washed with methanol, and air dried to yield 0.19 g (60%) of shiny purple solid. ^{1}H-NMR ($CDCl_3$): δ = 2.65 (s, 6 H, CH_3); 7.51 (d, 4 H); 8.02 (d, 4 H); 8.34 (d, 4 H); 8.57 (d, 4 H); 8.78 (d, 4 H, β_1-pyrrole); 8.96 (d, 4 H, β_2-pyrrole) ppm.

2.13.1.9 Zn-5,15-Bis(4-cyanophenyl)-10,20-di(4-nitrophenyl) porphyrin. Condensation of 5-(4-nitrophenyl)dipyrromethane (8 mmol, 2.14 gr) and 4-cyanobenzaldehyde (8 mmol; 1.05 gr) in CH_2Cl_2 (800 mL) with TFA (1.3 mL) gave a purple solid (0.42 g; 12 %) which was metallated using zinc acetate. ^{1}H-NMR ($CDCl_3$): δ = 7.98 (d, 4 H); 8.21 (d, 4 H); 8.27 (d, 4 H); 8.54 (d, 4 H); 8.78 (s, 8 H, β-pyrrole).

2.13.2 Thermal Analysis. Differential scanning calorimetry (DSC) measurements were carried out using DSC-2920 (TA Instruments) and thermal gravimetric analyses (TGA) were performed on TGA-2950 (TA Instruments). For DSC experiments, the samples were dispensed into aluminum pans that were crimped hermetically to ensure tight seal. For TGA experiments, the samples were loaded into open aluminum pans. In both cases the samples were heated from 30-350 °C at a heating rate of 10 °C/min under a purge of nitrogen gas. The DSC and TGA data were analyzed and processed using TA Universal Analysis software. For consistency between different experimental methods, the data were transferred to Microsoft Excel and the plots were generated using this program.

2.13.3 Powder X-Ray Diffraction Analysis. The PXRD were collected either on a Rigaku Geigerflex D-MAX/A diffractometer or Bruker D8 Advance diffractometer using Cu-Kα radiation. The instruments were equipped with vertical goniometers and scintillation counters as detectors. They both applied Bragg-Brentano geometry for data collection. X-rays were generated at a power setting of 35 kV and 35 mA on the Rigaku and, 40 kV and 40 mA on the Bruker diffractometers. Crystals of the solvated forms were used in diffraction analysis without pulverization; grinding of these crystals led to the partial loss of solvent. Samples were transferred to a glass sample holder that had loading dimensions 1.6 cm × 2 cm and exposed to X-rays over the 2θ range 5-50° in 0.05° steps and at a scan rate of 2° per minute. Small differences in the values of 2θ (between calculated and experimental patterns or between different patterns of the same substance) may arise due to the use of Bragg-Brentano geometry, the variations in sample holder position, the thickness of the sample and the difference in the temperature of data

collection. The data on the Rigaku diffractometer were analyzed using Jade software and on the Bruker diffractometer using the Eva software. In both cases, the data were transferred to Microsoft Excel and the plots were generated using this program.

2.13.4 Single Crystal X-Ray Diffraction Analysis. Crystals suitable for diffraction were selected under a microscope and mounted on a glass fiber, loop, or a kapton mesh using a small amount of paratone or mineral oil. X-ray data were collected using a Bruker SMART diffractometer or Bruker APEX II diffractometer equipped with CCD detectors and Oxford Cryostream or Oxford Cryostream Plus low-temperature device. On the SMART diffractometer, the data were measured using ω scans of 0.3° per frame; each frame was exposed to X-rays for 30 seconds. A total of 1271 frames, covering a hemisphere, were collected with a maximum resolution of 0.76 Å. The first 50 frames were recollected at the end of data collection to monitor for decay. Cell parameters were retrieved using SMART software and refined using the program SAINT on all observed reflections.

On the APEX II diffractometer, the data were measured using ϕ and ω scans of 0.5° per frame; each frame was exposed to X-rays for 10-60 seconds depending on the scattering power of the crystal. Unit cell parameters were determined using three mutually perpendicular ϕ scans with 12 frames per scan. Using the orientation matrix obtained from the unit cell, a hemisphere was searched with the program COSMO to determine the number of runs and frames needed for 0.75 Å resolution, 100 % completeness, and at least two fold redundancy when the crystal system is set to triclinic. Cell parameters were refined over all the equivalent reflections in the hemisphere during the data integration.

On both the diffractometers, data integration was performed using the program SAINT and absorption corrections were applied using SADABS multiscan technique. The structures were solved by the direct methods and refined by the least squares methods on F^2 using the program SHELXL-97[52] incorporated in SHELXTL-PC or APEX II. Typically, all the non-H-atoms were refined anisotropically and all H-atoms were calculated by geometrical methods and refined using a riding model. Structural analysis was performed by a combination of programs that include XP, XSHELL, Platon,[43] and Mercury.[53] Structural diagrams shown in this thesis were prepared using the program Mercury.

2.14 SUMMARY AND CONCLUSION

While contacts between Zn (and other metal) ions and O-atoms of nitro groups are seen in crystals before, we have used the Zn···NO_2 recognition as a synthon in the creation of coordination polymers with predetermined topology. We also showed that these polymers can incorporate nitrobenzene molecules (with some degree of selectivity) owing to the aromatic groups that partition the interlayer space. There are only few examples of porphyrin coordination polymers in which the network structure is intact after the removal of the guest. The coordination polymers reported in this work are built on weak coordination bonds in Zn···NO_2 and Co···NO_2 recognition; yet the networks retain their structure even after deintercalation of and reintercalation with nitrobenzene molecules.

These compounds also retain their overall crystallinity and macroscopic morphology through these reversible, solid-to-solid transformations. In addition, compound **1-Zn** is thermally stable and soluble in organic solvents; we expect that exploration of noncoordinating aryl groups on the metalloporphyrin core may lead to the design of processable porous materials that can be used as potential sensors for nitrated and other aromatic compounds. We showed that substitution of the nitro groups at the *meta* positions on the *meso*-phenyl rings is not a productive strategy to attain 4^4 networks. In addition it is possible to extend the Zn···NO_2 recognition to other metal ions such as Co^{2+}. We have described a lower *Z′* polymorph is discovered based on the concept of *crystal on the way*; this discovery has important implications in the cryogenic data collection and the relationship between the structures obtained at low temperature and the real structure at room temperature. Further exploration of Zn···NO_2 recognition can be achieve through the manipulation of substituents on the *meso*-phenyl rings; Chapter 3 presents a series of structures based on chlorophenyl and bromophenyl analogues of **1-Zn**.

2.15 REFERENCES

1. Batten, S. R.; Robson, R., Interpenetrating nets: ordered, periodic entanglement. *Angew. Chem. Int. Ed.* **1998,** *37*, 1461-1494.
2. Sanders, J. K. M.; Bampos, N.; Clyde-Watson, Z.; Darling, S. L.; Hawley, J. C.; Kim, H.-J.; Mak, C. C.; Webb, S. J., Axial coordination chemistry of metalloporphyrins. *Porphyrin Handbook* **2000,** *3*, 1-48.
3. Moulton, B.; Zaworotko, M. J., From molecules to crystal engineering. Supramolecular isomerism and polymorphism in network solids. *Chem. Rev.* **2001,** *101*, 1629-1658.
4. Evans, O. R.; Lin, W., Crystal Engineering of NLO Materials Based on Metal-Organic Coordination Networks. *Acc. Chem. Res.* **2002,** *35*, 511-522.
5. Seidel, S. R.; Stang, P. J., High-Symmetry Coordination Cages via Self-Assembly. *Acc. Chem. Res.* **2002,** *35*, 972-983.
6. Yaghi, O. M.; O'Keeffe, M.; Ockwig, N. W.; Chae, H. K.; Eddaoudi, M.; Kim, J., Reticular synthesis and the design of new materials. *Nature* **2003,** *423*, 705-714.
7. Kitagawa, S.; Kitaura, R.; Noro, S.-I., Functional porous coordination polymers. *Angew. Chem. Int. Ed.* **2004,** *43*, 2334-2375.
8. Rao, C. N. R.; Natarajan, S.; Vaidhyanathan, R., Metal carboxylates with open architectures. *Angew. Chem. Int. Ed.* **2004,** *43*, 1466-1496.
9. Rosseinsky, M. J., Recent developments in metal-organic framework chemistry: design, discovery, permanent porosity and flexibility. *Microporous and Mesoporous Materials* **2004,** *73*, 15-30.
10. Fujita, M.; Tominaga, M.; Hori, A.; Therrien, B., Coordination Assemblies from a Pd(II)-Cornered Square Complex. *Acc. Chem. Res.* **2005,** *38*, 369-378.
11. Goldberg, I., Crystal engineering of porphyrin framework solids. *Chem. Comm.* **2005**, 1243-1254.
12. Hosseini, M. W., Molecular Tectonics: From Simple Tectons to Complex Molecular Networks. *Acc. Chem. Res.* **2005,** *38*, 313-323.

13. Suslick, K. S.; Bhyrappa, P.; Chou, J. H.; Kosal, M. E.; Nakagaki, S.; Smithenry, D. W.; Wilson, S. R., Microporous Porphyrin Solids. *Acc. Chem. Res.* **2005,** *38*, 283-291.
14. Dastidar, P.; Stein, Z.; Goldberg, I.; Strouse, C. E., Supramolecular assembly of functionalized metalloporphyrins. Porous crystalline networks of zinc tetra(4-carboxyphenyl)porphyrin. *Supramolecular Chemistry* **1996,** *7*, 257-270.
15. Diskin-Posner, Y.; Patra, G. K.; Goldberg, I., Crystal engineering of 2-D and 3-D multiporphyrin architectures - The versatile topologies of tetracarboxyphenyl-porphyrin based materials. *European Journal of Inorganic Chemistry* **2001**, 2515-2523.
16. Kosal, M. E.; Chou, J.-H.; Wilson, S. R.; Suslick, K. S., A functional zeolite analogue assembled from metalloporphyrins. *Nature Materials* **2002,** *1*, 118-121.
17. Smithenry, D. W.; Wilson, S. R.; Suslick, K. S., A Robust Microporous Zinc Porphyrin Framework Solid. *Inorganic Chemistry* **2003,** *42*, 7719-7721.
18. Shmilovits, M.; Vinodu, M.; Goldberg, I., Coordination Polymers of Tetra(4-carboxyphenyl)porphyrins Sustained by Tetrahedral Zinc Ion Linkers. *Cryst. Growth & Design* **2004,** *4*, 633-638.
19. Vinodu, M.; Goldberg, I., Synthesis and versatile supramolecular self-assembly of the 5,15-bis(4-hydroxyphenyl)-10,20-bis(4-carboxyphenyl)porphyrin scaffold. *CrystEngComm* **2004,** *6*, 215-220.
20. Abrahams, B. F.; Hoskins, B. F.; Robson, R., A new type of infinite 3D polymeric network containing 4-connected, peripherally-linked metalloporphyrin building blocks. *J. Am. Chem. Soc.* **1991,** *113*, 3606-3607.
21. Fleischer, E. B.; Shachter, A. M., Coordination oligomers and a coordination polymer of zinc tetraarylporphyrins. *Inorganic Chemistry* **1991,** *30*, 3763-3769.
22. Drain, C. M.; Lehn, J.-M., Self-assembly of square multiporphyrin arrays by metal ion coordination. *J. Chem. Soc., Chem. Commun.* **1994**, 2313-2315.
23. Krupitsky, H.; Stein, Z.; Goldberg, I.; Strouse, C. E., Crystalline complexes, coordination polymers and aggregation modes of tetra(4-pyridyl)porphyrin. *Journal of Inclusion Phenomena and Molecular Recognition in Chemistry* **1994,** *18*, 177-192.
24. Kumar, R. K.; Goldberg, I., Supramolecular assembly of heterogeneous multiporphyrin arrays - structures of [{ZnII(tpp)}2(tpyp)] and the coordination polymer [{[MnIII(tpp)]2(tpyp)(ClO4)2}...]. *Angew. Chem. Int. Ed.* **1998,** *37*, 3027-3030.
25. Hagrman, D.; Hagrman, P. J.; Zubieta, J., Solid-state coordination chemistry: the self-assembly of microporous organic-inorganic hybrid frameworks constructed from tetrapyridylporphyrin and bimetallic oxide chains or oxide clusters. *Angew. Chem. Int. Ed.* **1999,** *38*, 3165-3168.
26. Lin, K.-J., SMTP-1: the first functionalized metalloporphyrin molecular sieves with large channels. *Angew. Chem. Int. Ed.* **1999,** *38*, 2730-2732.
27. Sharma, C. V. K.; Broker, G. A.; Huddleston, J. G.; Baldwin, J. W.; Metzger, R. M.; Rogers, R. D., Design Strategies for Solid-State Supramolecular Arrays Containing Both Mixed-Metalated and Freebase Porphyrins. *J. Am. Chem. Soc.* **1999,** *121*, 1137-1144.

28. Michelsen, U.; Hunter, C. A., Self-assembled porphyrin polymers. *Angew. Chem. Int. Ed.* **2000,** *39*, 764-767.
29. Pan, L.; Kelly, S.; Huang, X.; Li, J., Unique 2D metalloporphyrin networks constructed from iron(II) and meso-tetra(4-pyridyl)porphyrin. *Chem. Comm.* **2002**, 2334-2335.
30. Carlucci, L.; Ciani, G.; Proserpio, D. M.; Porta, F., Open network architectures from the self-assembly of AgNO3 and 5,10,15,20-tetra(4-pyridyl)porphyrin (H2tpyp) building blocks: The exceptional self-penetrating topology of the 3D network of [Ag8(ZnIItpyp)7(H2O)2](NO3)8. *Angew. Chem. Int. Ed.* **2003,** *42*, 317-322.
31. Deiters, E.; Bulach, V.; Kyritsakas, N.; Hosseini, M. W., Molecular tectonics: coordination networks based on porphyrins bearing pyridine N-oxide groups as coordinating sites. *New J. Chem.* **2005,** *29*, 1508-1513.
32. Deiters, E.; Bulach, V.; Hosseini, M. W., Reversible single-crystal-to-single-crystal guest exchange in a 3-D coordination network based on a zinc porphyrin. *Chem. Comm.* **2005**, 3906-3908.
33. Byrn, M. P.; Curtis, C. J.; Goldberg, I.; Hsiou, Y.; Khan, S. I.; Sawin, P. A.; Tendick, S. K.; Strouse, C. E., Porphyrin sponges: structural systematics of the host lattice. *J. Am. Chem. Soc.* **1991,** *113*, 6549-6557.
34. Desiraju, G. R., Supramolecular synthons in crystal engineering - a new organic synthesis. *Angew. Chem. Int. Ed.* **1995,** *34*, 2311-2327.
35. Ermer, O., Five-fold diamond structure of adamantane-1,3,5,7-tetracarboxylic acid. *J. Am. Chem. Soc.* **1988,** *110*, 3747-54.
36. Su, D.; Wang, X.; Simard, M.; Wuest, J. D., Molecular tectonics. *Supramolecular Chemistry* **1995,** *6*, 171-178.
37. Aoyama, Y., Functional organic zeolite analogs. *Topics in Current Chemistry* **1998,** *198*, 131-161.
38. Robson, R., Infinite frameworks [for crystal engineering]. *Comprehensive Supramolecular Chemistry* **1996,** *6*, 733-755.
39. Littler, B. J.; Miller, M. A.; Hung, C.-H.; Wagner, R. W.; O'Shea, D. F.; Boyle, P. D.; Lindsey, J. S., Refined Synthesis of 5-Substituted Dipyrromethanes. *J. Org. Chem.* **1999,** *64*, 1391-1396.
40. Littler, B. J.; Ciringh, Y.; Lindsey, J. S., Investigation of Conditions Giving Minimal Scrambling in the Synthesis of trans-Porphyrins from Dipyrromethanes and Aldehydes. *J. Org. Chem.* **1999,** *64*, 2864-2872.
41. It is difficult to ascertain if the shortening of N-O_b bond length is a real effect or an artifact of increased thermal vibration or a combination of both. Similar arguments are previously used to analyze the hydrogen bonding nature of C–H···O interactions formed by terminal alkynes. See
42. Steiner, T., Reduction of thermal vibrations by C-H...X hydrogen bonding: crystallographic evidence for terminal alkynes. *J. Chem. Soc., Chem. Commun.* **1994**, 101-102.
43. Spek, A. L., Single-crystal structure validation with the program PLATON. *J. Appl. Cryst.* **2003,** *36*, 7-13.
44. Fauvet, G.; Massaux, M.; Chevalier, R., Study of the crystal structure of benzonitrile at 198 K. *Acta Cryst.* **1978,** *B34*, 1376-8.

45. Thalladi, V. R.; Dabros, M.; Gehrke, A.; Weiss, H.-C.; Boese, R., Crystal Engineering with sbC-H...N and :C-H...N Hydrogen Bonds. *Cryst. Growth & Design* **2007,** *7*, 598-599.
46. Thalladi, V. R.; Weiss, H.-C.; Blaeser, D.; Boese, R.; Nangia, A.; Desiraju, G. R., C-H...F Interactions in the Crystal Structures of Some Fluorobenzenes. *J. Am. Chem. Soc.* **1998,** *120*, 8702-8710.
47. Langley, P. J.; Hulliger, J.; Thaimattam, R.; Desiraju, G. R., Supramolecular synthons mediated by weak hydrogen bonding: forming linear molecular arrays via C≡C–H···N≡C and C≡C–H···O_2N recognition. *New J. Chem.* **1998,** *22*, 1307-1309.
48. Allen, F. H.; Taylor, R., Research applications of the Cambridge Structural Database (CSD). *Chem. Soc. Rev.* **2004,** *33*, 463-475.
49. Steed, J. W., Should solid-state molecular packing have to obey the rules of crystallographic symmetry? *CrystEngComm* **2003,** *5*, 169-179.
50. Anderson, K. M.; Steed, J. W., Comment on "on the presence of multiple molecules in the crystal asymmetric unit (Z' > 1)" by Gautam R. Desiraju, CrystEngComm, 2007, 9, 91. *CrystEngComm* **2007,** *9*, 328-330.
51. Desiraju, G. R., On the presence of multiple molecules in the crystal asymmetric unit (Z' > 1). *CrystEngComm* **2007,** *9*, 91-92.
52. Sheldrick, G. M., A short history of SHELX. *Acta Cryst.* **2008,** *A64*, 112-122.
53. Macrae, C. F.; Bruno, I. J.; Chisholm, J. A.; Edgington, P. R.; McCabe, P.; Pidcock, E.; Rodriguez-Monge, L.; Taylor, R.; van de Streek, J.; Wood, P. A., Mercury CSD 2.0 - new features for the visualization and investigation of crystal structures. *J. Appl. Cryst.* **2008,** *41*, 466-470.

3 UNIVERSAL HOSTS – LAYERED PORPHYRIN SOLIDS BASED ON ZN···NO_2 RECOGNITION

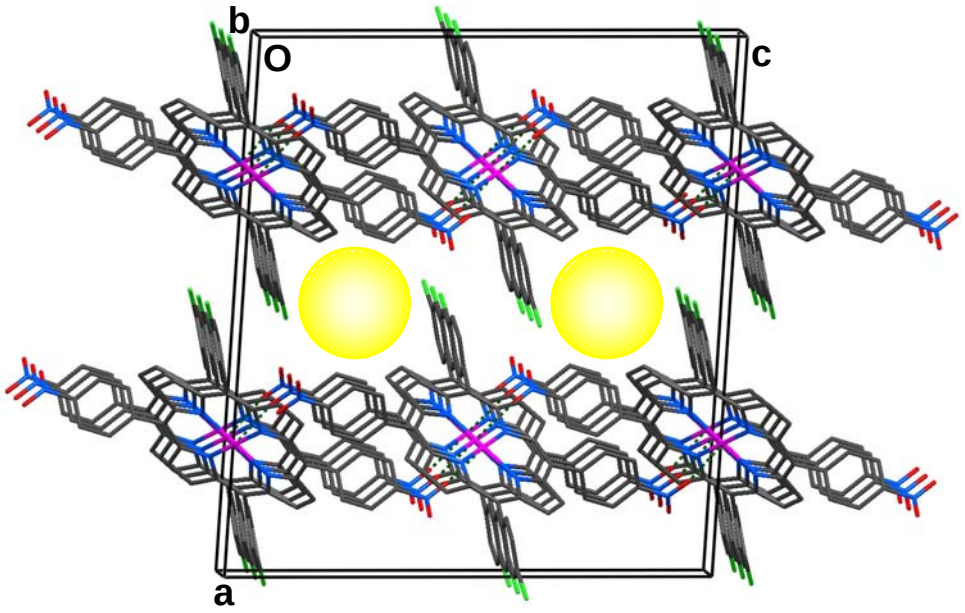

3.1 INTRODUCTION

Layered framework materials are good starting points to explore the utility of new coordination synthons in the design of porous solids,[1-3] especially synthons that are based on weak interactions.[4] In the previous chapter we showed that Zn···NO_2 recognition can be used as an effective synthon in the preparation of layered porphyrin solids.[5-22] In this chapter, we investigate the chlorophenyl and bromophenyl porphyrin derivatives, **2-Zn** and **3-Zn** (Figure 3.1), to explore their crystal structures, thermal properties and guest selection, and to test the robustness of Zn···NO_2 recognition in the formation of 4^4 networks. We have chosen **2-Zn** and **3-Zn** as candidates for further exploration of Zn···NO_2 recognition for several reasons. At the molecular level the difference between these two compounds and **1-Zn (**discussed in Chapter 2) is the replacement of methyl groups in **1-Zn** by chloro and bromo groups in **2-Zn** and **3-Zn**. These three groups – chloro, methyl, and bromo – are nearly spherical and have comparable sizes (20, 24, and 28 $Å^3$). They do differ from each other in their electronic character but in the context of structural chemistry the interchange of these groups should lead to predictable changes.

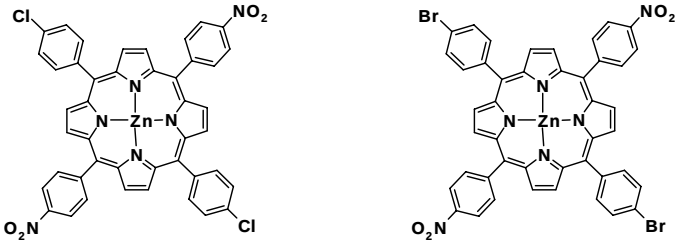

Figure 3.1 Molecular structures of **2-Zn** and **3-Zn**. These compounds differ from **1-Zn** only in the chloro and bromo substituents.

The concept of chloro-methyl exchange is used in crystal engineering to some degree of success in the preparation of isostructural solids.[23-24] Recently, this concept is extended to the preparation of multicomponent organic alloys using a supramolecular approach.[25] The chloro and methyl groups are structurally equivalent to a great extent but they are chemically distinct; these two contrasting properties makes **2-Zn** a primary alternative to **1-Zn** to test the efficacy of Zn···NO_2 recognition. In contrast to chloro-methyl exchange, the chloro-bromo and methyl-bromo exchanges are far less common in crystal engineering.[26-28] The bromo group is larger than the chloro and methyl groups, but the volume contribution of these groups to the overall size of the porphyrins **1-Zn**, **2-Zn**, and **3-Zn** is small. Electronically, the bromo group is similar to the chloro group but with one distinct difference. The bromo group can take part in polarization induced Br···NO_2 interactions.[26-28] These are attractive and stabilizing interactions that can interfere with the Zn···NO_2 recognition in a significant manner. Compound **3-Zn** is therefore an attractive alternative to **1-Zn** and **2-Zn** to test the robustness and competitiveness of Zn···NO_2 recognition in the design of 4^4 networks and layered solids. The most important consideration we used in the selection of **2-Zn** and **3-Zn** is that the chloro and bromo

groups do not bind to Zn^{2+} ion in competition with the nitro groups. We synthesized compounds **2-Zn** and **3-Zn** in a procedure analogous to the synthesis of **1-Zn**. Detailed experimental procedures and analyses are given in the experimental section at the end of the chapter.

3.2 COMPOUNDS 2-ZN AND 3-ZN ARE UNIVERSAL HOSTS

The key property that distinguishes compounds **2-Zn** and **3-Zn** from **1-Zn** is that they take up a range of guests when crystallized from solutions containing these guest species. Most of these guest included solids can be obtained as polycrystalline materials by slow evaporation of chloroform solutions. For a given solvate, the host-guest stoichiometry remained constant in the crystalline state, even if the guest is added in higher relative proportions in the solution. Unlike **1-Zn**, compounds **2-Zn** and **3-Zn** do not distinguish between the guests based on their size, shape, or electron deficient or electron rich character. For example, we have succeeded in crystallizing solvates of **2-Zn** that contain smaller guests such as chloroform or larger guests such as *o*-nitrotoluene. We analyzed the different solvates of **2-Zn** and **3-Zn** by thermal gravimetric analysis (TGA) to determine the host-guest stoichiometry of the bulk crystalline samples (Table 3.1). Analysis of these samples by differential scanning calorimetry (DSC) showed that all the solvates showed endotherms corresponding to desolvation; no other phase transitions are seen when the samples are heated up to 350 °C. It can be seen from Table 3.1 that these

Table 3.1 TGA Results for the porphyrin solvates studied in this chapter. Ratio refers to porphyrin-guest stoichiometry and *o*NT to *o*-nitrotoluene.

Porphyrin	Guest	Solvate	Ratio	% Guest	
				calcd.	exptl.
2-Zn	$CHCl_3$	**2-Zn-$CHCl_3$**	1:1	12.48	12.17
2-Zn	$PhCH_3$	**2-Zn-$PhCH_3$**	1:2	18.04	13.67
2-Zn	PhCl	**2-Zn-PhCl**	1:1	11.85	11.71
2-Zn	PhBr	**2-Zn-PhBr**	1:1	15.80	13.32
2-Zn	PhCN	**2-Zn-PhCN**	1:1	10.97	11.73
2-Zn	$PhNO_2$	**2-Zn-$PhNO_2$**	1:2	22.73	22.82
2-Zn	*o*NT	**2-Zn-*o*NT**	1:1	14.08	14.57
3-Zn	$CHCl_3$	**3-Zn-$CHCl_3$**	1:1	11.42	10.92
3-Zn	$PhCH_3$	**3-Zn-$PhCH_3$**	1:2	16.60	15.45
3-Zn	PhCl	**3-Zn-PhCl**	1:2	19.56	19.11
3-Zn	PhBr	**3-Zn-PhBr**	1:2	24.08	25.33
3-Zn	PhCN	**3-Zn-PhCN**	1:2	18.22	15.58
3-Zn	$PhNO_2$	**3-Zn-$PhNO_2$**	3:4	15.06	14.60

Table 3.2 Unit cell and space group (SPGR) data for porphyrin solvates discussed in Chapters 2 and 3. The *a*, *b*, and *c* axes are given in Å units, α, β, and γ angles in °, V (volume) in $Å^3$, and T (temperature) in K. There are six types of layered structures that contain 4^4 networks and Zn···NO_2 recognition; space groups of different types are shaded in unique colors. Structures that lack Zn···NO_2 recognition are not shaded.

Compound	SPGR	*Z*	*a*	*b*	*c*	α	β	γ	*V*	T
1-Zn	$P2_1/n$	2	10.194	9.061	20.667	90	102.475	90	1863.80	193
1-Zn-PhCN	$C2/c$	4	22.958	8.591	21.459	90	92.087	90	4229.60	193
1-Zn-PhNO$_2$-HT	$P2_1/c$	2	11.321	11.925	18.146	90	94.312	90	2443.00	193
1-Zn-PhNO$_2$-LT	$P2_1/c$	6	11.098	35.294	18.260	90	94.982	90	7125.39	100
1'-Zn-PhNO$_2$	$P\bar{1}$	1	10.371	10.538	12.712	70.371	77.297	62.679	1158.95	100
1-Co-PhNO$_2$-HT	$P2_1/c$	2	11.552	11.830	18.663	90	94.741	90	2541.77	273
1-Co-PhNO$_2$-LT	$P2_1/c$	6	11.201	34.571	18.223	90	95.777	90	7020.80	100
1-Co-CHCl$_3$	$P\bar{1}$	2	10.027	12.443	16.293	74.708	83.860	87.732	1949.45	100
2-Zn	$P2_1/n$	2	10.237	8.951	20.693	90	102.533	90	1851.06	163
2-Zn-CHCl$_3$	$C2/c$	4	23.832	8.029	21.446	90	93.737	90	4094.76	193
2-Zn-PhCH$_3$	$P2_1/c$	2	14.241	8.043	21.027	90	91.659	90	2407.40	193
2-Zn-PhCl	$C2/c$	4	23.400	8.223	21.384	90	93.130	90	4108.28	100
2-Zn-PhCN	$C2/c$	4	22.875	8.483	21.208	90	92.153	90	4112.43	100
2-Zn-PhNO$_2$	$P2_1/c$	6	11.131	35.375	18.439	90	95.080	90	7232.00	193
3-Zn	$P2_1/n$	2	10.026	9.016	20.885	90	103.000	90	1839.41	100
3-Zn-CHCl$_3$	$C2/c$	4	23.968	8.090	21.436	90	94.491	90	4144.00	193
3-Zn-PhCH$_3$	$P2_1/c$	2	14.124	8.070	20.891	90	90.579	90	2381.13	100
3-Zn-PhCl	$P2_1/n$	2	15.387	7.989	20.919	90	110.939	90	2401.60	100
3-Zn-PhBr	$P2_1/n$	2	15.675	7.966	20.776	90	110.723	90	2426.32	100
3-Zn-PhCN	$P2_1/c$	2	14.476	7.937	21.220	90	96.237	90	2423.78	100
3-Zn-PhNO$_2$	$P\bar{1}$	1	13.561	16.538	16.873	61.112	86.267	89.276	3305.60	193

two porphyrins incorporate a range of guests in different stoichiometries in the solid state. Only single crystal X-ray diffraction analysis can unequivocally prove whether these solvates possess the 4^4 networks based on Zn···NO_2 recognition and the guest species are located between the layers. Table 3.2 shows the unit cell parameters of various solvates described in this chapter along with the **1-Zn** and **1-Co** structures reported in the previous chapter. Further details of TGA and DSC experiments and structural analysis of individual solvates are given in the following sections.

3.3 SMALLER CRYSTALS AND STRUCTURAL LIMITATIONS

Compounds **2-Zn** and **3-Zn** readily dissolve in solvents such as chloroform and dichloromethane and most of the solvate crystals used in this work are grown from chloroform solutions. One vexing problem with porphyrin compounds studied in this work is their tendency to grow as thin plate-like polycrystalline materials. The small size of these crystals combined with the larger size of the porphyrin moieties often result in poor X-ray datasets. It has been very common for the compounds studied in this work to diffract only up to 1.0-1.1 Å resolution. In addition, solvates of **1-Zn**, **2-Zn** and **3-Zn** show problems typical of layered materials, namely misalignment of layers in the crystals and increased mosaicity. Almost all the solvates discussed in this chapter contain guest species in channels confined to the interlayer region. Often, these guest molecules are loosely bound to the host porphyrins and exhibit positional and orientational disorders. All these problems culminate in crystal structures that contain some isotropically refined heavy atoms (C, N, O, Zn etc), incompletely refined solvent molecules, or portions of molecules that are subjected to crystallographic constraints and restraints. In this context,

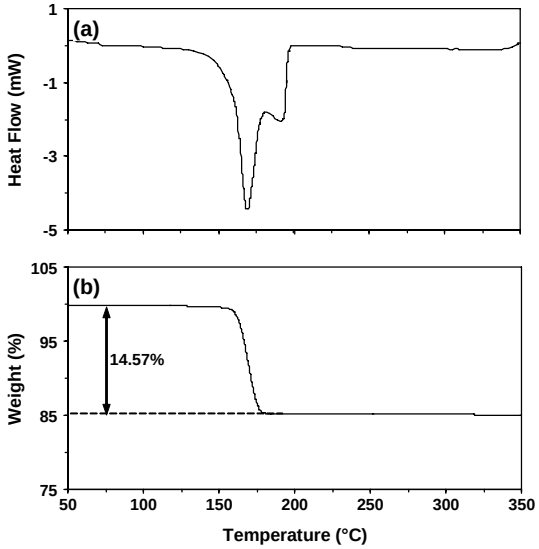

Figure 3.2 (a) DSC and **(b)** TGA plots of **2-Zn-*o*NT**. The endotherm in **(a)** and weight loss in **(b)** correspond to the desolvation of *o*-nitrotoluene from the crystals.

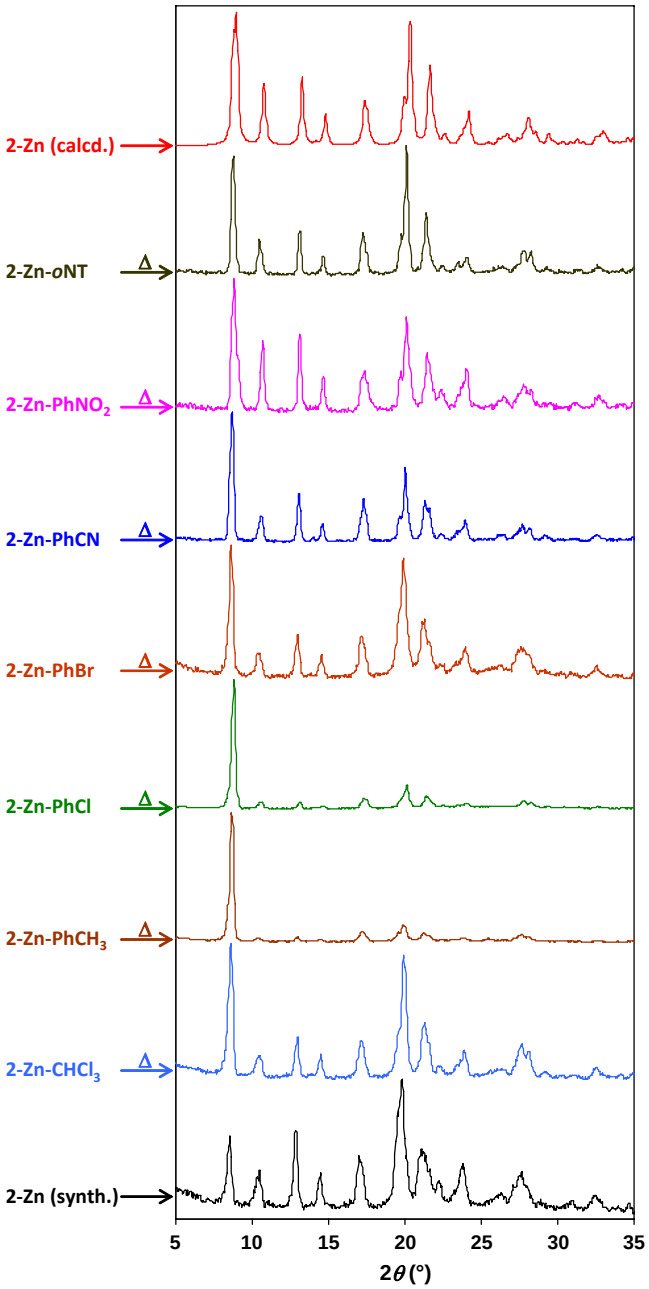

Figure 3.3 PXRD Patterns of as synthesized **2-Zn** (bottom) and desolvated crystals of different **2-Zn** solvates. At the top, the PXRD pattern calculated from the single crystal structure of **2-Zn** is given for comparison. The desolvated samples of **2-Zn-PhCH$_3$** and **2-Zn-PhCl** were not pulverized; their patterns show significant preferred orientation.

the parameters for Zn···NO_2 recognition – Zn···O distances, N–O distances, U_{eq} values of nitro O-atoms etc – are only refined in some solvates where the quality of the data permitted such refinement. Thus, the values of some or all of these parameters are not explicitly given in the following sections. Stating the same observations in a positive sense, the crystal structures reported here are a tribute to the cryogenic data collection, CCD (charge coupled device) detectors, and advanced integration and absorption methods. If not for these technological advancements, most of the crystal structures in this thesis would not have been realized. Despite the limitations in the quality of the data, the space groups of the structures are determined unequivocally and the atomic positions of the porphyrin molecules and most of the guests are unambiguously established. Details of X-ray data collection are given in the experimental section at the end of the chapter and, unit cell data and refinement parameters are provided in Appendix 1.

3.4 DESOLVATION OF 2-ZN SOLVATES

As discussed in Section 3.1 compound **2-Zn** forms solvated crystals with a range of guest species. In Table 3.1 we listed only those solvates for which we collected the single crystal or powder diffraction data, with the exception of the *o*-nitrotoluene solvate of **2-Zn**. Crystals of the solvate **2-Zn-*o*NT** grown from chloroform solution are very small and to date we did not succeed in obtaining X-ray data beyond a resolution of 2.4 Å. The crystals of **2-Zn-*o*NT**, however, showed sharp mass loss in TGA between 165-175 °C and a corresponding endotherm in DSC (Figure 3.2). The TGA data indicated that **2-Zn-*o*NT** is a 1:1 solvate. We present this solvate at the beginning of this chapter to emphasize that **2-Zn** is capable of forming solvates with larger molecules such as *o*-nitrotoluene (and *o*-xylene; data not shown here) that are banished by **1-Zn**. Though the **2-Zn** solvates shown in Table 3.1 exhibit some differences in their crystal structures (discussed below), they all contain 4^4 networks based on Zn···NO_2 recognition and all of them revert to the structure of non-solvate after heat induced desolvation (Figure 3.3). We made several unsuccessful attempts to obtain the crystal structure of the non-solvate from these desolvated materials. All the solvates yielded polycrystalline **2-Zn** after desolvation; these desolvated crystals are not suitable for single crystal X-ray diffraction. In other words, the conversion of any **2-Zn** solvate (listed in Table 3.1) into the **2-Zn** non-solvate does not follow the process of single crystal to single crystal transformation.

3.5 LAYERED STRUCTURE OF 2-ZN AND 4^4 NETWORKS

Despite repeated attempts, we could not grow single crystals of unsolvated **2-Zn** from solvents as small as acetonitrile and as large as *o*-xylene or *o*-nitrotoluene. All our attempts to crystallize **2-Zn** as a non-solvate led only to the solvated crystals. The desolvation of these solvated crystals involved explicit or internal shattering; the **2-Zn** crystals obtained in this manner are not suitable for single crystal X-ray diffraction analysis. Fortunately, we obtained a single crystal of **2-Zn** through a remarkable multi-step desolvation and ligand removal from a pyridine complex of **2-Zn**. The details of this pyridine complex and its transformation to **2-Zn** are discussed in detail in Chapter 4. Crystals of **2-Zn** obtained in this manner, though single crystalline in nature, diffracted to a lower resolution. The poor quality of the data may have its origins in the heating of the

pyridine complex beyond 250 °C, the intrinsic disorder that accrues as a result of ligand removal and desolvation, and more than 20% reduction in the unit cell volume that occurs when the pyridine complex is transformed to **2-Zn**. Interpretation of the results from the X-ray data of these **2-Zn** crystals is carried out with appropriate attention to the quality of the data.

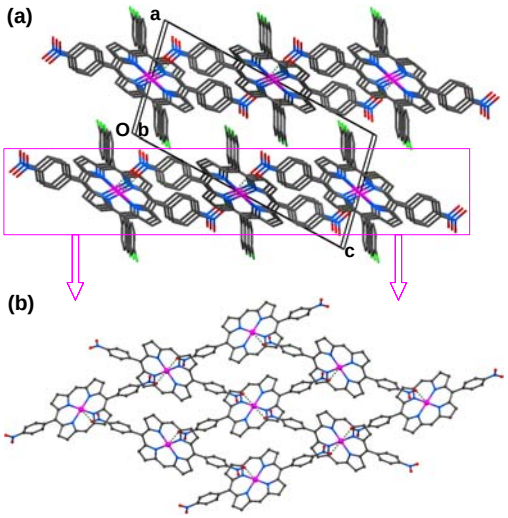

Figure 3.4 Crystal structure of **2-Zn**. **(a)** Interlayer stacking. Notice interdigitated packing and offset of layers. H-atoms are omitted. **(b)** 4^4 Networks formed by Zn···NO_2 recognition. Chlorophenyl groups and H-atoms are omitted. Color scheme: Zn-magenta; Cl-green, O-red; N-blue; and C-grey.

Crystals of **2-Zn** are isostructural to **1-Zn** and belong to the space group $P2_1/n$. Both crystals have practically similar unit cell dimensions (Table 3.2). The structure consists of layers that are offset stacked and the interlayer regions are walled by chlorophenyl groups (Figure 3.4a). Within each layer the molecules are connected to each other through Zn···NO_2 recognition to form 4^4 networks (Figure 3.4b). It must be mentioned that the chlorophenyl and nitrophenyl rings are disordered such that the *para* positions on any phenyl ring is occupied by nitro and chloro groups, with the overall occupancy being equal to two nitro and two chloro groups per porphyrin molecule. The structures drawn in Figure 3.4 use those positions that permit Zn···NO_2 recognition. Given the structural similarity between **1-Zn** and **2-Zn** it is reasonable to describe the structure of **2-Zn** in the above manner. The extensive disorder of the chloro and nitro groups required the fixing of bond lengths and angles of these groups using the geometric constraints.

3.6 CHLOROFORM SOLVATE OF 2-ZN

Unlike **1-Zn**, compound **2-Zn** yields solvated crystals, **2-Zn-$CHCl_3$**, when crystallized from chloroform. These crystals undergo partial loss of solvent and become slightly

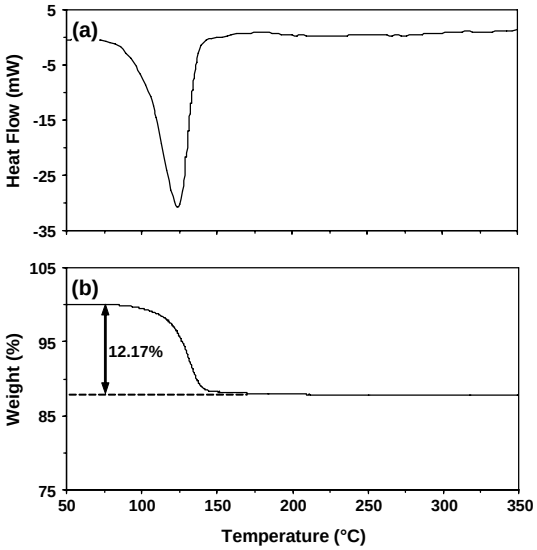

Figure 3.5 (a) DSC and **(b)** TGA plots of **2-Zn-CHCl$_3$**. The endotherm in **(a)** and weight loss in **(b)** correspond to the desolvation of chloroform from the crystals.

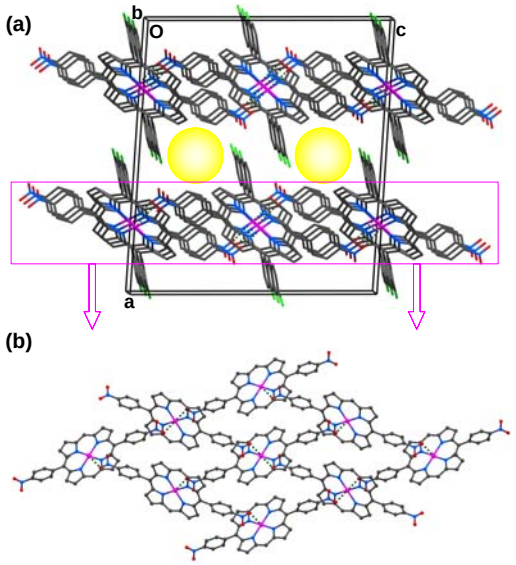

Figure 3.6 Crystal structure of **2-Zn-CHCl$_3$**. **(a)** Interlayer stacking. Notice interdigitated packing. Contrast this figure with the unsolvated **2-Zn** (Figure 3.4a) to note the decrease in the offset of layers. Reduction in the offset allows the sorption of guests in the interlayer region. Disordered solvent molecules (not shown) are located in the voids represented by yellow spheres. H-atoms are omitted. **(b)** 4^4 Networks formed by Zn···NO_2 recognition. Chlorophenyl groups and H-atoms are omitted.

opaque when left at ambient temperature. Given that **1-Zn** does not form chloroform solvate, it is interesting to note that **2-Zn** crystals grown from chloroform solutions lose solvent when exposed to open air. Thermal analysis of these crystals (Figure 3.5) revealed an endotherm in DSC at 125 °C and 12.17 % mass loss in TGA. The TGA data suggests that the porphyrin and the guest are in 1:1 stoichiometry in **2-Zn-$CHCl_3$**.

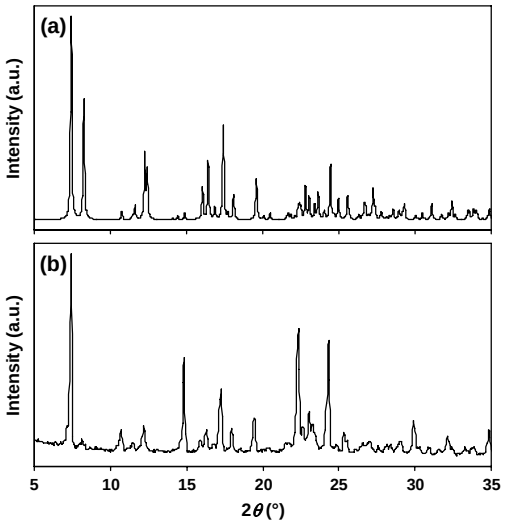

Figure 3.7 (a) Calculated and **(b)** experimental PXRD patterns of **2-Zn-$CHCl_3$**. These patterns indicate that the crystals in bulk samples have the same structure as the one reported above. The diffraction from the disordered chloroform molecules is included in the calculated pattern shown in **(a)**. The differences in the relative intensities of the peaks can be attributed to the anisotropic shapes of the crystals and partial preferred orientation of the non-pulverized samples. The minor variations in the peak positions can be attributed to the difference in the temperature of X-ray data collection: **(a)** at -80 °C and **(b)** at 25 °C.

Crystals of **2-Zn-$CHCl_3$** belong to the space group *C*2/*c* and display all the important characteristics of our design: porphyrin molecules are interconnected by Zn···NO_2 recognition to form 4^4 networks (Figure 3.6b) and these networks stack on each other to form a layered structure (Figure 3.6a). Surprisingly, **2-Zn-$CHCl_3$** is isostructural to **1-Zn-PhCN** (Table 3.2) Unfortunately, the solvent molecules in **2-Zn-$CHCl_3$** are highly disordered; we could not determine the guest-guest or host-guest interactions. Recall that in **1-Zn-PhCN**. the benzonitrile guest molecules are joined by C–H···N interactions to form linear arrays between the host layers (Figure 2.16). We could locate the electron density corresponding to one chloroform molecule (per porphyrin molecule) between the layers, but could not refine the positions and occupancies of different atoms of the solvent. We therefore used the SQUEEZE routine in PLATON program to eliminate the contribution of the solvent to the overall diffraction, and refined the structure to a reasonable *R* value (Appendix 1). Figure 3.7 shows the calculated (from single crystal data) and experimental PXRD patterns. These patterns illustrate that the crystals in the bulk sample possess the same structure as that displayed in Figure 3.6. In the context of

crystal engineering, **2-Zn-CHCl$_3$** represents yet another structure in which our design principles are successfully employed resulting in a layered intercalated material.

3.7 ABUTTING LAYERS IN 2-ZN-PHCH$_3$

Crystals of toluene solvate of **2-Zn** belong to the space group $P2_1/c$. The crystal structure of **2-Zn-PhCH$_3$** is similar to **1-Zn** solvates and **2-Zn-CHCl$_3$** in that it exhibits Zn···NO$_2$ recognition, 4^4 networks, and layered structure but yet different in that the adjacent layers in **2-Zn-PhCH$_3$** are juxtaposed but not interdigitated. It is for this reason the unit cell of **2-Zn-PhCH$_3$** is unique compared to the other solvates reported so far (Table 3.2).

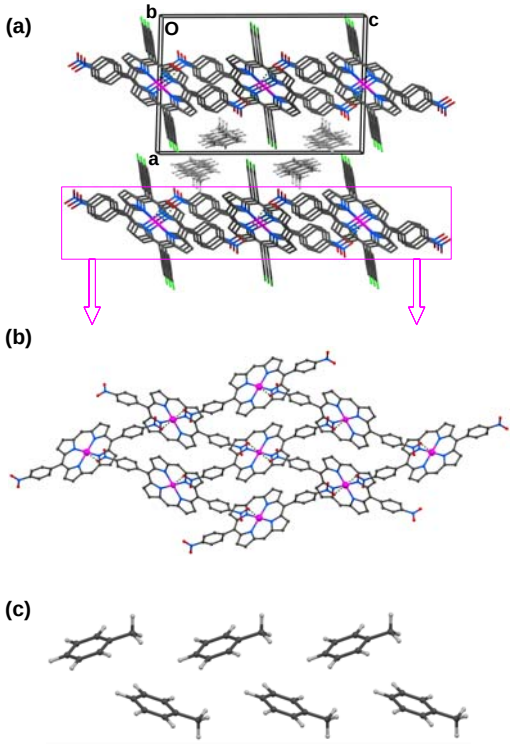

Figure 3.8 Crystal structure of **2-Zn-PhCH$_3$**. **(a)** Interlayer stacking. Notice that the chlorophenyl groups do not interlock as in **2-Zn** (Figure 3.4a) or **2-Zn-CHCl$_3$** (Figure 3.6a). Notice also the decrease in the offset of layers and increase in the separation between the layers. Toluene molecules are drawn with lighter colors. H-atoms of the porphyrin are omitted. **(b)** 4^4 Networks formed by Zn···NO$_2$ recognition. Chlorophenyl groups and H-atoms are omitted. Notice the similarity between this network and the 4^4 networks of **2-Zn** (Figure 3.4b) or **2-Zn-CHCl$_3$** (Figure 3.6b). (**c**) One-dimensional bimolecular arrays of guest species confined to the interlayer region.

Figure 3.8a shows the interlayer packing in **2-Zn-PhCH$_3$**. Adjacent layers do not interlock as seen in previous solvates; they abut each other. The porphyrin and the

toluene are in 1:2 stoichiometry within the crystals. Thus, larger space is needed in the interlayer region in **2-Zn-PhCH$_3$** compared to **2-Zn-CHCl$_3$** in which porphyrin and guest are in 1:1 ratio. The demand for the increased space for guests in **2-Zn-PhCH$_3$** is met by a decrease in interlayer offset (0.412 Å) and an increase in interlayer separation (14.235 Å). For comparison, the interlayer offset and separation in **2-Zn-CHCl$_3$** are 0.639 and 11.683 Å. It is pertinent to note that accommodation of toluene molecules is achieved by varying the *interlayer* region but not the *intralayer* region (Figure 3.8b). That is, the differences in the non-solvate and different solvates are overcome by tweaking the interlayer region while preserving the Zn···NO_2 recognition and the 4^4 networks. These observations again testify the robustness of the relatively weak Zn···NO_2 recognition and its utility in design of predictable crystal structures. The arrangement of toluene molecules confined to the interlayer region is shown in Figure 3.8c. These molecules are housed between the chlorophenyl groups by van der Waals interactions.

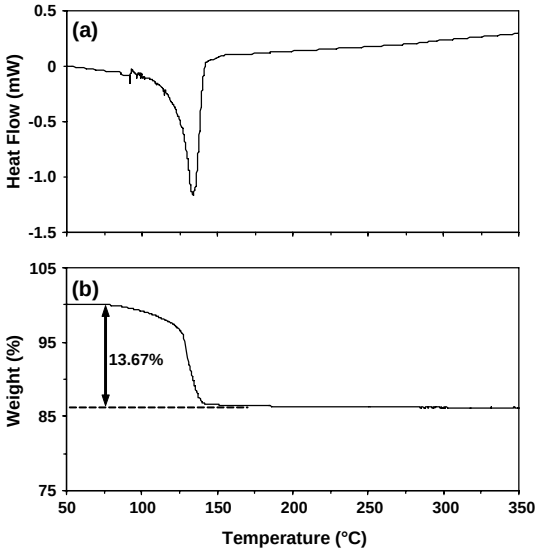

Figure 3.9 (a) DSC and **(b)** TGA plots of **2-Zn-PhCH$_3$** obtained from a solution of chloroform and toluene. Note that the weight loss in TGA is significantly smaller than expected (Table 3.1).

Compound **2-Zn** is sparingly soluble in toluene and crystals of **2-Zn-PhCH$_3$** obtained from toluene solutions are very small (~ 50 μm in longest dimension) and unusable for X-ray diffraction. Decent sized (> 300 μm in longest dimension) crystals of **2-Zn-PhCH$_3$**, however, can be easily obtained from a solution of **2-Zn** in chloroform and toluene. Single crystal X-ray analysis was performed on a crystal that is obtained from this mixture of solvents. For consistency, powder X-ray diffraction and thermal analyses are also performed on crystals obtained from the same batch of crystals. Analysis by DSC (Figure 3.9a) showed an endotherm related to absorption of desolvation energy. When the solvated crystals are subjected to TGA (Figure 3.9b), the mass loss corresponding to the

solvent removal, however, is significantly less than expected (13.67 versus 18.04; Table 3.1) for a 1:2 solvate.

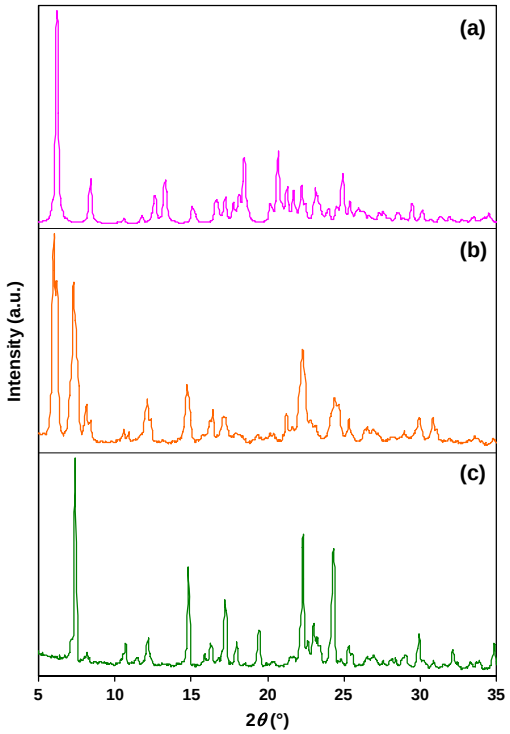

Figure 3.10 (a) Calculated and **(b)** experimental PXRD patterns of **2-Zn-PhCH$_3$**. The experimental pattern in **(b)** shows several additional peaks; these peaks correspond to the crystals of **2-Zn-CHCl$_3$**. For comparison the experimental PXRD pattern of **2-Zn-CHCl$_3$** is shown in **(c)**. The peak in **(b)** at $2\theta = 6°$ clearly distinguishes **2-Zn-PhCH$_3$** from **2-Zn-CHCl$_3$**.

Given that the solvated crystals are grown from a mixture of solvents and that **2-Zn** is capable of forming chloroform and toluene solvates, it is likely that the bulk sample contains both **2-Zn-PhCH$_3$** and **2-Zn-CHCl$_3$**. The presence of both solvates in the crystals grown from chloroform and toluene solutions is confirmed by PXRD analysis. Diffraction peaks corresponding to both **2-Zn-PhCH$_3$** and **2-Zn-CHCl$_3$** can be clearly identified in the powder X-ray pattern (Figure 3.10). These observations suggest that **2-Zn** does not discriminate between chloroform and toluene and formation of both types of structures are equally favorable under the experimental conditions. These experiments also suggest that it is important to carry out the characterization of bulk samples by methods such as PXRD and TGA to confirm or provide context for the results of single crystal X-ray diffraction analysis.

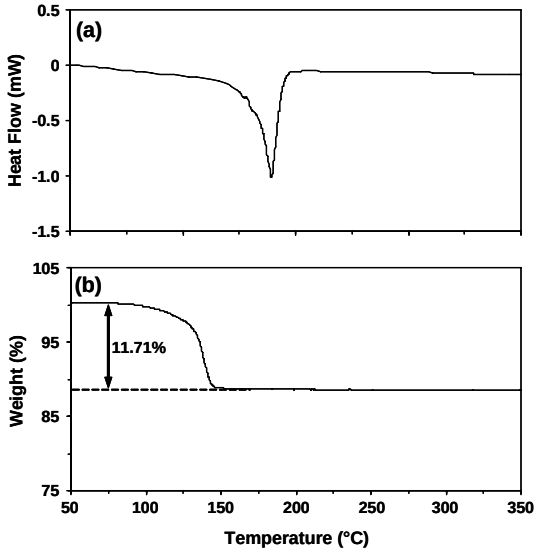

Figure 3.11 (a) DSC and **(b)** TGA plots of **2-Zn-PhCl** obtained from a solution of chloroform and chlorobenzene.

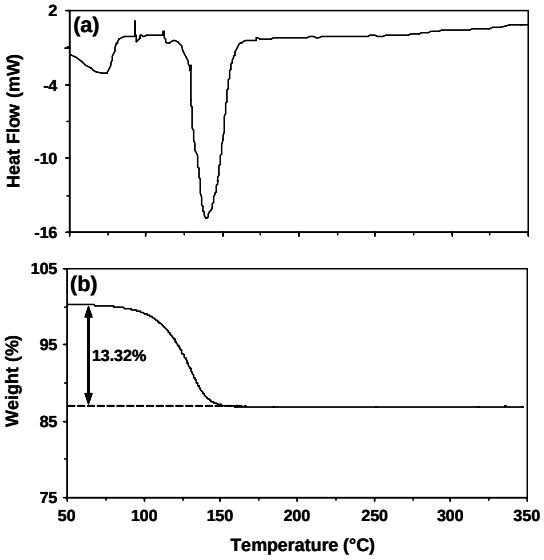

Figure 3.12 (a) DSC and **(b)** TGA plots of **2-Zn-PhBr** obtained from a solution of chloroform and bromobenzene. In **(a)**, the endotherm near 60 °C corresponds to the removal of physisorbed solvent.

3.8 CHLOROBENZENE AND BROMOBENZENE SOLVATES OF 2-ZN

Slow evaporation of chloroform solutions containing **2-Zn** and chlorobenzene or bromobenzene produces **2-Zn-PhCl** or **2-Zn-PhBr** in quantitative yields. In both cases the crystals have plate like morphologies and they do not lose solvent as fast as **2-Zn-$CHCl_3$**. Analysis of these crystals by DSC revealed that each solvate exhibits a desolvation endotherm and neither shows additional phase transitions at least until 350 °C (Figures 3.11a and 3.12a). The TGA experiments showed that both **2-Zn-PhCl** and **2-Zn-PhBr** are 1:1 solvates; that is in each case the porphyrin and the guest are in 1:1 stoichiometry (Figures 3.11b and 3.12b). Under evaporation conditions, both solvates usually grow as very small crystals and for a long time we could not carry out single crystal X-ray diffraction analysis of these samples. Analysis of these crystals by PXRD, however, showed that both solvates exhibit similarities in the diffraction patterns (Figure 3.13). Given that chlorobenzene and bromobenzene molecules have similar shapes, sizes and electronic distributions, and that **2-Zn-PhCl** and **2-Zn-PhBr** have host and guest in 1:1 stoichiometry, it is possible that the two **2-Zn** solvates have similar structures and therefore display similar diffraction patterns.

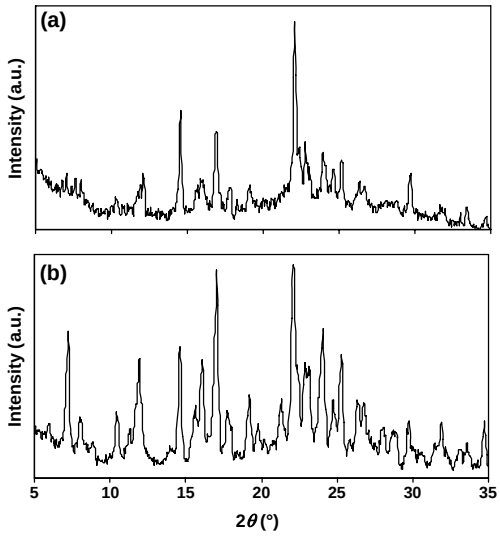

Figure 3.13 Experimental PXRD patterns of **(a) 2-Zn-PhCl** and **(b) 2-Zn-PhBr**. In the top pattern **2-Zn-PhCl** crystals adopt partial preferred orientation and display fewer peaks than expected. The similarity between the patterns in **(a)** and **(b)** suggests that **2-Zn-PhCl** and **2-Zn-PhBr** most likely adopt similar crystal structures.

After repeated crystallization attempts, we have been able to grow crystals of **2-Zn-PhCl** suitable for single crystal X-ray analysis. Crystals of **2-Zn-PhCl** are isostructural to **1-Zn-PhCN** (and **2-Zn-$CHCl_3$**) and belong to the space group *C*2/*c*. Unlike in **2-Zn-$PhCH_3$** the layers are interdigitated (Figure 3.14a) with larger interlayer offset (0.639 Å) and shorter interlayer separation (11.683 Å). Within each layer the porphyrin molecules form 4^4 networks through Zn···NO_2 recognition (Figure 3.14b).

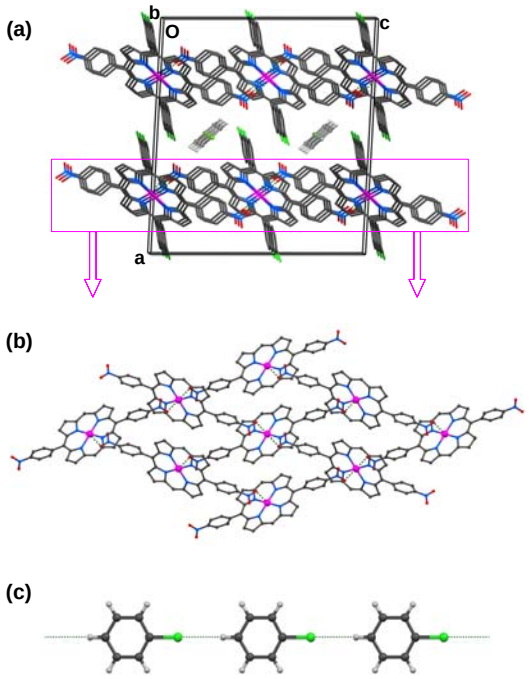

Figure 3.14 Crystal structure of **2-Zn-PhCl**. **(a)** Interlayer stacking. Notice interdigitated packing. Compare this figure with **2-Zn-$CHCl_3$** (Figure 3.6a) and **1-Zn-PhCN** (Figure 2.15). Guest molecules are drawn with lighter colors. H-atoms of the porphyrin are omitted. **(b)** 4^4 Networks formed by Zn···NO_2 recognition. Chlorophenyl groups and H-atoms are omitted. Notice the similarity between this network and the 4^4 networks of **2-Zn** (Figure 3.4b) or **2-Zn-$CHCl_3$** (Figure 3.6b) or **2-Zn-$PhCH_3$** (Figure 3.8b). (**c**) One-dimensional arrays of chlorobenzene molecules confined to the interlayer region. Compare this figure with Figure 2.16 to note that the C–H···Cl interactions can be as effective in forming linear chains as other well known interactions. Chlorobenzene molecules are disordered over two positions; only one position is shown here. In both positions, the guest molecules form one-dimensional arrays with short, linear C–H···Cl interactions.

An interesting feature of the structure of **2-Zn-PhCl** lies in the guest assembly in the interlayer region. The chlorobenzene molecules are bisected by crystallographic 2-fold axes; they form closely spaced linear arrays along the 2-fold axes. Within each array adjacent molecules are connected by short, linear C–H···Cl interactions (H···Cl: 2.67 Å; C···Cl: 3.75 Å; C–H···Cl: 180°) as shown in Figure 3.14c. Recall that similar linear arrays of guest molecules are seen in **1-Zn-PhCN** (Figure 2.16), which is isostructural to the current **2-Zn-PhCl**. In these two cases the guest molecules have similar shapes, sizes and electronic distributions in the context of C–H···N/Cl interactions. While the C–H···N mediated linear assemblies are previously known, the current host system enables the production of linear molecular arrays that are stabilized by C–H···Cl interactions. The design of guest assembly based on host architecture has been used for applications such as nonlinear optics, nano-sized flourous droplets, and stereospecific reactions. Here we

show the use of host architecture in the realization of supramolecular structures sustained by previously under-explored weak intermolecular interactions. Based on the similarities between the PXRD patterns of **2-Zn-PhCl** and **2-Zn-PhBr** we surmise that the latter solvate has linear arrays of bromobenzene molecules joined together by C–H···Br interactions. Single crystal X-ray analysis needs to be performed to prove this hypothesis.

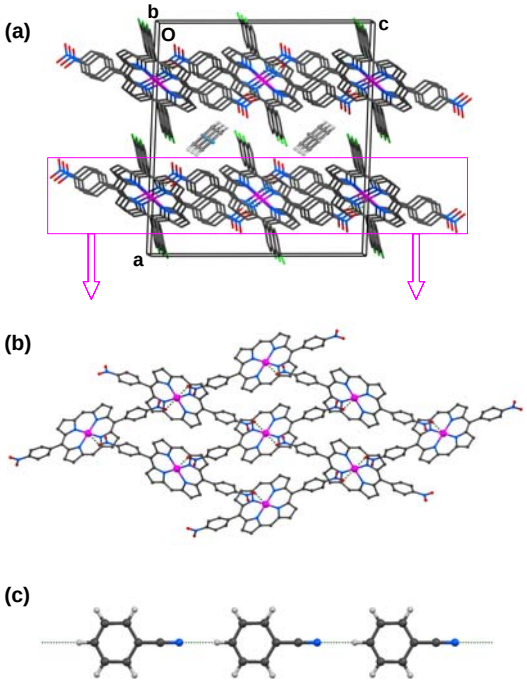

Figure 3.15 Crystal structure of **2-Zn-PhCN**. **(a)** Interlayer stacking. Notice interdigitated packing. Compare this figure with **2-Zn-CHCl$_3$** (Figure 3.6a), **2-Zn-PhCl** (Figure 3.14a), and **1-Zn-PhCN** (Figure 2.15). Guest molecules are drawn with lighter colors. H-atoms of the porphyrin are omitted. **(b)** 4^4 Networks formed by Zn···NO$_2$ recognition. Chlorophenyl groups and H-atoms are omitted. Notice the similarity between this network and the 4^4 networks discussed so far. (**c**) One-dimensional C–H···N hydrogen bonded arrays of benzonitrile molecules confined to the interlayer region. Compare this figure with Figure 2.16 and Figure 3.14c.

3.9 LINEAR C–H···N ARRAYS OF GUEST MOLECULES IN 2-ZN-PHCN

Noting that **2-Zn-PhCl** is isostructural to **1-Zn-PhCN** and that guest molecules form linear supramolecular assemblies in these structures, our quest to determine the crystal structure of **2-Zn-PhCN** had two goals. One is to ensure the host architecture remained the same (a layered structure with 4^4 networks and Zn···NO$_2$ recognition) and the other is to attain the 1:1 host-guest stoichiometry with linear hydrogen bonded arrays of

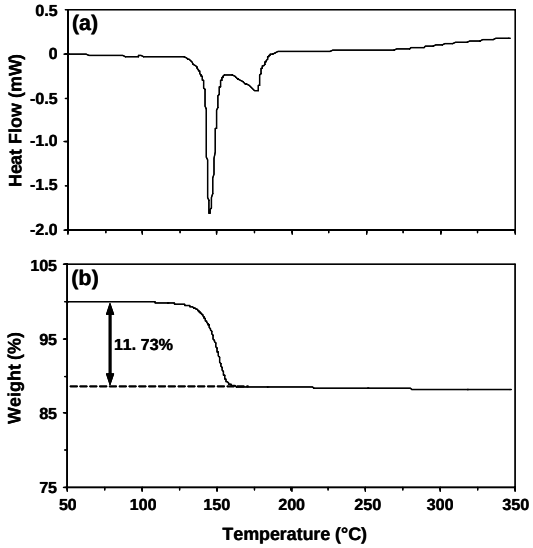

Figure 3.16 (a) DSC and **(b)** TGA plots of **2-Zn-PhCN** obtained from a solution of chloroform and benzonitrile. In **(a)**, the double endotherm suggests that the desolvation is a two step process when **2-Zn-PhCN** is heated in sealed pans.

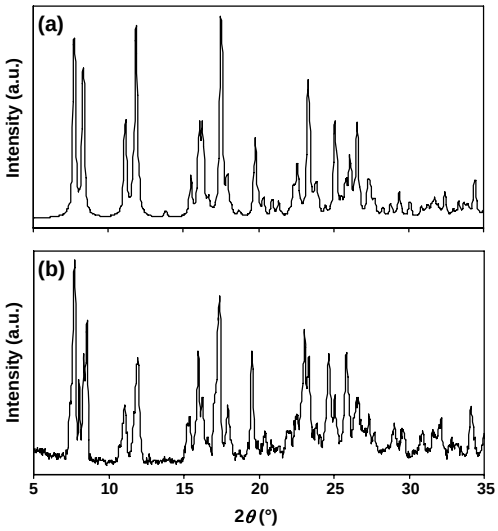

Figure 3.17 (a) Calculated and **(b)** experimental PXRD patterns of **2-Zn-PhCN**. These patterns indicate that the crystals in bulk samples have the same structure as the one reported above. Minor variations in the peak positions can be attributed to the difference in the temperature of X-ray data collection: **(a)** at -173 °C and **(b)** at 25 °C.

benzonitrile molecules. Indeed, the crystals of **2-Zn-PhCN** are fully isostructural to **1-Zn-PhCN** and **2-Zn-PhCl** and belong to the space group *C*2/*c* (Table 3.2 and Figure 3.15). Again, the benzonitrile molecules are confined to the interlayer region and form linear arrays (Figure 3.15c) held together by C–H···N hydrogen bonds (H···N: 2.19 Å; C···N: 3.27 Å; C–H···N: 180°). We evaluated the presence of benzonitrile solvate in the bulk sample by DSC, TGA (Figure 3.16) and PXRD (Figure 3.17). The TGA and PXRD experiments revealed that the bulk sample has the same host-guest stoichiometry and solid state structure as those revealed from the single crystal diffraction analysis.

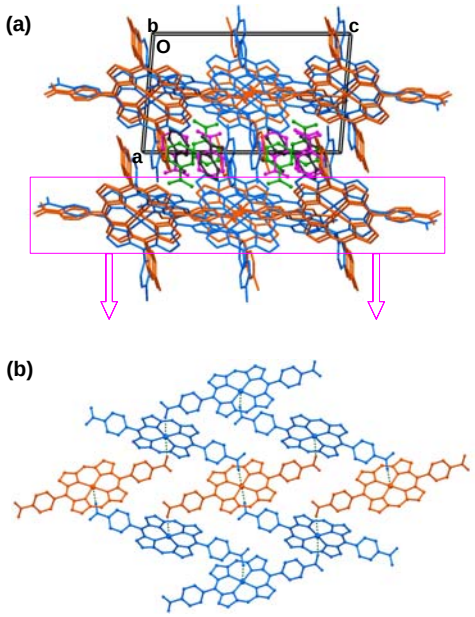

Figure 3.18 Crystal structure of **2-Zn-PhNO$_2$** determined at -80 °C. **(a)** Interlayer stacking showing the intercalation of nitrobenzene between the layers. Symmetry independent host (orange and blue) and guest (black, magenta, and green) are colored differently. One of the three nitrobenzene molecules is disordered over two positions; only one position is shown. H-atoms are omitted. Compare and contrast this structure with the lower *Z*′ structures of **1-Zn-PhNO$_2$** (Figure 2.6) and **1-Co-PhNO$_2$** (Figure 2.24). **(b)** 4^4 Networks formed by Co···NO$_2$ recognition. *p*-Tolyl groups and H-atoms are omitted. Note that each 4^4 network in the crystal contains both symmetry independent porphyrin molecules. Each orange molecule is connected to four blue molecules, whereas each blue molecule is connected to two orange and two blue molecules.

3.10 HIGHER Z′ STRUCTURE OF 2-ZN-PHNO$_2$

Crystals of **2-Zn-PhNO$_2$** in which porphyrin and the guest are in 1:2 stoichiometry are obtained from a chloroform solution containing **2-Zn** and excess nitrobenzene. Single crystal X-ray data collected -80 °C revealed that **2-Zn-PhNO$_2$** has the same structure (Figure 3.18) as **1-Co-PhNO$_2$** at -80 °C (Figure 2.22) or **1-Zn-PhNO$_2$** at -173 °C. That is,

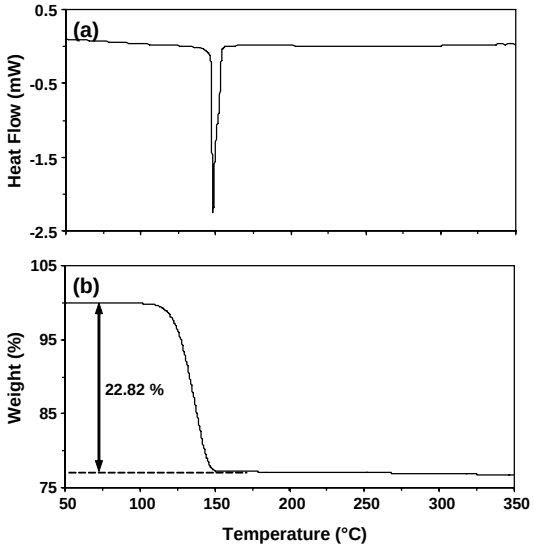

Figure 3.19 (a) DSC and **(b)** TGA plots of **2-Zn-PhNO$_2$** obtained from a solution of chloroform and nitrobenzene. The endotherm in **(a)** and weight loss in **(b)** correspond to the desolvation of nitrobenzene from the crystals.

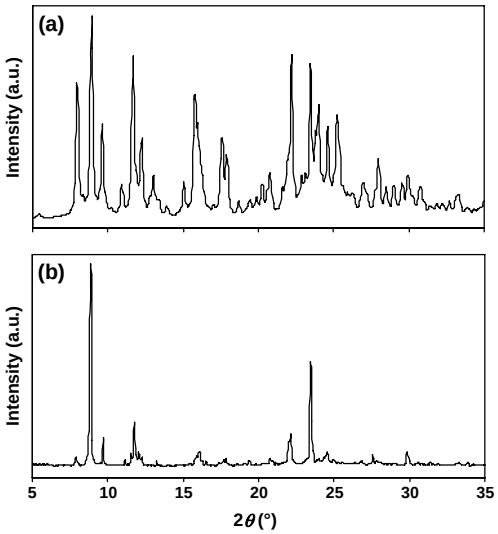

Figure 3.20 (a) Calculated and **(b)** experimental PXRD patterns of **2-Zn-PhNO$_2$**. The differences in the relative intensities of the peaks can be attributed to the anisotropic shapes of the crystals and partial preferred orientation of the non-pulverized samples. Minor variations in the peak positions can be attributed to the difference in the temperature of X-ray data collection: **(a)** at -80 °C and **(b)** at 25 °C.

2-Zn-PhNO$_2$ at -80 °C has the higher *Z*′ structure reported in Chapter 2. Crystals of **2-Zn-PhNO$_2$** are more akin to **1-Co-PhNO$_2$** (than **1-Zn-PhNO$_2$**) in terms of the temperature at which higher *Z*′ structure is adopted. We should mention here that, at the time of data acquisition of **2-Zn-PhNO$_2$** we did not notice the similarities between lower *Z*′ and higher *Z*′ structures and hence did not collect X-ray data at higher temperature on these crystals. We believe that if these crystals are brought to higher temperature (e.g., room temperature) they will transform to a lower *Z*′ structure similar to that seen in Figures 2.6 and 2.24. In the bulk samples, we determined the desolvation endotherms by DSC (Figure 3.19a), established the stoichiometry by TGA (Figure 3.19b) and confirmed the crystallinity by PXRD (Figure 3.20).

3.11 DESOLVATION AND RESOLVATION OF 2-ZN-PHNO$_2$

Heating of the crystals of **2-Zn-PhNO$_2$** to 200 °C in a TGA chamber (Figure 3.19b) led to the complete loss of the guest molecules. It can be seen from Figures 3.21a-b that the crystals retained their morphology after this heat induced desolvation. Powder X-ray analysis showed that the crystals also retained crystallinity to some extent (Figures 3.21e-f). From morphology it appeared that the desolvation of **2-Zn-PhNO$_2$** to **2-Zn** is a single crystal to single crystal phase transition. Yet, when subjected to single crystal X-ray diffraction these desolvated crystals resulted in highly diffuse reflections and powder rings as opposed to discrete spots. Thus we concluded that the prismatic blocks in Figure 3.21b (obtained after desolvation) are not single crystals; most likely they are polycrystalline solids. When we attempted the resolvation of these desolvated crystals (by soaking the crystals with a very small volume, 0.2 mL, of nitrobenzene) we noticed significant dissolution of the crystals followed by the growth of new solvated crystals (Figure 3.21c). This result is in stark contrast to the resolvation of **1-Zn** crystals with nitrobenzene (Section 2.7) but similar to that seen for **1-Co** (Section 2.10.3.3). It appears that **2-Zn** (like **1-Co**) has far greater solubility in nitrobenzene than **1-Zn**. In the case of **2-Zn** the rate of dissolution is faster than the rate of diffusion of nitrobenzene into the solid, leading to a greater amount of re-grown **2-Zn-PhNO$_2$** (small dark crystals in Figure 3.21c) than resolvated **2-Zn-PhNO$_2$** (reddish-orange blocks). TGA analysis (Figure 3.22) of these re-grown and resolvated crystals showed near complete inclusion of guest molecules into the crystals. Analysis of these nitrobenzene soaked samples by PXRD (Figure 3.22g) confirmed that these crystals belong to **2-Zn-PhNO$_2$**.

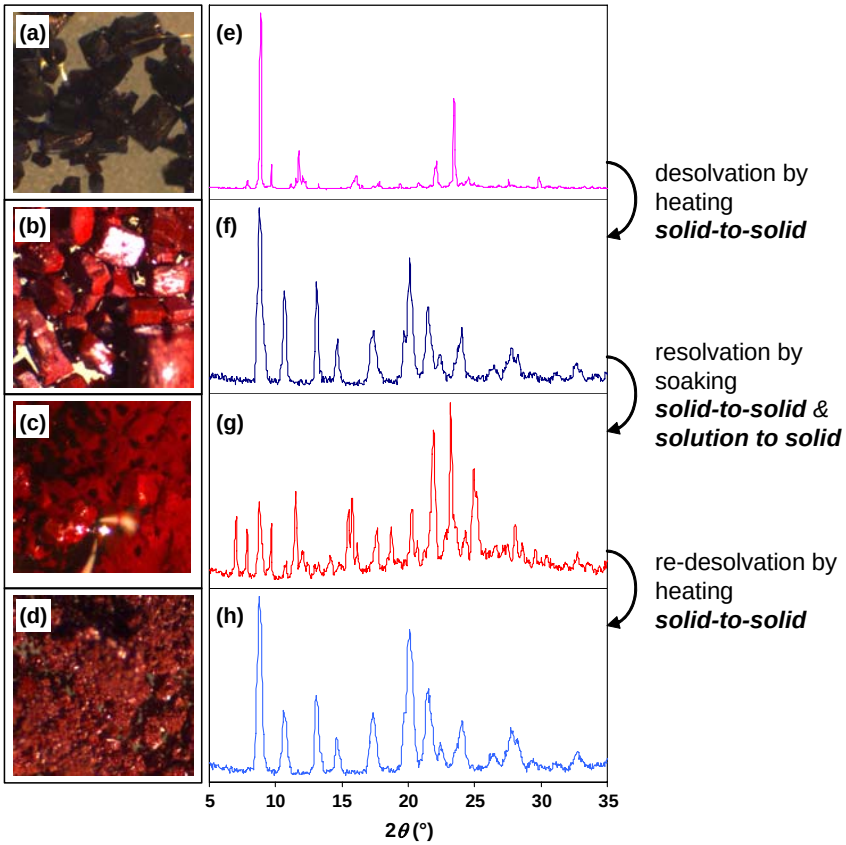

Figure 3.21 Desolvation, resolvation, and re-desolvation of **2-Zn-PhNO$_2$** monitored by **(a-d)** optical microscopy and **(e-h)** PXRD analysis. The solution grown crystals of **2-Zn-PhNO$_2$ (a)** show fewer peaks in the powder diffraction pattern **(e)** than expected. The crystals are not pulverized to avoid grinding induced desolvation; they adopt preferred orientation on sample holders and give fewer diffraction peaks. The desolvated crystals **(b)** show distinct color but retain the morphology of **2-Zn-PhNO$_2$**. The powder diffraction pattern **(f)** of desolvated crystals confirm the phase transition of **2-Zn-PhNO$_2$** to **2-Zn**. **(c)** Microscopic image of the desolvated crystals soaked in nitrobenzene for 15 minutes. Notice the growth of small dark crystals and some remnants of reddish-orange crystals. **(g)** Powder diffraction pattern of the crystals shown in **(c)**. Notice the disappearance of peaks corresponding to **2-Zn** and emergence of peaks corresponding to **2-Zn-PhNO$_2$**. The crystals in **(c)** do not adopt preferred orientation on the sample holder; this is the reason for the difference in relative intensities in diffraction patterns shown in **(e)** and **(g)**. Compare **(g)** with calculated powder pattern of **2-Zn-PhNO$_2$** (Figure 3.20a) to note that pattern in **(g)** displays all the expected diffraction peaks. (**d**) Re-desolvated material and (**h**) its diffraction pattern confirming the full desolvation in the second cycle. For PXRD patterns in **(e-h)**, the *y*-axis refers to diffraction intensity in arbitrary units.

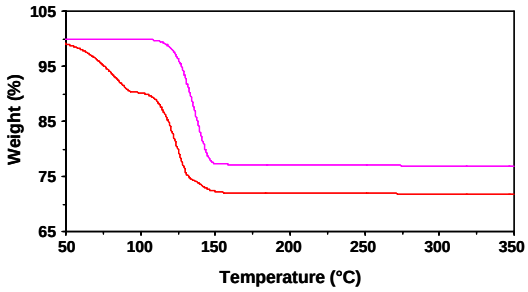

Figure 3.22 TGA plots of the solution grown crystals of **2-Zn-PhNO$_2$** (magenta) and samples of **2-Zn-PhNO$_2$** (red) obtained by soaking desolvated crystals in nitrobenzene for 15 minutes. Notice that the red plot involved the weight loss corresponding the physisorbed nitrobenzene solvent. After accounting for this physisorbed solvent, there is a close match of weight loss between magenta and red plots. The resolvated material (that is subjected to the TGA experiment, blue plot) contained small dark crystals (grown after dissolution) and reddish-orange blocks (crystals that remained intact at the end of soaking) of **2-Zn-PhNO$_2$**. This result shows that resolvation of 2-**Zn** involves two mechanisms: (a) dissolution of **2-Zn** followed by the re-growth of **2-Zn-PhNO$_2$** and (b) diffusion of nitrobenzene into the solid **2-Zn**. The relative masses of two types of crystals have not been determined.

3.12 LAYERED STRUCTURE OF 3-ZN AND 4^4 NETWORKS

Like **2-Zn**, compound **3-Zn** cannot be crystallized as a non-solvate whether the solvent used is small (e.g., acetonitrile) or large (*o*-xylene). Repeated attempts to crystallize **3-Zn** as a non-solvate led only to the solvated crystals (Table 3.1). The desolvation of these solvated crystals led to polycrystalline **3-Zn** that was not suitable for single crystal X-ray diffraction analysis. Following the lines of **2-Zn**, we have been able to obtain a single crystal of **3-Zn** through a multi-step desolvation and ligand removal from a pyridine complex of **3-Zn**. Chapter 4 provides the details of this pyridine complex and its transformation to **3-Zn**. The X-ray data collected on **3-Zn** crystals obtained by this process is of poor quality for the same reasons that are mentioned in Section 3.5. Structural interpretation of **3-Zn** is carried out with appropriate attention to the quality of the data.

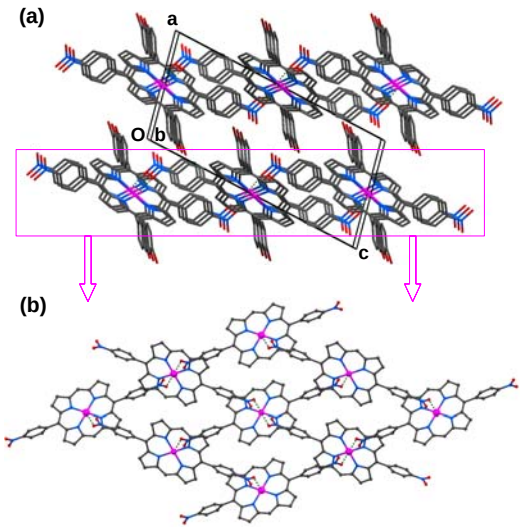

Figure 3.23 Crystal structure of **3-Zn**. **(a)** Interlayer stacking. Notice interdigitated packing and offset of layers. H-atoms are omitted. **(b)** 4^4 Networks formed by Zn···NO_2 recognition. Bromophenyl groups and H-atoms are omitted. Color scheme: Zn-magenta; Br-crimson red, O-red; N-blue; and C-grey.

Crystals of **3-Zn** are isostructural to **1-Zn** and **2-Zn**, and belong to the space group $P2_1/n$. All the three non-solvates have practically similar unit cell dimensions (Table 3.2). The structure consists of layers that are offset stacked and the interlayer regions are walled by bromophenyl groups (Figure 3.23a). Within each layer the molecules are connected to each other through Zn···NO_2 recognition to form 4^4 networks (Figure 3.23b). The bromophenyl and nitrophenyl rings are disordered such that the *para* positions on any phenyl ring is occupied by nitro and bromo groups, with the overall occupancy being equal to two nitro and two bromo groups per porphyrin molecule. The structures drawn in Figure 3.23 use those positions that permit Zn···NO_2 recognition. Given the structural similarity between **3-Zn**, **1-Zn** and **2-Zn** it is reasonable to describe the structure of **3-Zn** in the above manner. The extensive disorder of the bromo and nitro groups required the fixing of bond lengths and angles of these groups using the geometric constraints.

3.13 PARTIAL ZN···NO_2 RECOGNITION IN 3-ZN-$PHNO_2$

At the outset of our work on **3-Zn** solvates, we wished to explore **3-Zn-$PhNO_2$** because nitrobenzene solvates of **1-Zn**, **1-Co** and **2-Zn** exhibit rich structural chemistry in terms of single crystal to single crystal transformations (higher Z' to lower Z' structures). Crystallization of **3-Zn** from a solution of chloroform and nitrobenzene readily results in well-formed block like crystals of **3-Zn-$PhNO_2$** in quantitative yields. Thermal analysis of these crystals showed a desolvation endotherm near 150 °C in DSC and 14.60 % weight loss in TGA (Figure 3.24). This mass loss is well below the value for the expected 1:2 solvate (21.01 %) and well above the value for a 1:1 solvate (11.74 %). In fact, this mass loss corresponds to a solvate in which the porphyrin and nitrobenzene molecules are

in 3:4 stoichiometry (Table 3.1). This is the first time in the series of **1-Zn**, **2-Zn** and **3-Zn** solvates the porphyrin and the guest are present in a 3:4 ratio. It will be of interest to know whether this stoichiometry is compatible with 4^4 networks or whether the structure of **3-Zn-PhNO$_2$** contains Zn···NO$_2$ recognition albeit with a different network topology.

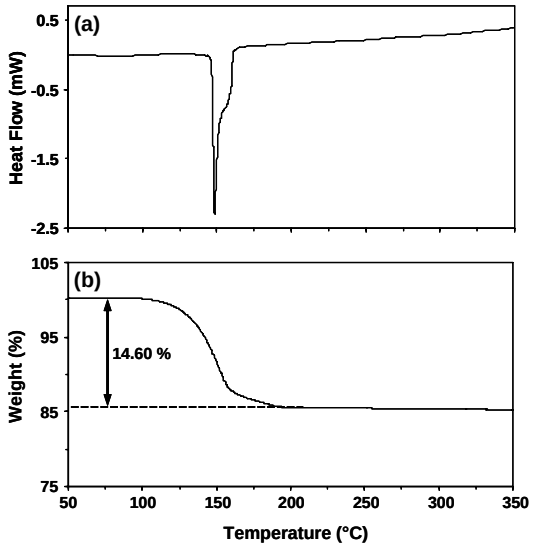

Figure 3.24 (a) DSC and **(b)** TGA plots of **3-Zn-PhNO$_2$** obtained from a solution of chloroform and nitrobenzene. The endotherm in **(a)** and weight loss in **(b)** correspond to the desolvation of nitrobenzene from the crystals.

Crystals of **3-Zn-PhNO$_2$** belong to the space group $P\bar{1}$ in which the asymmetric unit contains one and half molecules of porphyrin and two molecules of nitrobenzene. The overall structure of this solvate is totally different from any of the **1-Zn** or **2-Zn** solvates we have studied so far. The structure does not contain 4^4 networks based on Zn···NO$_2$ recognition. There is, however, partial and much weaker Zn···NO$_2$ recognition between the two symmetry independent molecules: one molecule (blue in Figure 3.25a) provides the nitro groups and the other (orange in Figure 3.25a) provides the Zn^{2+} ion. One of the nitro groups of the blue molecule and both nitro groups and the Zn^{2+} ion of the orange molecule do not participate in Zn···NO$_2$ recognition. Why does **3-Zn-PhNO$_2$** adopt a different structure and form insufficient and weaker Zn···O contacts? The answer to this question may be gleaned from other interactions in the structure of **3-Zn-PhNO$_2$**.

Figure 3.25b shows the layered structure of **3-Zn-PhNO$_2$**. The two symmetry independent porphyrin molecules pack into layers parallel to *bc*-plane. The **3-Zn** molecule sitting on an inversion center (Z' = 0.5; orange in Figure 3.25) is flat and located at (100) and the other porphyrin molecule located on a general position (Z' = 1; blue in Figure 3.25) is located at (300). Each independent molecule connects with symmetry related molecules (orange to orange and blue to blue) to form layers and these layers stack along the *a*-axis in ABBABB… pattern. The nitrobenzene guest molecules

are sandwiched between the layers such that one of them (green) is stacked above the porphyrin core of orange molecule and the other is located in some interstitial space.

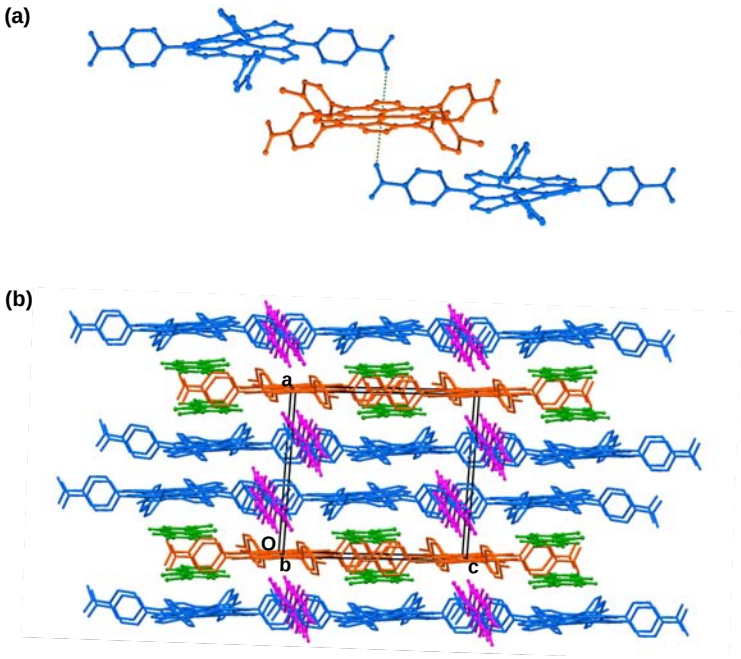

Figure 3.25 Crystal structure of **3-Zn-PhNO$_2$**. **(a)** Zn···NO_2 recognition between the Zn^{2+} ion of Z' = 1 porphyrin (orange) and one of the nitro groups of Z' = 0.5 porphyrin (blue). The Zn···O contacts are longer (3.15 Å) and weaker compared to those in other solvates discussed before. **(b)** Layered packing showing the ABBABB… pattern. For every layer of orange molecules there are two layers of blue molecules. Note that orange and blue molecules are at different heights along the *a*-axis. Notice the stacking of green nitrobenzene molecules on one side of the blue porphyrin core. The Zn^{2+} ion of blue porphyrin does not participate in Zn···NO_2 recognition. H-atoms are omitted.

Though there are two symmetry independent porphyrin layers, within each layer adjacent **3-Zn** molecules are connected by similar sets of interactions. For example, in the orange layer (Figure 3.26a), inversion related molecules along [110] are connected by short C–H···O hydrogen bonds (H···O: 2.65/2.71 Å; C···O: 3.69/3.72 Å; C–H···O: 159.3/154.7 °) to form one-dimensional tapes. These tapes are further linked by Br···NO_2 contacts (Br···O: 3.39/3.39 Å; C–Br···O: 147.0/143.7 °) along [01 $\bar{1}$] to form the layered structure. Similarly, the blue layer (Figure 3.26b) also consists of C–H···O hydrogen bond (H···O: 2.45/2.56 Å; C···O: 3.52/3.52 Å; C–H···O: 172.7/144.9 °) mediated tapes along [001] that are interconnected by Br···NO_2 contacts (Br···O: 3.26/3.48 Å; C–Br···O: 141.6/152.0 °) along [010]. It seems likely that these Br···NO_2 interactions combined with the C–H···O hydrogen bonds compete successfully with the Zn^{2+} ion so that only one of the two Zn^{2+} ions forms Zn···NO_2 recognition. We have also confirmed by PXRD (Figure 3.27) that the bulk samples of **3-Zn-PhNO$_2$** have the structure as the one discussed here.

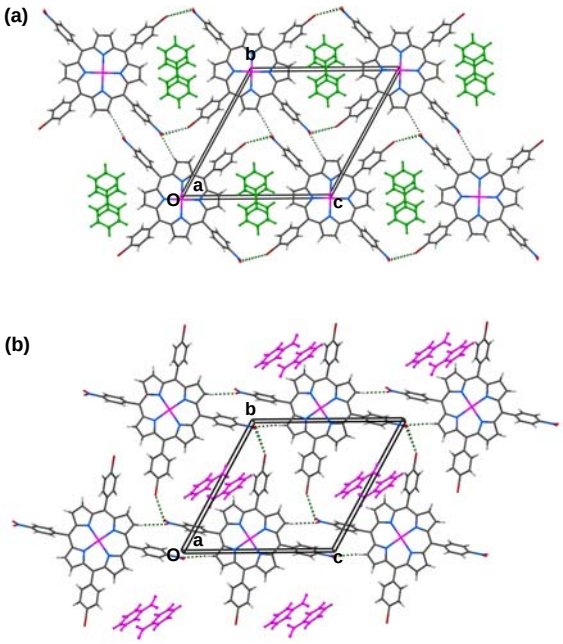

Figure 3.26 (a) Orange and **(b)** blue porphyrin layers in **3-Zn-PhNO$_2$**. In both cases, porphyrin molecules form linear tapes based on C–H···O hydrogen bonds. These tapes are further connected by Br···O interactions between -Br and -NO$_2$ groups. Superposition of the layers in **(a)** and **(b)** leads to the three-dimensional structure of **3-Zn-PhNO$_2$**.

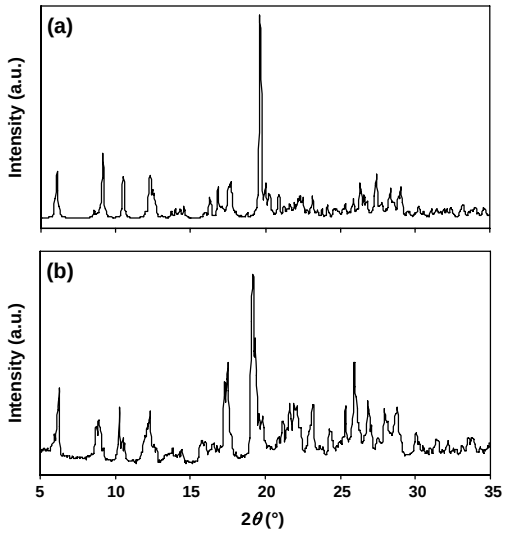

Figure 3.27 (a) Calculated and **(b)** experimental PXRD patterns of **3-Zn-PhNO$_2$**. Minor variations in the peak positions can be attributed to the difference in the temperature of X-ray data collection: **(a)** at -80 °C and **(b)** at 25 °C.

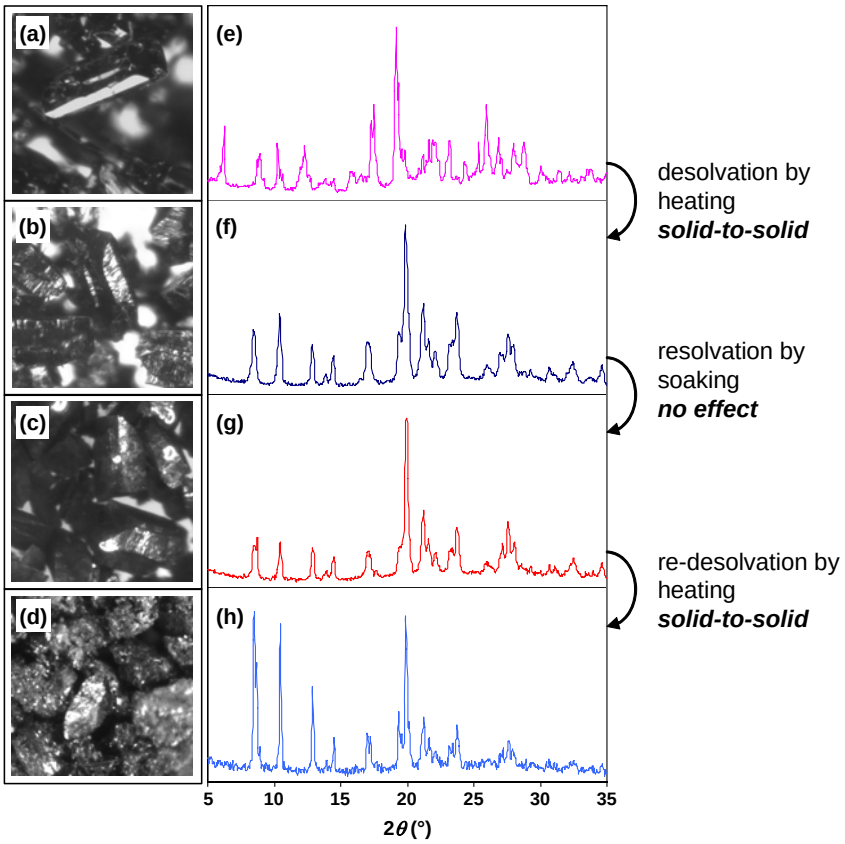

Figure 3.28 Desolvation, attempted resolvation, and re-desolvation of **3-Zn-PhNO$_2$** monitored by **(a-d)** optical microscopy and **(e-h)** PXRD analysis. The solution grown crystals of **3-Zn-PhNO$_2$ (a)** show a powder diffraction pattern **(e)** that is expected from single crystal structure described above. The crystals are not pulverized to avoid grinding induced desolvation. The desolvated crystals **(b)** show distinct color but retain the outward morphology of **3-Zn-PhNO$_2$**. The powder diffraction pattern **(f)** of desolvated crystals confirm the phase transition of **3-Zn-PhNO$_2$** to **3-Zn**. **(c)** Microscopic image of the desolvated crystals soaked in nitrobenzene for 1.5 hours. The crystals do not change their size (no dissolution) or color. **(g)** Powder diffraction pattern of the crystals shown in **(c)**. Notice the similarity of this pattern to that in **(e)**; no resolvation occurs when 3-Zn crystals are soaked in nitrobenzene for four hours or longer. (**d**) Re-desolvated material and (**h**) its diffraction pattern showing that no change occurs during this desolvation, because the crystals before and after the heating belong to the unsolvated phase of **3-Zn**. For PXRD patterns in **(e-h)**, the *y*-axis refers to diffraction intensity in arbitrary units.

3.14 DESOLVATION AND ATTEMPTED RESOLVATION OF 3-ZN-PHNO$_2$

We showed that **1-Zn** and **2-Zn** can reversibly intercalate nitrobenzene molecules through diffusion or dissolution mediated processes. Given that **3-Zn-PhNO$_2$** has a completely different structure, it is worth examining whether this solvate can be desolvated and resolvated. We followed the same procedure that we used for **1-Zn** and **2-Zn** resolvation. We obtained the crystals of **3-Zn-PhNO$_2$** (Figure 3.28a) by evaporating a solution of chloroform and nitrobenzene and collected powder X-ray data (Figure 3.28e) on these crystals to verify the bulk structure. We subject these crystals to heating in a TGA chamber to ensure complete desolvation and collected the powder X-ray pattern (Figure 3.28f) of these desolvated crystals (Figure 3.28b). It is surprising to note that desolvation of **3-Zn-PhNO$_2$**, which does not possess the Zn···NO$_2$ recognition mediated 4^4 networks, leads to **3-Zn**, which does possess these characteristics. It seems that in the absence of solvents **3-Zn** is capable of forming Zn···NO$_2$ recognition. We added two drops of nitrobenzene to the desolvated materials and allowed the crystals to soak in the solvent for two hours (Figure 3.28c). The PXRD pattern (Figure 3.28g) of these crystals showed no sign of resolvation and TGA experiment has confirmed this result (Figure 3.29). The re-desolvated crystals (Figure 3.28d) thus obtained belonged to the **3-Zn** non-solvate (Figure 3.28h).

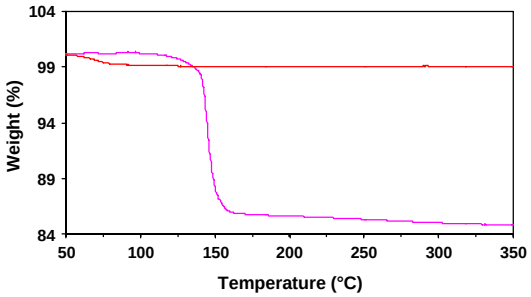

Figure 3.29 TGA plots of the solution grown crystals of **3-Zn-PhNO$_2$** (magenta) and samples of **3-Zn-PhNO$_2$** (red) obtained by soaking desolvated crystals in nitrobenzene for 1.5 hours. Notice that the red plot shows, at the onset of heating, a small percent of mass loss corresponding the physisorbed nitrobenzene solvent. No further desolvation occurs upon further heating indicating that resolvation of **3-Zn** does not lead to the formation of **3-Zn-PhNO$_2$**.

3.15 CHLOROFORM SOLVATE OF 3-ZN

Like **2-Zn**, compound **3-Zn** yields solvated crystals, **3-Zn-CHCl$_3$**, when crystallized from chloroform. These crystals undergo partial loss of solvent and become opaque when left at ambient temperature. Thermal analysis of these crystals (Figure 3.30) revealed a broad endotherm in DSC between 50-130 °C and 10.92 % mass loss in TGA (Table 3.1). The TGA data suggests that the porphyrin and the guest are in 1:1 stoichiometry in **3-Zn-CHCl$_3$**.

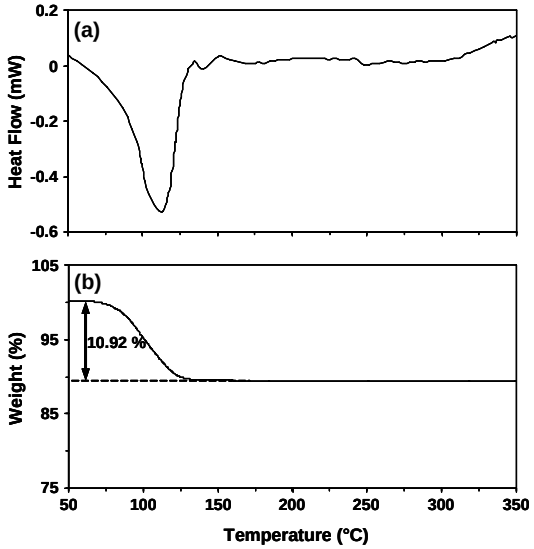

Figure 3.30 (a) DSC and **(b)** TGA plots of **3-Zn-CHCl$_3$**. The endotherm in **(a)** and weight loss in **(b)** correspond to the desolvation of chloroform from the crystals.

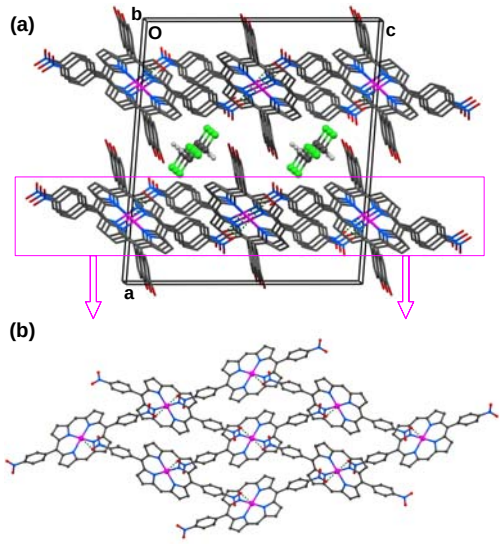

Figure 3.31 Crystal structure of **3-Zn-CHCl$_3$**. **(a)** Interlayer stacking. Notice interdigitated packing. Contrast this figure with the unsolvated **3-Zn** (Figure 3.23a) to note the decrease in the offset of layers. Disordered solvent molecules are located in the interlayer region. H-atoms are omitted. **(b)** 4^4 Networks formed by Zn···NO_2 recognition. Bromophenyl groups and H-atoms are omitted.

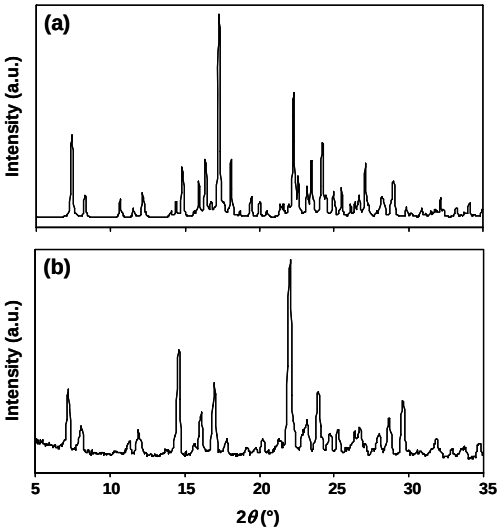

Figure 3.32 (a) Calculated and **(b)** experimental PXRD patterns of **3-Zn-CHCl$_3$**. These patterns indicate that the crystals in bulk samples have the same structure as the one reported above. The diffraction from the disordered chloroform molecules is included in the calculated pattern shown in **(a)**.

Crystals of **3-Zn-CHCl$_3$** belong to the space group *C*2/*c*; they are isostructural to **2-Zn-CHCl$_3$** and other related structures discussed before. They possess Zn···NO_2 recognition, 4^4 networks (Figure 3.31b) and the expected layered structure (Figure 3.31a). This result is in contrast to the structure of **3-Zn-PhNO$_2$** and more in line with our design principles. It seems that **3-Zn** can adopt the designed 4^4 network or a different structure depending on whether Zn^{2+} ions can compete successfully with C–Br and C–H groups for the nitro groups. The solvent molecules in **3-Zn-CHCl$_3$** are highly disordered; we located only some portions of these partially disordered molecules. Figure 3.32 shows the calculated (from single crystal data) and experimental PXRD patterns of **3-Zn-CHCl$_3$**. These patterns illustrate that the crystals in the bulk sample possess the same structure as that displayed in Figure 3.31.

3.16 ABUTTING LAYERS IN 3-ZN-PHCH$_3$, 3-ZN-PHCL, 3-ZN-PHBR AND 3-ZN-PHCN

Compound **3-Zn** forms 1:2 solvates with toluene, chlorobenzene, bromobenzene, and benzonitrile. All the solvates show desolvation endotherms in DSC (Figure 3.33).and appropriate weight loss corresponding to the solvent loss in TGA (Figure 3.34). The toluene and benzonitrile solvates are isostructural but they differ slightly from the chlorobenzene and bromobenzene solvates. All the four solvates possess the layered structures and the 4^4 networks stabilized by Zn···NO_2 recognition (Figures 3.35-3.37). Adjacent layers in all the solvates abut each other; they do not interlock as in the unsolvated **3-Zn** or the chloroform solvate. It is interesting to note that the benzonitrile

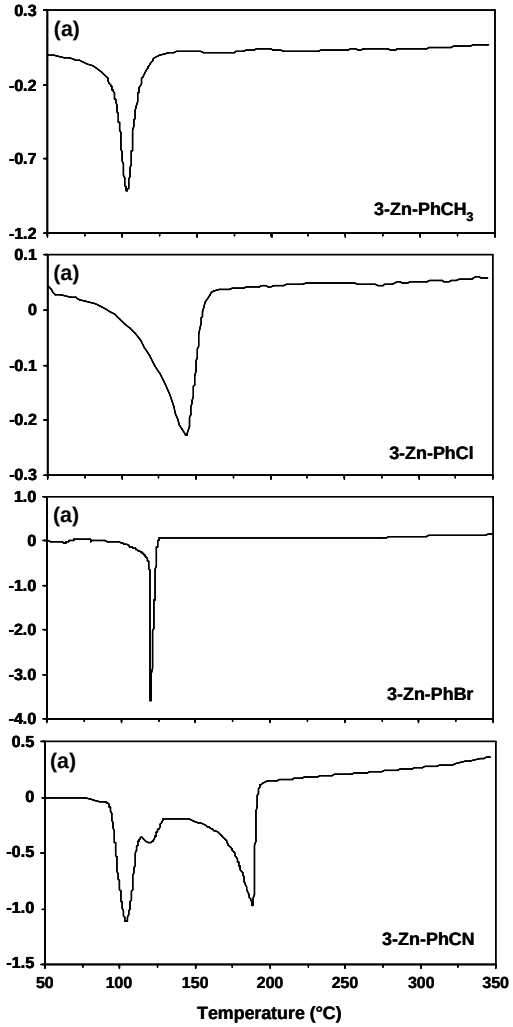

Figure 3.33 DSC plots of various solvates of **3-Zn**. In each case the endotherm corresponds to the desolvation of respective guest species from the crystals. The benzonitrile solvate shows two widely separated minima; these minima may correspond to sequential desolvation events.

solvate adopts a structure in which the guest molecules adopt a different pattern. In this pattern, the cyano group forms C–H···N interactions with the *meta*-C–H group of the adjacent benzonitrile molecule (H···N: 2.76 Å; C···N: 3.61 Å; C–H···N: 135.0 °) in addition to two more C–H···N interactions with the porphyrin C–H groups (H···N: 2.35/2.53 Å; C···N: 3.36/3.44 Å; C–H···N: 153.47/141.4 °). Similarly, the chlorbenzene and bromobenzene molecules adopt a different set of interactions in these **3-Zn** solvates.

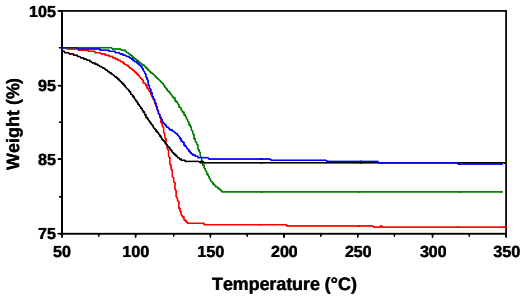

Figure 3.34 TGA plots of various solvates of **3-Zn**: black: **3-Zn-PhCH$_3$**, green: **3-Zn-PhCl**, red: **3-Zn-PhBr**, blue: **3-Zn-PhCN**.

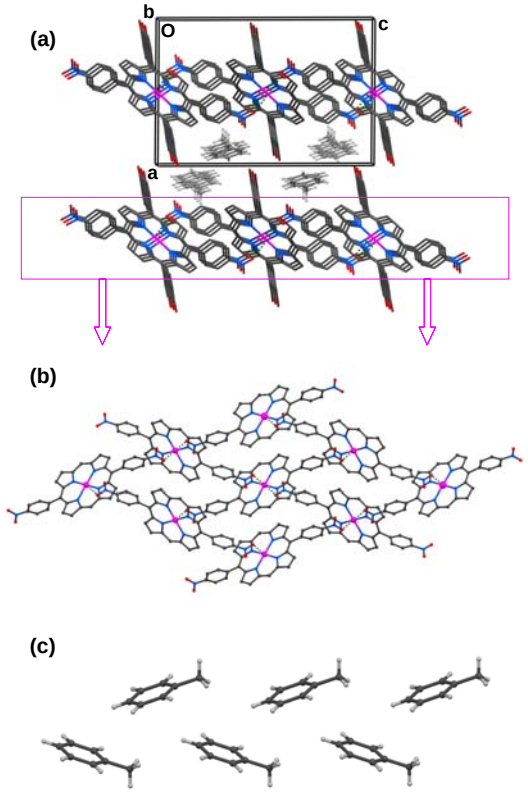

Figure 3.35 Crystal structure of **3-Zn-PhCH$_3$**. **(a)** Interlayer stacking. Notice that the chlorophenyl groups do not interlock as in **3-Zn** (Figure 3.23a) or **3-Zn-CHCl$_3$** (Figure 3.31a). Notice also the decrease in the offset of layers and increase in the separation between the layers. Toluene molecules are drawn with lighter colors. H-atoms of the porphyrin are omitted. **(b)** 4^4 Networks formed by Zn···NO$_2$ recognition. Bromophenyl groups and H-atoms are omitted. (**c**) One-dimensional bimolecular arrays of guest species confined to the interlayer region.

It is interesting to note that **3-Zn** adopts four different types of structures (non-solvate, chloroform solvate, toluene/benzonitrile solvates, and chlorobenzene/bromobenzene solvates; Table 3.2) that contain the Zn···NO_2 recognition and the 4^4 networks. Between all the solvates of **1-Zn**, **2-Zn**, and **3-Zn**, only one structure (**3-Zn-PhNO$_2$**) does not possess the expected layer structure. Even in this structure, one third of the Zn^{2+} ions participate in Zn···NO_2 recognition. All these structures indicate that Zn···NO_2 recognition is an effective coordination synthon that can be employed reliably and consistently to create predictable solid state structures that can function as sorption materials, reversible intercalators, and create guest assemblies with unique geometries.

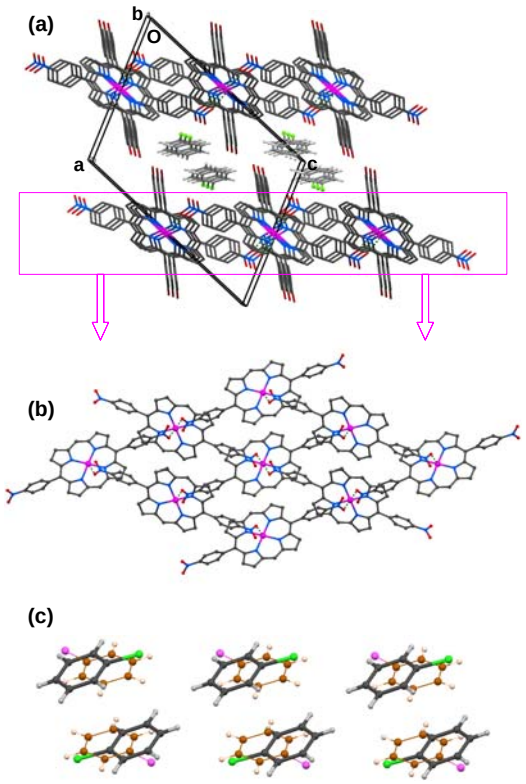

Figure 3.36 Crystal structure of **3-Zn-PhCl**. **(a)** Interlayer stacking. As in **3-Zn-PhCH$_3$** (Figure 3.35a) the chlorophenyl groups abut each other and do not interlock. Notice the small differences in the offsets, guest arrangements, and the unit cell geometries. Chlorobenzene molecules are drawn with lighter colors. H-atoms of the porphyrin are omitted. **(b)** 4^4 Networks formed by Zn···NO_2 recognition. Bromophenyl groups and H-atoms are omitted. (**c**) One-dimensional bimolecular arrays of guest species confined to the interlayer region. Chlorobenzene molecules are disordered over two positions and here each position is shown with a unique color scheme. Crystals of **3-Zn-PhBr** are isostructural to **3-Zn-PhCl** and display the same packing features shown here.

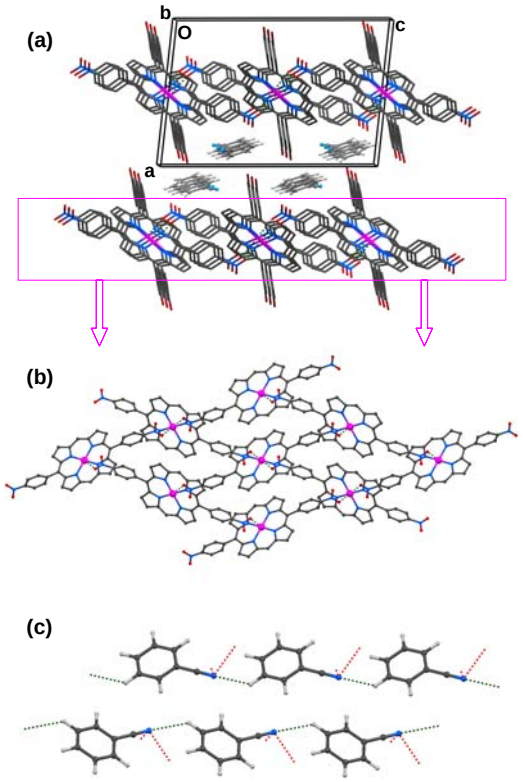

Figure 3.37 Crystal structure of **3-Zn-PhCN**. **(a)** Interlayer stacking. Notice the close similarity between this structure and that of **3-Zn-PhCH$_3$** (Figure 3.35a). Notice the differences in the orientations of the guest species within the interlayer region. Benzonitrile molecules are drawn with lighter colors. H-atoms of the porphyrin are omitted. **(b)** 4^4 Networks formed by Zn···NO_2 recognition. Bromophenyl groups and H-atoms are omitted. (**c**) One-dimensional bimolecular arrays of guest species confined to the interlayer region. Notice the C–H···N interactions (green dashed lines) between successive benzonitrile molecules. The C–H···N interactions between porphyrin and guest species are indicated with red dashed lines.

3.17 DESOLVATION AND RESOLVATION OF 3-ZN-PHCH$_3$

Noting that crystals of **3-Zn-PhNO$_2$** resist resolvation, we wished to test if this resistance is specific to the solvate or generic to the host **3-Zn** itself. The **3-Zn-PhNO$_2$** has a structure that did not favor the resolvation, so it seemed reasonable to test one of the solvates discussed in Section 3.16 for resolvation experiments. Compound **3-Zn** is sparingly soluble in toluene, and we studied the resolvation using this solvate. We obtained the crystals of **3-Zn-PhCH$_3$** (Figure 3.38a) by evaporating a solution of chloroform and toluene and collected powder X-ray data (Figure 3.38e) on these crystals to verify the bulk structure. We subject these crystals heating in a TGA chamber to

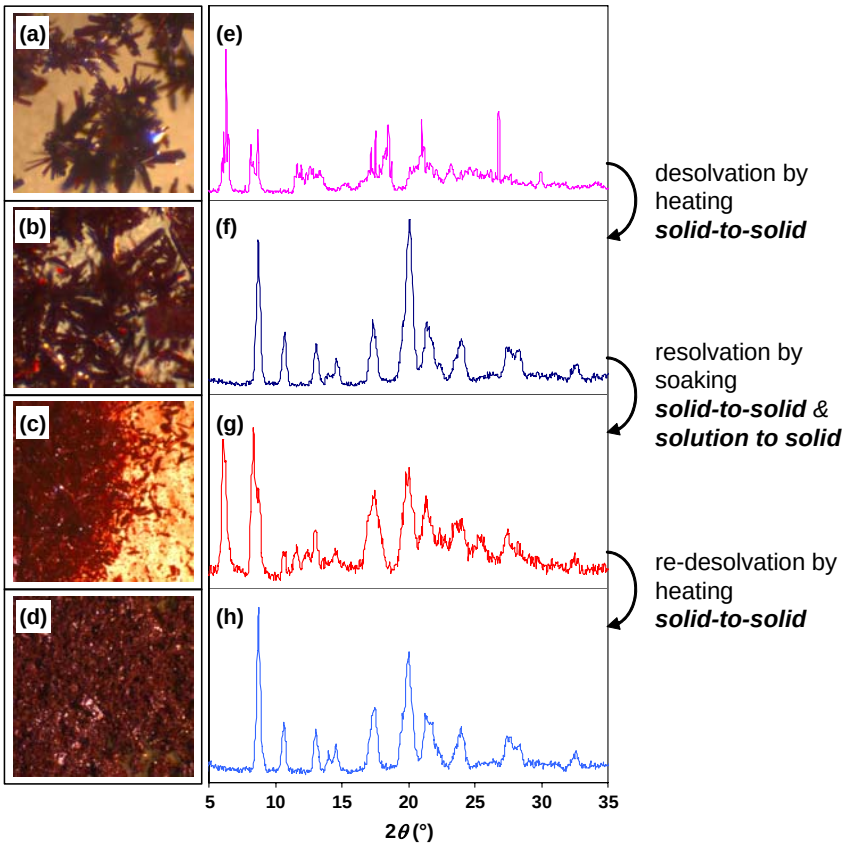

Figure 3.38 Desolvation, resolvation, and re-desolvation of **3-Zn-PhCH$_3$** monitored by **(a-d)** optical microscopy and **(e-h)** PXRD analysis. The solution grown crystals of **2-Zn-PhNO$_2$ (a)** show fewer peaks in the powder diffraction pattern **(e)** than expected. The crystals are not pulverized to avoid grinding induced desolvation; they adopt preferred orientation on sample holders and give fewer diffraction peaks. The desolvated crystals **(b)** become slightly opaque but retain the morphology of **3-Zn-PhCH$_3$**. The powder diffraction pattern **(f)** of desolvated crystals confirm the phase transition of **3-Zn-PhCH$_3$** to **3-Zn**. **(c)** Microscopic image of the desolvated crystals soaked in toluene for two hours. The crystals do not change in size or morphology; their dissolution in toluene is minimal. **(g)** Powder diffraction pattern of the crystals shown in **(c)**. Notice the peaks corresponding to **3-Zn** as well as **3-Zn-PhCH$_3$**. (**d**) Re-desolvated material and (**h**) its diffraction pattern confirming the full desolvation in the second cycle. For PXRD patterns in **(e-h)**, the *y*-axis refers to diffraction intensity in arbitrary units.

ensure complete desolvation and collected the powder X-ray pattern (Figure 3.38f) of these desolvated crystals (Figure 3.38b). These crystals possessed the structure of **3-Zn** non-solvate discussed in Section 3.12. We added few drops of toluene to the desolvated materials and allowed the crystals to soak in the solvent for two hours (Figure 3.38c). The

PXRD pattern (Figure 3.38g) of these crystals showed peaks corresponding to both the non-solvate and the solvate, and TGA experiment has confirmed this result (Figure 3.39). The re-desolvated crystals (Figure 3.38d) obtained from the TGA experiment belonged to the **3-Zn** non-solvate (Figure 3.38h).

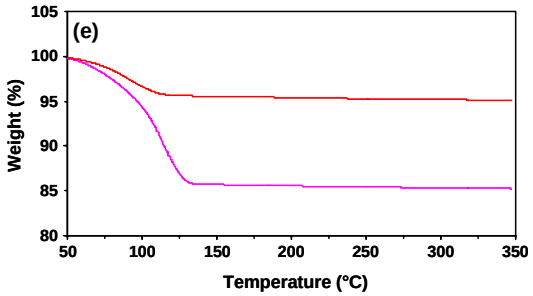

Figure 3.39 TGA plots of the solution grown crystals of **3-Zn-PhCH$_3$** (magenta) and samples of **3-Zn-PhCH$_3$** (red) obtained by soaking desolvated crystals in nitrobenzene for two hours. The red plot is result of heating the resolvated crystals of **3-Zn-PhCH$_3$** and un-resolvated **3-Zn**; this is the reason the red plot shows a smaller percentage of weight loss.

3.18 EXPERIMENTAL

3.18.1 Synthesis. All the solvents were purchased from Pharmco and rest of the chemicals were purchased from Alfa Aesar and used as received in the synthesis (Figure 2.3) and crystallization. Dueterated solvents were purchased from Norell. The NMR spectra were recorded on a Bruker 400 MHz or a Bruker 500 MHz spectrometer. The IR spectra were recorded in the ATR (attenuated total reflection) mode on a Perkin Elmer Spectrum One spectrometer. Thermal and diffraction methods are described in Chapter 1.

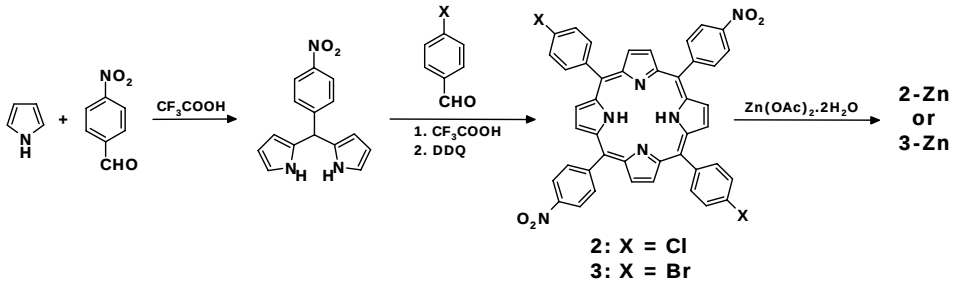

Figure 3.40 Modular synthesis of metalloporphyrins **2-Zn** and **3-Zn** starting from pyrrole, *p*-nitrobenzaldehyde and 4-chlorobenzaldehyde or 4-bromobenzaldehyde.

3.18.1.1 Synthesis of 5,15-di(4-nitrophenyl)-10,20-di(4-chorophenyl)porphyrin (2) and 2-Zn. Condensation of 5-4-nitrophenyldipyrromethane (4 mmol, 1.07 g) and 4-chlorobenzaldehyde (4 mmol, 0.56 g) in CH_2Cl_2 (400 mL) with TFA (7.12 mmol, 0.55

mL) gave a purple solid (0.175 g; 11.3%). The procedure for the synthesis of **1** described in Chapter 2 is used for this synthesis. ^{1}H-NMR ($CDCl_3$): -2.83 (br. s, 2 H, NH); 7.76 (d, 4 H); 8.13 (d, 4 H); 8.39 (d, 4 H); 8.66 (d, 4 H); 8.78 (d, 4 H, β_1-pyrrole); 8.88 (d, 4 H, β_2-pyrrole). Metallation of **2** is performed using zinc acetate dihydrate using the procedure in Chapter 2.

3.18.1.2 Synthesis of 5,15-di(4-nitrophenyl)-10,20-di(4-bromophenyl)porphyrin (3) and 3-Zn. Condensation of 5-4-nitrophenyldipyrromethane (4 mmol, 1.07 g) and 4-bromobenzaldehyde (4 mmol, 0.74 g) in CH_2Cl_2 (400 mL) with TFA (7.12 mmol, 0.55 mL) gave a purple solid (0.16 g; 9.3 %). The procedure for the synthesis of **1** described in Chapter 2 is used for this synthesis. ^{1}H-NMR ($CDCl_3$): -2.84 (br. s, 2 H, NH); 7.92 (d, 4 H); 8.07 (d, 4 H); 8.39 (d, 4 H); 8.66 (d, 4 H); 8.78 (d, 4 H, β_1-pyrrole); 8.90 (d, 4 H, β_2-pyrrole). Metallation of **3** is performed using zinc acetate dihydrate using the procedure in Chapter 2.

3.19 SUMMARY AND CONCLUSION

This effect of introducing the chloro and bromo groups on the porphyrin template **1-Zn** is explored in this chapter. Chloro, methyl, and bromo groups are often used as structural equivalents in crystal engineering. In this work, we showed that compared to **1-Zn**, chloro and bormo substituted porphyrins **2-Zn** and **3-Zn** display dramatically different guest inclusion properties. These compounds can intercalate guest species as small as acetonitrile or as large as *o*-nitrotoluene. Remarkably, this inclusion of various guests occurs while preserving the salient features of our crystal design: Zn···NO_2 recognition, nearly flat 4^4 networks, and layered structures with interlayer spaces for housing the guests. At the same time, insertion of guests of different steric and electronic character resulted in a rich variety of structures. To date, we have determined six different types of crystal structures (Table 3.2) that abide by our design principles. In these six types of structures, most of the changes occur in the interlayer region while conserving the intralayer arrangements. Typically, the layers shift with respect one another laterally (offset) or vertically (separation) to enlarge or shrink space available for the guests.

Among the many solvates based on Zn-metallated porphyrins, only one solvate does not contain the predicted 4^4 network. It does, however, exhibit Zn···NO_2 recognition, albeit with weaker Zn···O bonds. In this case, the bromo group competes successfully with the Zn^{2+} ion for the nitro group and forms polarization induced Br···O contacts. In the next chapter, we will discuss the effect of introducing stronger ligands that can bind to Zn^{2+} ions and some interesting architectures and properties that develop from these new metal ligand bonds. Overall, the work presented in Chapters 2 and 3 clearly illustrates that the Zn···NO_2 recognition is an effective synthon that can be used to design layered porous solids whose chemical and geometrical attributes can be controlled by several independent modifications. These changes include replacement of metal cations (e.g. Co^{2+}), nitro groups (e.g., acetyl), side arm groups (e.g., naphthyl), and other substituents on the periphery of the porphyrin. By tailoring these changes judiciously, we believe that it will be possible to design materials that can selectively absorb specific guest species.

3.20 REFERENCES

1. Holman, K. T.; Pivovar, A. M.; Swift, J. A.; Ward, M. D., Metric Engineering of Soft Molecular Host Frameworks. *Acc. Chem. Res.* **2001,** *34*, 107-118.
2. Biradha, K.; Fujita, M., Layered materials by design: 2D coordination polymeric networks containing large cavities/channels. *Perspectives in Supramolecular Chemistry* **2003,** *7*, 211-239.
3. Nakano, K.; Sada, K.; Nakagawa, K.; Aburaya, K.; Yoswathananont, N.; Tohnai, N.; Miyata, M., Organic intercalation material: reversible change in interlayer distances by guest release and insertion in sandwich-type inclusion crystals of cholic acid. *Chem. Eur. J.* **2005,** *11*, 1725-33.
4. Desiraju, G. R., Supramolecular synthons in crystal engineering - a new organic synthesis. *Angew. Chem. Int. Ed.* **1995,** *34*, 2311-2327.
5. Fleischer, E. B.; Shachter, A. M., Coordination oligomers and a coordination polymer of zinc tetraarylporphyrins. *Inorganic Chemistry* **1991,** *30*, 3763-3769.
6. Abrahams, B. F.; Hoskins, B. F.; Michall, D. M.; Robson, R., Assembly of porphyrin building blocks into network structures with large channels. *Nature* **1994,** *369*, 727-729.
7. Drain, C. M.; Lehn, J.-M., Self-assembly of square multiporphyrin arrays by metal ion coordination. *J. Chem. Soc., Chem. Commun.* **1994**, 2313-2315.
8. Krupitsky, H.; Stein, Z.; Goldberg, I.; Strouse, C. E., Crystalline complexes, coordination polymers and aggregation modes of tetra(4-pyridyl)porphyrin. *J. Incl. Phenom. Mol. Recog.* **1994,** *18*, 177-192.
9. Lin, K.-J., SMTP-1: the first functionalized metalloporphyrin molecular sieves with large channels. *Angew. Chem. Int. Ed.* **1999,** *38*, 2730-2732.
10. Pan, L.; Wang, X.; Noll, B. C., Self-assembly of free-base tetrapyridylporphyrin units by metal ion coordination. *Chem. Commun.* **1999**, 157-158.
11. Diskin-Posner, Y.; Dahal, S.; Goldberg, I., New effective synthons for supramolecular self-assembly of meso-carboxyphenylporphyrins. *Chem. Commun.* **2000**, 585-586.
12. Haycock, R. A.; Hunter, C. A.; James, D. A.; Michelsen, U.; Sutton, L. R., Self-Assembly of Oligomeric Porphyrin Rings. *Organic Letters* **2000,** *2*, 2435-2438.
13. Michelsen, U.; Hunter, C. A., Self-assembled porphyrin polymers. *Angew. Chem. Int. Ed.* **2000,** *39*, 764-767.
14. Sanders, J. K. M.; Bampos, N.; Clyde-Watson, Z.; Darling, S. L.; Hawley, J. C.; Kim, H.-J.; Mak, C. C.; Webb, S. J., Axial coordination chemistry of metalloporphyrins. *Porphyrin Handbook* **2000,** *3*, 1-48.
15. Diskin-Posner, Y.; Patra, G. K.; Goldberg, I., Crystal engineering of 2-D and 3-D multiporphyrin architectures - The versatile topologies of tetracarboxyphenyl-porphyrin based materials. *Eur. J. Inorg. Chem.* **2001**, 2515-2523.
16. Diskin-Posner, Y.; Patra, G. K.; Goldberg, I., Crystal engineering of metalloporphyrin assemblies. New supramolecular architectures mediated by bipyridyl ligands. *Chem. Comm.* **2002**, 1420-1421.
17. Kosal, M. E.; Chou, J.-H.; Wilson, S. R.; Suslick, K. S., A functional zeolite analogue assembled from metalloporphyrins. *Nature Materials* **2002,** *1*, 118-121.

18. Shmilovits, M.; Vinodu, M.; Goldberg, I., Coordination Polymers of Tetra(4-carboxyphenyl)porphyrins Sustained by Tetrahedral Zinc Ion Linkers. *Cryst. Growth Des.* **2004,** *4*, 633-638.
19. Deiters, E.; Bulach, V.; Kyritsakas, N.; Hosseini, M. W., Molecular tectonics: coordination networks based on porphyrins bearing pyridine N-oxide groups as coordinating sites. *New J. Chem.* **2005,** *29*, 1508-1513.
20. Goldberg, I., Crystal engineering of porphyrin framework solids. *Chem. Comm.* **2005**, 1243-1254.
21. Hosseini, M. W., Molecular Tectonics: From Simple Tectons to Complex Molecular Networks. *Acc. Chem. Res.* **2005,** *38*, 313-323.
22. Suslick, K. S.; Bhyrappa, P.; Chou, J. H.; Kosal, M. E.; Nakagaki, S.; Smithenry, D. W.; Wilson, S. R., Microporous Porphyrin Solids. *Acc. Chem. Res.* **2005,** *38*, 283-291.
23. Desiraju, G. R.; Sarma, J. A. R. P., The chloro-methyl exchange rule and its violations in the packing of organic molecular solids. *Pro. Ind. Acad. Sci.* **1986,** *96*, 599-605.
24. Edwards, M. R.; Jones, W.; Motherwell, W. D. S., Cocrystal formation of 4-methyl and 4-chlorobenzamide with carboxylic acids: chloro/methyl interchange and crystal structure. *CrystEngComm* **2006,** *8*, 545-551.
25. Dabros, M.; Emery, P. R.; Thalladi, V. R., A supramolecular approach to organic alloys: cocrystals and three- and four-component solid solutions of 1,4-diazabicyclo[2.2.2]octane and 4-X-phenols (X = Cl, CH3, Br). *Angew. Chem. Int. Ed.* **2007,** *46*, 4132-4135.
26. Pedireddi, V. R.; Sarma, J. A. R. P.; Desiraju, G. R., Crystal engineering and solid state chemistry of some b-nitrostyrenes. *J. Chem. Soc. Perkin Trans. 2* **1992**, 311-20.
27. Desiraju, G. R.; Pedireddi, V. R.; Sarma, J. A. R. P.; Zacharias, D. E., Determination of the crystal structure of 4-iodo-b-nitrostyrene with the aid of packing considerations: a study of halogen...nitro interactions. *Acta Chim. Hungar.* **1993,** *130*, 451-65.
28. Thalladi, V. R.; Goud, B. S.; Hoy, V. J.; Allen, F. H.; Howard, J. A. K.; Desiraju, G. R., Supramolecular synthons in crystal engineering. Structure simplification, synthon robustness and supramolecular retrosynthesis. *Chem. Commmun.* **1996**, 401-2.

4 MULTI-STEP SINGLE CRYSTAL TO SINGLE CRYSTAL TRANSFORMATIONS IN DIPYRIDYL PORPHYRINS

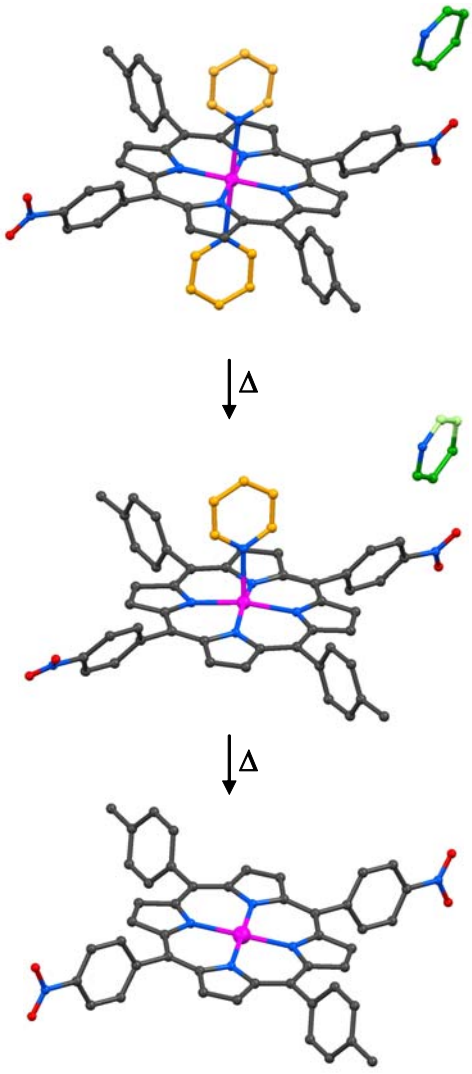

4.1 INTRODUCTION

In previous chapters, we discussed the application of a new coordination synthon, Zn···NO_2 recognition, in forming predictable network structures. This synthon is based on weak bonding between nitro groups and Zn^{2+} ions embedded in the porphyrin core. We witnessed that introduction of the bromo group on the porphyrin can potentially disrupt the formation of this synthon. The bromo group and the Zn^{2+} ion compete with each other to interact with the nitro group; in our work, the latter always succeeded in this competition except in one instance. We wished to create new structures with ligands that can form stronger bonds with Zn^{2+} ions; in this context we prepared several new coordination complexes of **1-Zn**, **2-Zn** and **3-Zn** with aniline and its derivatives and pyridine and its derivatives. These new complexes exhibit rich structural diversity; in this chapter we discuss the pyridine complexes of **1-Zn**, **2-Zn** and **3-Zn** because they display remarkable multi-step single crystal to single crystal (**scsc**) transformations.[1]

Solid to solid phase transitions involve change in crystal structure and also often change in mass. These transitions rarely retain the integrity of single crystals because the components are subjected to large motions to adjust to the changes in local environments and overall volume of the crystals.[2-4] For this reason, most **scsc** transformations are discovered only in metal-organic frameworks or other kinds of extended solids.[5-7] In these solids, the phase change typically involves loss of solvent or ligands that are not integral to the framework, or minor rearrangements of the networks that do not destroy the bonds responsible for building the frameworks. In this context, the experiments reported in this chapter offer one of the first examples of **scsc** transformations that involve multi-step desolvation and de-ligation (removal of ligand) and drastic changes in the structure and volume of the crystals.

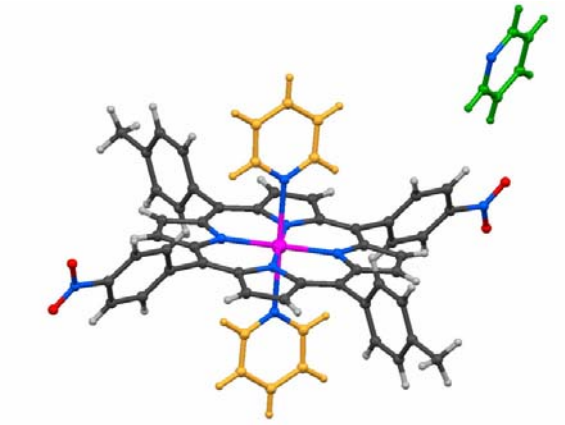

Figure 4.1 Molecular structure of **1-Zn-Py$_3$**. Notice the tetragonal coordination environment around the zinc at the center of porphyrin. Ligand pyridine molecules are drawn in yellow and the solvated pyridine in green. Color scheme: Zn-magenta; O-red; N-blue; and C-grey. Similar color scheme is followed for other figures in this thesis.

4.2 ISOSTRUCTURAL PYRIDINE COMPLEXES OF 1-ZN, 2-ZN AND 3-ZN

The pyridine ligand has a much higher affinity for the Zn^{2+} ion than the nitro group. Crystallization of the porphyrins **1-Zn**, **2-Zn** and **3-Zn** from solutions containing pyridine resulted in *discrete* coordination complexes containing the porphyrins and pyridine in 1:3 ratio. All the three crystals, **1-Zn-Py$_3$, 2-Zn-Py$_3$** and **3-Zn-Py$_3$**, are isostructural and belong to the space group *C2*/c. Two of the pyridine molecules act as ligands and the third is a solvated guest molecule. When the difference between these ligand (**L**) and solvate (**S**) pyridine molecules need to be emphasized, we denote these systems in the manner **1-Zn-L$_2$-S$_1$**. The asymmetric unit in each of the crystals contains half metallo-porphyrin that is located on an inversion center, one pyridine ligand, and half pyridine solvate that is located on a 2-fold axis. Molecular structure of **1-Zn-Py$_3$** is shown in Figure 4.1; the other two complexes have similar structures. The two pyridine ligands bind the Zn^{2+} ion at the axial positions to create a discrete complex that has six arms. The hub-and-spoke shape of this molecule limits its close packing and solvated pyridine is an integral part of the overall packing in the crystal. This solvated pyridine is attached to neighboring host molecules through short intermolecular C–H···N (Table 1), C–H···O, and C–H···π interactions in all the three crystals. In these interactions, the solvated pyridine acts as donor as well as acceptors.

Table 3.1 Parameters for C–H···O and C–H···N interactions in the pyridine complexes of **1-Zn**, **2-Zn** and **3-Zn**. Interaction **(a)** refers to the 2^2 network, **(b)** to the connection between 2^2 networks and **(c)** to the binding of the complex with pyridine solvate.

Compound	Interaction	D–H···A	H···A (Å)	D–H···A (°)
1-Zn-Py$_3$	**(a)**	C–H···O	2.52	143
	(b)	C–H···O	2.57	168
	(c)	C–H···N	2.59	152
2-Zn-Py$_3$	**(a)**	C–H···O	2.49	143
	(b)	C–H···O	2.56	164
	(c)	C–H···N	2.56	155
3-Zn-Py$_3$	**(a)**	C–H···O	2.56	143
	(b)	C–H···O	2.57	168
	(c)	C–H···N	2.59	152

4.3 FROM 4^4 NETWORKS TO 2^2 NETWORKS

We showed in previous chapters that unperturbed Zn···NO_2 recognition leads to 4^4 coordination networks. In these networks, each porphyrin donates two and accepts two Zn···O contacts and connects to four other neighbors (Figure 4.2a). The smallest loop in the network contains four porphyrins. When the metallo-porphyrins are bound to pyridine ligands, the nitro groups form short C–H···O hydrogen bonds (Table 3.1; interaction **a**) with the C–H groups of the pyridine ligands. Each porphyrin donates two and accepts two C–H···O hydrogen bonds but connects to only *two* other neighbors. Successive porphyrins connected through these interactions lead to 2^2 networks (Figure 4.2b). The

smallest loop in these networks contains *two* porphyrins. Formation of a 4^4 network leads to greater void spaces compared to the 2^2 network (Figure 4.2). In pyridine complexes the C–H···O bonds are formed at the periphery of the pyridyl ligands. If these bonds were to be part of a 4^4 network, they would lead to large voids that must be filled with solvent molecules or by another network through interpenetration. The problem of void spaces in pyridine complexes is minimized by adopting networks with 2^2 topologies (Figure 4.3).

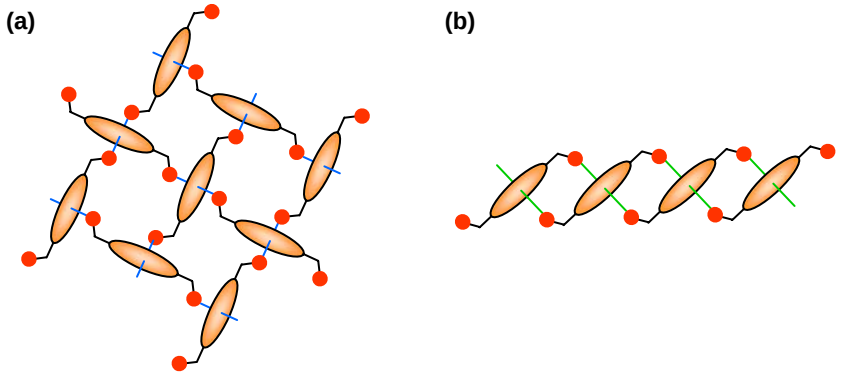

Figure 4.2 Schematic representations of 4^4 and 2^2 networks formed by porphyrins. Notice the larger voids in 4^4 networks compared to the 2^2 networks. Blue and green lines indicate Zn···O contacts and C–H···O interactions respectively.

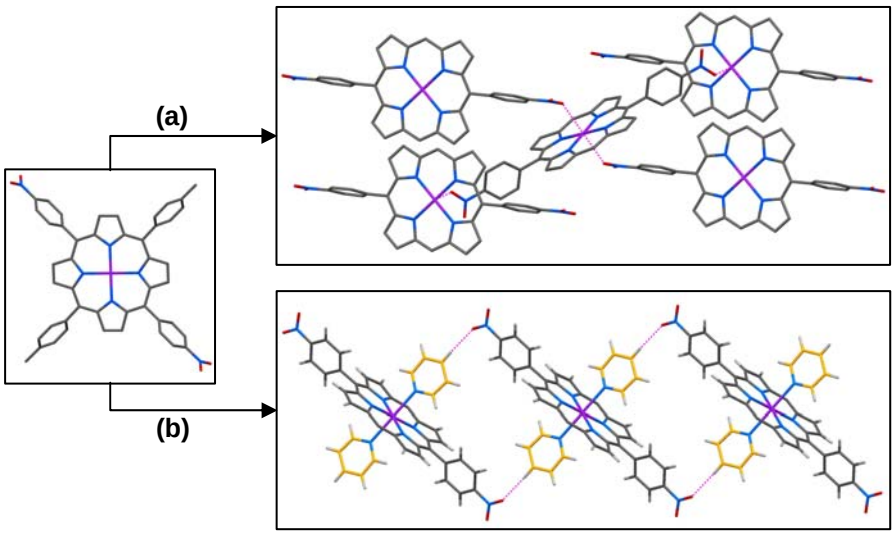

Figure 4.3 Crystal structures of **(a) 1-Zn** and **(b)** its pyridine complex showing 4^4 networks in the former and 2^2 networks in the latter.

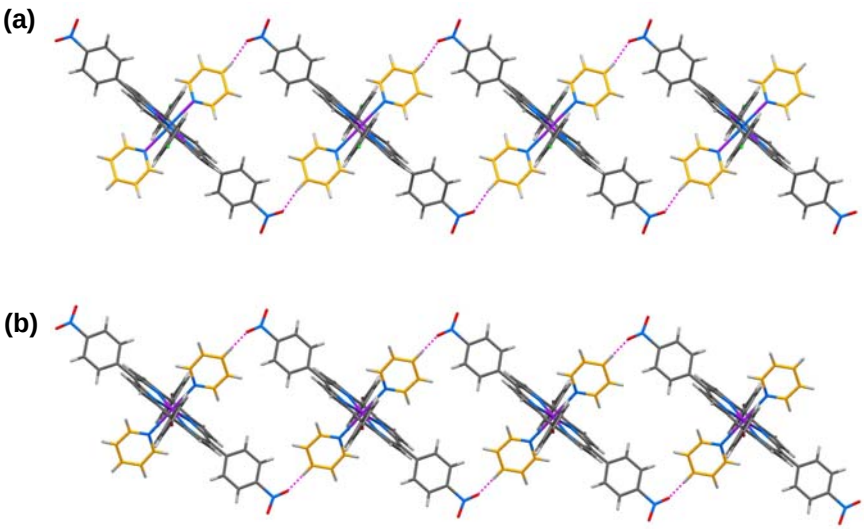

Figure 4.4 Crystal structures of **(a) 2-Zn-Py$_3$** and **(b) 3-Zn-Py$_3$** showing 2^2 networks built on C–H···O hydrogen bonds.

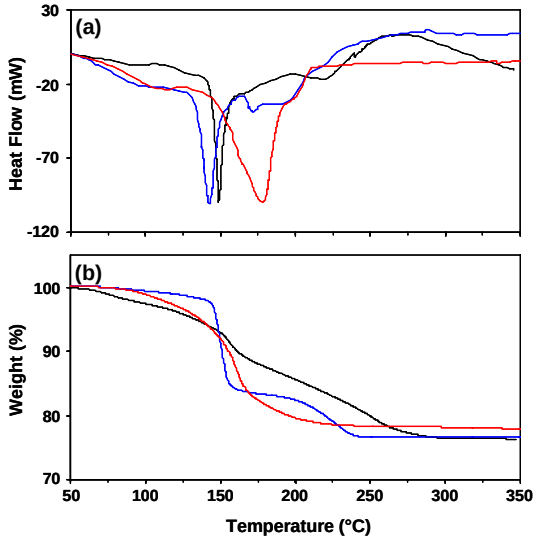

Figure 4.5 (a) DSC and **(b)** TGA plots of **1-Zn-Py$_3$** (black), **2-Zn-Py$_3$** (blue) and **3-Zn-Py$_3$** (red). Notice the two step mass loss in blue and black TGA plots and the corresponding endotherms in DSC plots.

4.4 THERMAL ANALYSIS OF PYRIDINE COMPLEXES

In order to establish the stoichiometry in bulk samples, the three pyridine complexes listed above are subjected to thermal analysis by DSC and TGA methods. For crystals of **1-Zn-Py$_3$** and **2-Zn-Py$_3$** TGA plots showed two step desolvation process (Figure 4.5). While the two steps are not clearly separated, it seems that the first step involves the loss of half of the pyridine molecules. This first step can be seen as a nearly vertical drop in the graph around 150 ºC in the TGA. It is difficult to ascertain the origin of this loss of one and half molecules of pyridine. It is likely that the solvated pyridine is removed during this first step, but the loss of half a pyridine molecule from **1-Zn-L$_2$** or **2-Zn-L$_2$** is hard to fathom. During the second stage of the heating (150-250 ºC) the remaining pyridine molecules are lost and result in the de-pyridinated porphyrins. In **3-Zn-Py$_3$** the loss of pyridines appears continuous at the rate of heating (10 ºC per minute) we used in the TGA experiments.

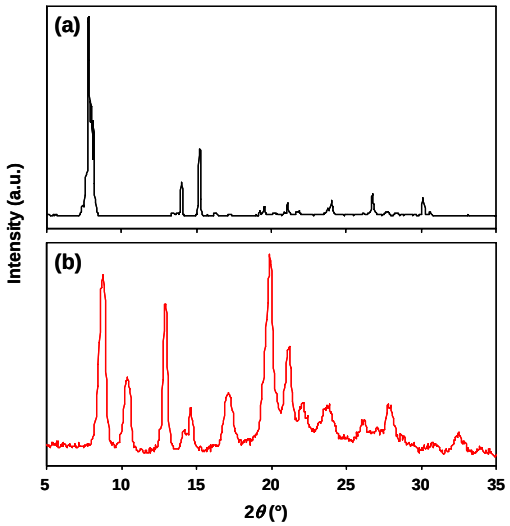

Figure 4.6 PXRD patterns of **1-Zn-Py$_3$** crystals collected **(a)** immediately after taken out of solution and **(b)** after heating to 160 °C. Notice the distinct differences between the two patterns. The material used in **(a)** is not pulverized; fewer peaks than expected show in this pattern due to the partial preferred orientation of the crystals. Compare pattern **(b)** to that in Figure 2.8b to note that heating of **1-Zn-Py$_3$** results in the crystals of unsolvated **1-Zn**.

4.5 POWDER DIFFRACTION ANALYSIS OF DE-PYRIDINATED CRYSTALS

Crystals of **1-Zn-Py$_3$**, **2-Zn-Py$_3$** and **3-Zn-Py$_3$** subjected to TGA appeared unchanged even after the removal of solvated and bound pyridine molecules. There is no discernible change in the morphology under an optical microscope and no signs of crystal shattering are observed. This is surprising given that heating, and loss of solvent and ligand molecules, should involve large movement of porphyrin molecules in the crystal lattice. After de-pyridination, powder X-ray diffraction (PXRD) was carried out in order to

verify whether or not the resulting solid was crystalline. Figures 4.6-4.7 show the diffraction patterns recorded before and after TGA of **1-Zn-Py$_3$**, **2-Zn-Py$_3$** and **3-Zn-Py$_3$**. In all three cases, the PXRD analyses show that the solid products obtained after the heating are indeed crystalline; however, the patterns show definite differences from the patterns of *fully-solvated* crystals. These results indicate that the products have different crystal structures than the fully-solvated crystals; indeed the patterns of heated products match the patterns of unsolvated and un-ligated **1-Zn**, **2-Zn** and **3-Zn** obtained directly from the synthesis (*cf*. Figures 2.8, 3.3 and 3.28).

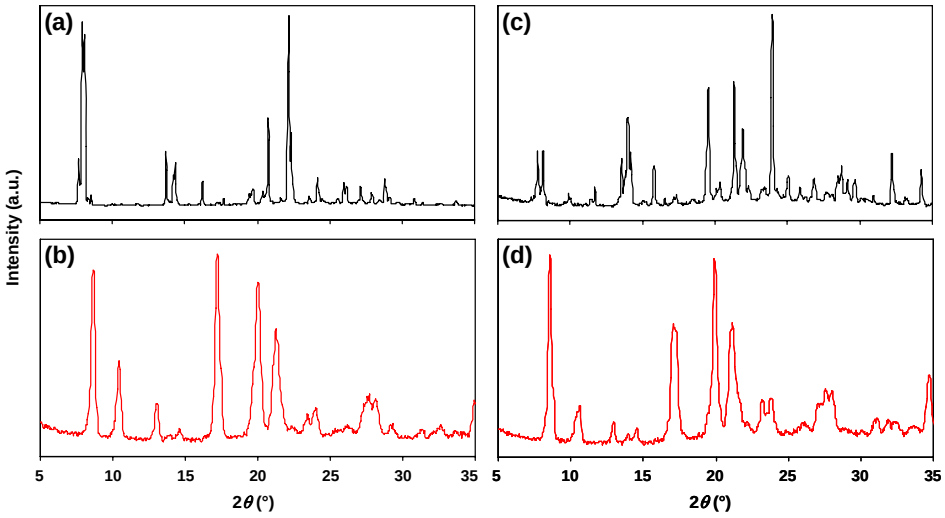

Figure 4.7 PXRD patterns of (left) **2-Zn-Py$_3$** and (right) **3-Zn-Py$_3$** crystals collected **(a** and **c)** immediately after taken out of solution and **(b** and **d)** after heating to 160 °C. Notice the distinct differences between the two patterns. The materials used in **(a** and **c)** are not pulverized. Compare patterns **(b** and **d)** to those in Figures 3.3 and 3.28f to note that heating of **1-Zn-Py$_3$** results in the crystals of unsolvated **2-Zn** and **3-Zn**.

4.6 STEPWISE DESOLVATION AND DE-LIGATION

The thermal analysis discussed in Section 4.4 provides evidence of a two step desolvation process. PXRD and optical microscopy indicate that the de-pyridination results in a crystalline solid without change in morphology or structural integrity (crystals do not shatter). We used single crystal X-ray diffraction to determine if the transformation occurred in a **scsc** manner and to elucidate the orientation of the resulting components at each interval. From the TGA experiments, the first step in the de-pyridination process occurred at around 160 °C for each of the three porphyrin derivatives. We collected full data sets at or below room temperature (to confirm the structure of fully-solvated system) and then heated the sample to 160 °C and collected a subsequent data set. The quality of the data in the case of **2-Zn-Py$_3$** is poor and we determined the full structures only in the case of heated products of **1-Zn-Py$_3$** and **3-Zn-Py$_3$**. Both these heated products are isostructural; they crystallize in the space group *I*2/*a* with porphyrin and pyridine in 1:1.5 ratio. We call these structures *half-baked* as it is the first of two steps towards de-

pyridination and the porphyrin-pyridine ratio changed from 1:3 to 1:1.5. The molecular structure of resultant product (as obtained from single crystal X-ray analysis) of **1-Zn-Py$_3$** is shown in Figure 4.8. Of the one and half pyridine molecules in the asymmetric unit, one molecule acts as the ligand and binds to the Zn^{2+} ion on one of the axial positions. The half pyridine molecule (located on the 2-fold axis) is not coordinated to the porphyrin; it is a solvate. We refer to these half-baked structures in the manner **1-Zn-L$_1$-S$_{½}$** when distinguishing between the two types of ligands or making comparisons between different phases. When the crystals are heated further on the diffractometer up to 350 °C they undergo full de-pyrdination to result in the formation of *fully-baked* structures that are devoid of pyridine. We cooled these crystals to room temperature and collected the full data sets on all three porphyrins. Porphyrins **1-Zn**, **2-Zn** and **3-Zn** are isostructural; they belong to the space group $P2_1/n$ (Table 2.2 in Chapter 2) with half a molecule in the asymmetric unit.

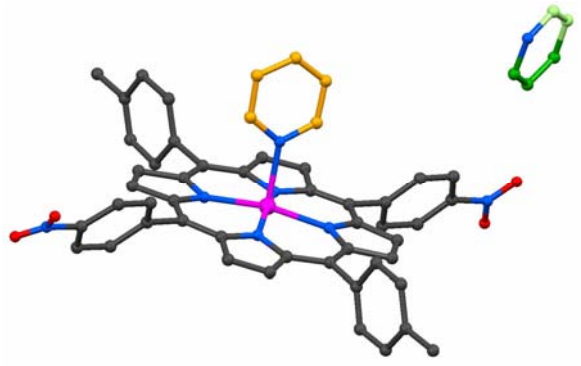

Figure 4.8 Molecular structure of **1-Zn-Py$_{1½}$**. Notice the square-pyramidal coordination environment around the zinc at the center of porphyrin. Ligand pyridine molecule is drawn in yellow and the solvated pyridine in green. Symmetry related C-atoms in solvated pyridine are shaded with different intensities.

4.7 COMPARISON OF FULLY-SOLVATED, HALF-BAKED AND FULL-BAKED STRUCTURES

Figures 4.9, 4.10 and 4.11 display the crystal structures of the fully-solvated, half-baked and fully-baked porphyrin solids. The structures are drawn to highlight the similarities and to show the possible relationships between them. In each case 12 porphyrin molecules that lie in a plane are taken to retain the clarity while displaying the essential differences between structures. In the fully-solvated structure 24 ligand pyridines along with 12 (Figure 4.9) solvated pyridines (corresponding to 12 porphyrin molecules) are shown; the guest molecules line in the cavities walled by *p*-tolyl groups. When heated to 160 °C, the resultant structure (Figure 4.10) contains 12 ligand pyridines along with six solvent pyridines. The loss of pyridines seem to occur along an axis during the heating; when pyridine is lost in this manner the *p*-tolyl groups that walled the cavities in the fully-solvated structure now collapse to fill the space. Concurrent with this solvent loss is the loss of half (12) of the ligand pyridines. It can be seen from Figures 4.9 and 4.10 that

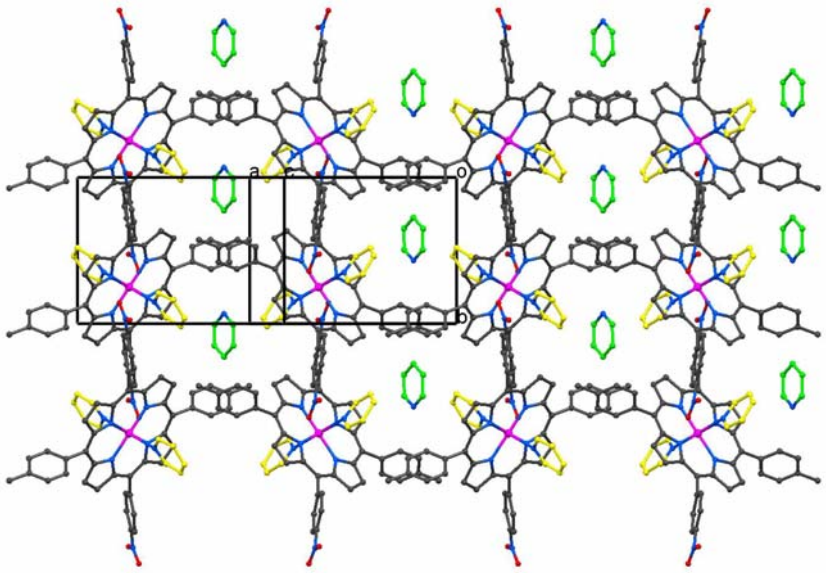

Figure 4.9 Crystal structure of **1-Zn-Py$_3$** showing the relative orientations of porphyrin, ligand and guest molecules in a layer.

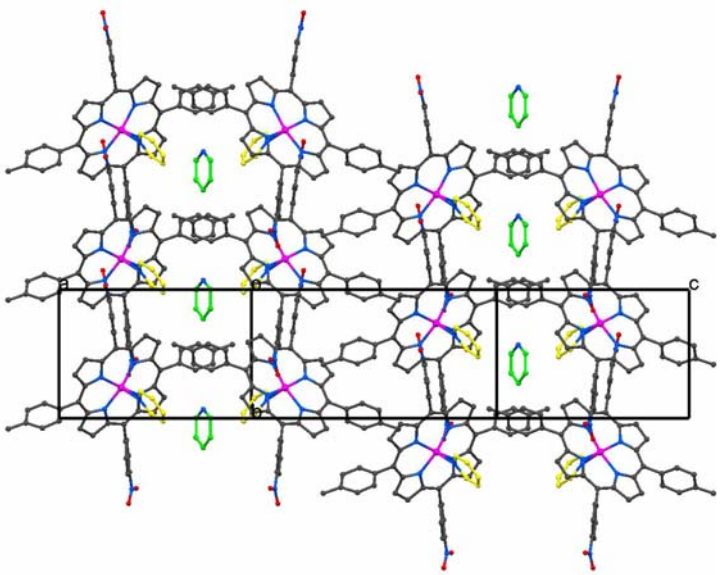

Figure 4.10 Crystal structure of **1-Zn-Py$_{1½}$** showing the relative orientations of porphyrin, ligand and guest molecules in a layer. Contrast central portion of this figure with Figure 4.10 to note the collapse of *p*-tolyl rings into the void space. This collapsing involves half translations of host molecules along the *b*-axis. Compare the left and right portions with the previous figure to note the similarities between the fully-solvated and half-baked structures.

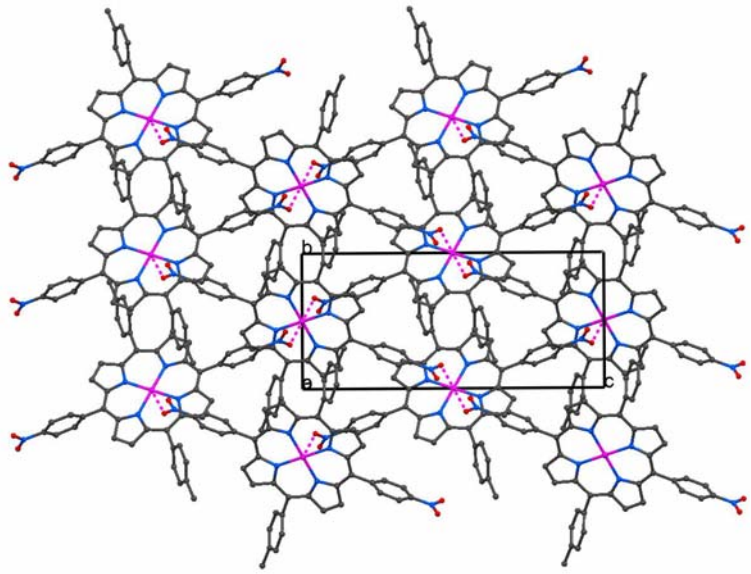

Figure 4.11 Crystal structure of the fully-baked **1-Zn** obtained after heating **1-Zn-Py$_3$** up to 350 °C. Compare this figure with structure of **1-Zn** (Figure 2.5 in Chapter 2) obtained directly from solution crystallization.

those portions in the half-baked structure that do not lose the solvated or ligated pyridines are very similar to the corresponding portions in the fully-solvated structure. Further heating of the half-baked structure results in the fully-baked de-pyrdinated structure; Figure 4.11 attempts to show the similarities between the this structure and the parent structures. When the remaining pyridines are lost from the half-baked structure the remaining cavities are filled by rearrangement of the *p*-tolyl and nitrophenyl groups (most likely involving rotations of porphyrins) to attain what seems to be a stable structure of non-solvated **1-Zn**. Similar structural features are seen in **3-Zn** systems. For **2-Zn-Py$_3$**, though the poor quality of the X-ray data did not allow the structure determination of the half-baked structure, we obtained reasonable data for the fully-baked **2-Zn**. Based on this data we established that the path of de-pyridination is similar in all the three porphyrin systems studied here. In these heating experiments, an interesting observation is that one of the axial ligands seems to have evaporated even before part of the solvated pyridine is removed. One reason for this early removal of coordinated pyridine might lie in the preferred coordination geometries of the Zn^{2+} ion.

4.8 STABILITY OF THE HALF-BAKED COMPLEXES

It is widely known that Zn^{2+} ion embedded in the porphyrin core frequently adopts a penta-coordinated square-pyramidal geometry.[8] For example, in the literature, except for one example,[9] all the pyridine containing zinc-metallated porphyrins contain this square-pyramidal geometry. In this geometry, aza ligands bind strongly to the Zn^{2+} ion and often distort away from the porphyrin plane, towards the ligand. The bonds are necessarily

weaker in the hexa-coordination geometry. The same results are borne out in our porphyrin structures. For example, in the **1-Zn-Py$_3$** system, the length of the Zn–N bond in the fully solvated structure is 2.43 Å and in the half-baked structure it is 2.20 Å. The corresponding values for the **3-Zn-Py$_3$** system are 2.41 and 2.20 Å. Stronger association of pyridine ligands in the square-pyramidal geometry is, we believe, one of the reasons for the stability of the intermediate complex formed in the heating process.

4.9 POSSIBLE MECHANISM OF DE-PYRIDINATION

The preceding discussion is based on the experimental observations that there appears to be two steps in the de-pyrdination process in TGA. Accordingly, we determined the structures of the products at the end of each step. Structural analysis, however, reveals that the loss of pyridine is 'unexpected' from the considerations of energies involved host-ligand and host-guest bonding. Obviously, the ligand pyridines are attached to the porphyrin by strong coordination bonds, while the solvated pyridines are only bound by weak intermolecular interactions. It is therefore surprising that during the first step in the heating process *half* of the ligands (12 of 24) are removed along with half of the solvate molecules (6 of 12). Consideration of these uncommon results led us to propose the mechanism depicted in Figure 4.12 to describe the de-pyridination process. Below we discuss the mechanism using the example **1-Zn-Py$_3$**; it is equally suitable for other two porphyrin systems studied here.

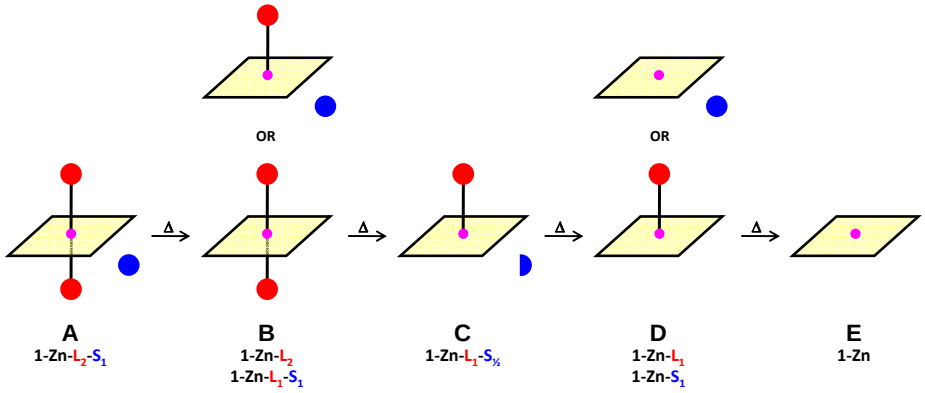

Figure 4.12 Proposed mechanism for the step-wise de-pyridination of **X-Zn-Py$_3$** (**X** = **1**, **2**, or **3**). **A**, **C** and **E** correspond to fully-solvated, half-baked and fully-baked structures respectively. **B** and **D** are possible intermediates that could not be characterized with single crystal X-ray diffraction analysis. Yellow square: porphyrin; magenta dot: metal cation; red cirle: ligand pyridine; blue circle or semi-circle: solvated pyridine.

We surmise that there are at least three intermediates (**B**-**D**) during the conversion of **1-Zn-L$_2$-S$_1$ (A)** to **1-Zn (E)**. The origin of this supposition comes from the experimentally observed intermediate **1-Zn-L$_2$-S$_{½}$ (C)**. As pointed above, loss of ligand pyridine while retaining the solvent pyridine is an energetically unfavorable process. We believe that the conversion of **A** to **C** goes through the intermediate **B** in the configuration **1-Zn-L$_2$**. We

made several unsuccessful attempts (with three different porphyrin systems) with varying temperatures and crystal encasing (in oil and paraffin wax) experiments to stop the transition at this level and determine the crystal structure. These attempts led to either no desolvation or half-baked structure. Given that the data obtained in some of these cases are not easily processable, it is possible that we have produced partially desolvated crystals that contain domains of **1-Zn-L_2** and **1-Zn-L_2-S_1** (and **1-Zn-L_2** with some fraction of **S**). Owing to the space- and time-averaged nature of X-ray diffraction analysis, it was impossible to deduce real structure of the intermediate between **A** and **C** (if it existed).

We believe that **B** or some variant of it does exist as an intermediate between fully-solvated and half-baked structures. The ephemeral existence of **B** is driven by two distinct but related issues: **(a)** penta-coordinated geometry around Zn^{2+} ion is intrinsically more stable than the hexa-coordination geometry and **(b)** the cavities that are left after the evaporation of solvated pyridine bestow enormous instability to the crystal. The first of these two problems has its origin in a molecular level transition and the second in a supramolecular level transition. We propose that the molecular transition (**1-Zn-L_2** to **1-Zn-L**) is a result of supramolecular transition (**1-Zn-L_2-S_1** to **1-Zn-L_2**). We attempted to monitor this transition by IR spectroscopy as detailed below.

In addition to **B**, we assume that there is another intermediate **D** between half-baked (**C**) and fully-baked (**E**) solids. We have also tried to harness the second stage of the desolvation to catch **D** or a related variant through diffraction experiments. Again, the time required to collect X-ray data (at least two hours) is much longer than the life of potential intermediates (**D** or **B**) that lie between the thermodynamic minima (**A**, **C** or **E**) and these structures could not be determined by X-ray diffraction. We should note that we have tried experiments where the crystal is heated to a temperature at which **B** or **D** is expected to be present and flash froze the crystal to -173 °C. Even in these cases, we could not determine with certainty that **B** or **D** is present without their predecessors (**A** or **C**). The problems here stem from the space-averaged nature of the diffraction, poor scattering power of the crystals and increased mosaicity associated with the loss of the solvent. For these reasons, we used IR spectroscopy to garner details on possible phases in the heating process.

Figure 4.13 shows IR spectra of **1-Zn-Py_3** at various stages of the heating process. It can be seen that at each stage of this process, until the formation of **1-Zn**, absorptions corresponding the pyridine molecules are present. Normalization of spectra and approximate weighting of the peaks showed that there is a gradual loss of pyridine in this heating process. If there were only one intermediate (**C**) in the conversion of **1-Zn-Py_3** to **1-Zn** then the relative absorption intensities of pyridine should be discontinuous, not gradual. These results suggest that the mechanism showed in Figure 4.12 is most likely operational in the multi-step phase transitions seen in three different porphyrin complexes.

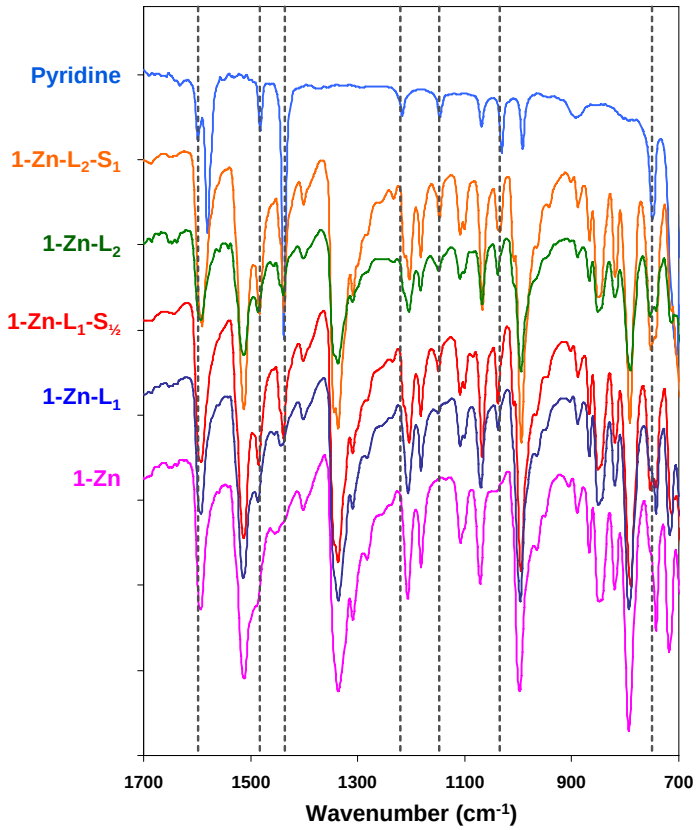

Figure 4.13 IR Spectra of pure pyridine, **1-Zn-Py$_3$** and products obtained when **1-Zn-Py$_3$** is subjected to different heating temperatures:

4.11 EXPERIMENTAL

Synthesis of compounds **1-Zn**, **2-Zn** and **3-Zn** are described in Chapters 2 and 3. Crystals of **1-Zn-Py$_3$, 2-Zn-Py$_3$** and **3-Zn-Py$_3$** are grown from chloroform solutions containing the respective porphyrins and excess pyridine. Crystals were analyzed by DSC, TGA, IR and NMR spectroscopy, PXRD and SXRD methods as described in the previous chapters.

To monitor **scsc** transformations, we mounted fully-solvated crystals (in mineral or paratone oil or paraffin wax) onto a cold nitrogen stream on the Bruker APEX II single crystal X-ray diffractometer. Initially, the data were collected at a low temperature (-80 or -173 °C) to ascertain the structures of fully-solvated complexes. Crystals were then heated to the required temperature (e.g., 160 °C) through a ramping program (e.g., 6 °C per minute). The temperature and time required to achieve a particular result is guided by the TGA experiments but mostly determined by trial and error by several repeats. Once

the crystal has reached the target temperature (some times it is kept at that temperature for a short while, usually in the order of 10-30 min), it was cooled to -50 or -80 °C and the X-ray data were collected. Using this process, the crystal structures of the half-baked and fully-baked porphyrins were determined.

4.12 SUMMARY AND CONCLUSION

Crystals of (fully-solvated) **1-Zn-Py$_3$, 2-Zn-Py$_3$** and **3-Zn-Py$_3$** exhibit 2^2 networks made of C–H···O interactions as opposed to the 4^4 networks made of Zn···O contacts. Heating of these crystals leads to the unsolvated (fully-baked) porphyrins **1-Zn, 2-Zn** and **3-Zn** through one distinctly stable (half-baked) intermediate in each case. The conversion of the fully-solvated crystals to half-baked crystals involves the net loss of half pyridine molecules. This conversion, however, is unusual in that the half-baked structure seems to have formed from the loss of a ligand pyridine while retaining the solvated pyridine. To account for this observation a mechanism is proposed based on the molecular and supramolecular level relative stabilities of possible intermediates between fully-solvated and half-baked transition, as well as between half-baked and fully-baked transition. The limitations of the X-ray diffraction methods (information gathered is based on space- and time-averaged data) are alluded to and presence of possible intermediates is garnered by IR spectroscopic analysis.

SCSC Transformations are extremely rare and multi-step **scsc** transitions are even rarer. The transition of fully-solvated crystals to the fully-baked crystals through the half-baked intermediates is remarkable for any solid; especially for neutral and discrete molecular complexes. This work suggests that the **scsc** transformations can also be achieved in solids in which domains of one set of interactions or patterns are segregated from others. One of the useful outcomes of these **scsc** transformations is that they allowed the full structure determinations of compounds **2-Zn** and **3-Zn** that are otherwise impossible to grow as solvent-free crystals.

4.13 REFERENCES

1. Barbour, L. J., Single Crystal to Single Crystal Transformations. *Aust. J. Chem.* **2006,** *59*, 595-596.
2. Kaupp, G., Solid-state reactions, dynamics in molecular crystals. *Curr. Opn. Solid State Mater. Sci* **2002,** *6*, 131-138.
3. Friscic, T.; MacGillivray, L. R., Single-crystal-to-single-crystal [2+2] photodimerizations: From discovery to design. *Z. Kristallogr.* **2005,** *220*, 351-363.
4. Garcia-Garibay, M. A., Molecular crystals on the move: from single-crystal-to-single-crystal photoreactions to molecular machinery. *Angew. Chem. Int. Ed.* **2007,** *46*, 8945-8947.
5. Halder, G. J.; Kepert, C. J., Single Crystal to Single Crystal Structural Transformations in Molecular Framework Materials. *Aust. J. Chem.* **2006,** *59*, 597-604.

6. Suh, M. P.; Cheon, Y. E., Recent Advances in the Dynamics of Single Crystal to Single Crystal Transformations in Metal-Organic Open Frameworks. *Aust. J. Chem.* **2006,** *59*, 605-612.
7. Kawano, M.; Fujita, M., Direct observation of crystalline-state guest exchange in coordination networks. *Coord. Chem. Rev.* **2007,** *251*, 2592-2605.
8. Goldberg, I., Crystal engineering of porphyrin framework solids. *Chem. Commun.* **2005**, 1243-1254.
9. Diskin-Posner, Y.; Patra, G. K.; Goldberg, I., Supramolecular assembly of metalloporphyrins in crystals by axial coordination through amine ligands. *J. Chem. Soc., Dalton Trans.* **2001**, 2775-2782.

5 CUBES AS DIMERS OF SQUARES – MODULAR SYNTHESIS OF COFACIAL PORPHYRIN DIMERS

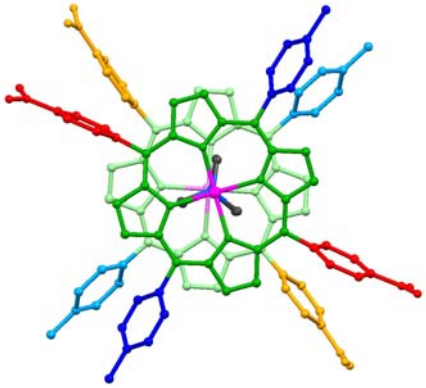

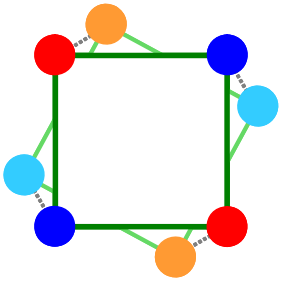

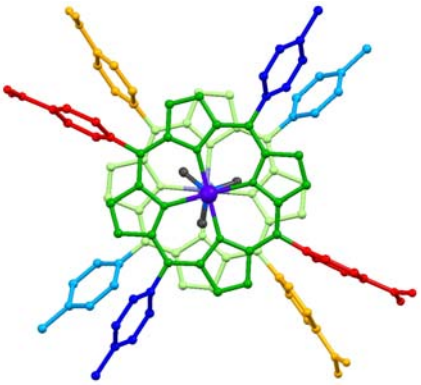

5.1 INTRODUCTION

The concept of supramolecular chemistry emphasizes that assemblies of molecules show properties that are unavailable to molecules themselves.[1] A crystal is a collection of millions of molecules and it is termed as 'the supramolecular par excellence'.[2] In previous chapters we prepared and studied several porphyrin crystals, the *infinite* supermolecules of porphyrins. Here we explore the synthesis, structures and properties of *finite* assemblies of porphyrin derivatives. The impetus for this work comes from the realization that these discrete assemblies are important starting points for applications such as two photon absorption (TPA)[3] and second order nonlinear optics (NLO).[4-5]

5.1.1 Two-Photon Absorption. The process of simultaneous absorption of two photons of identical or different energies is referred to as TPA. The absorption probability is dependent on the square of the intensity and hence TPA is a nonlinear process that is much weaker than the linear absorption. Molecules that possess large TPA cross sections are coveted targets due to their applications in, among others, biological imaging, three-dimensional nanofabrication and optical limiting.[6-8] It has been recognized that *J*-aggregates (Figure 5.1a) of a tetrasulfonatophenyl derivative of porphyrin in aqueous solutions show thirty fold enhancement in TPA cross section compared to the corresponding monomers.[9] The *J*-aggregates refer to offset stacking of molecules in solution; they can adopt several configurations based on the differences between the mutual orientation and separation between the porphyrin units. Adjoining the porphyrin units by covalent linkages (Figure 5.1b) fixes the mutual separation between porphyrins; this cross-linking led to several hundred fold increase in the values of TPA cross section.[10] Covalent cross-linking is usually a laborious, time-consuming, and low-yielding process and disfavors the easy synthesis and exploration of structure-property relationships between multiple related derivatives.[3] We envisaged that it is easier to prepare a large set of structurally related porphyrin systems if we apply the principles of supramolecular synthesis to several monomers we created in previous chapters. The types of porphyrin assemblies we created are also guided by their potential applications in NLO materials as discussed below.

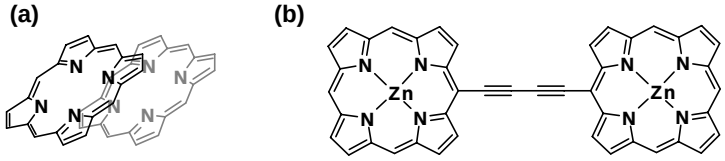

Figure 5.1 (a) Schematic representation of a *J*-aggregate. The two porphyrin units are assembled by π-stacking interactions. **(b)** Covalent dimerization of porphyrin units. Most covalent synthetic methods link the neighboring porphyrins at the *meso* positions.

5.1.2 Second Order Nonlinear Optics. There is a growing research interest in organic materials with second order NLO properties for possible applications in optoelectronic and photonic devices.[4-5] Traditionally, the materials of choice have been based on inorganic systems.[11] The use of organic materials for NLO applications has emerged in

the mid 1970s, and today, some of the most successful organic systems are used in commercial devices.[12-13] Organic NLO molecules have advantages over inorganic ones such as fast response time and optimization of optical properties at the molecular and crystalline level through chemical modification. Donor-acceptor substituted aromatic molecules (Figure 5.2a) have been the most investigated NLO chromophores. These molecules represent the prevailing dipolar model of organic nonlinear optics. Dipolar molecules, however, have several limitations.[14-16] The most important of these is their strong tendency to adopt anti-parallel packing in the solid state. This centrosymmetric anti-parallel alignment nullifies bulk nonlinearity in dipolar materials.

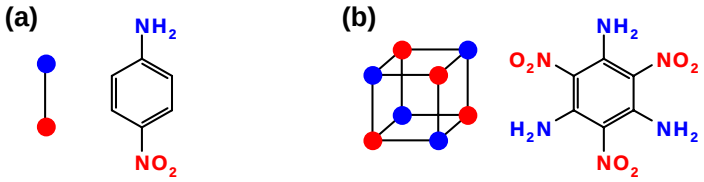

Figure 5.2 Schematic representation of **(a)** dipoles and **(b)** octupoles and classical examples of each system.

Recently, a new class of materials based on octupolar symmetries has been proposed for NLO applications.[17-19] Octupolar molecules (Figure 5.2b) lack permanent dipole moments and have better chances to adopt noncentrosymmetric packing. Another significant advantage of octupolar systems is that their hyperpolarizability (β) increases steadily as the extent of charge transfer increases, whereas the β of dipolar molecules increases to a maximum value and then decreases as the length of the conjugation increases.[16] The objective of this work is to develop a hierarchical strategy for the synthesis of cubic octupoles (Figure 5.2b); these cubic systems are expected to show high nonlinearities at molecular as well as crystalline scale.

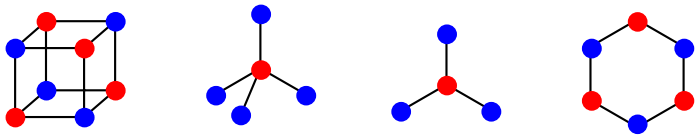

Figure 5.3 Octupolar systems with different symmetries. The system on the left represents an ideal octupole with eight point charges at the corners of a cube; we term this system a cubic octupole. Tetrahedral and trigonal octupoles can be derived from the cubic octupole through projection of charges into the center of the cube, or onto a plane respectively.

5.2 PORPHYRINS AS TEMPLATES FOR COFACIAL DIMERS

Octupoles can be expressed in several symmetries as shown in Figure 5.3. Our initial goal in this work is to make donor and acceptor substituted porphyrin dimers that can be used as templates for cubic octupoles. We have started this work with porphyrin derivatives because they have several desirable properties: (a) their central tetra-pyrrole core is planar and possesses rigid geometry; (b) they can be synthesized with established synthetic methods;[20] (c) their ring system can be built in a modular fashion so that donor

and acceptor groups can be introduced in *trans*-positions required for cubic octupoles; (d) they have extended conjugation required for high β; and, (e) they represent molecules that display highest β in dipolar realm.[21]

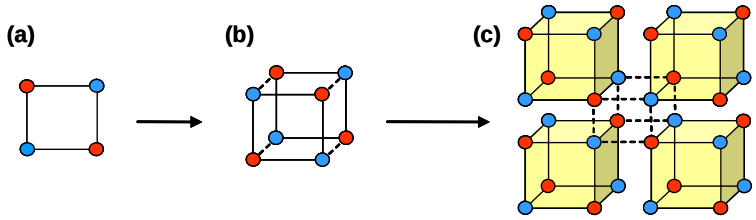

Figure 5.4 (a) Schematic of a molecule with square geometry; it has donor and acceptor groups positioned in the trans orientation. **(b)** A cubic octupole formed by the cofacial dimerization of square-shaped molecules. In this work the square units are made by covalent synthesis; cubes are made from square units by metal-ligand coordination. **(c)** Targeted acentric, octupolar assembly of cubes in the solid state. Cubes are filled with solid color to distinguish intra- and intermolecular regions. Dashed lines highlight a supramolecular cubic octupole.

5.3 DESIGN OF CUBIC OCTUPOLES

Our strategy for making cubic octupoles and their possible assembly into 3D noncentrosymmetric structures is shown in Figure 5.4. We begin with the molecular synthesis of the square unit shown in Figure 5.4a. Synthetically, it is easy to substitute porphyrin molecules at the *meso* positions. We have chosen *meso* substituted *trans*-$\mathbf{A_2D_2}$ porphyrin (**A**: acceptor; **D**: donor) to synthesize the square unit shown in Figure 5.4. To obtain *trans*-$\mathbf{A_2D_2}$ porphyrin we use a modular method in which a dipyrromethane consisting of **A** (or **D**) groups is synthesized first. This dipyrromethane is then reacted with an aldehyde containing **D** (or **A**) groups to yield the *trans*-$\mathbf{A_2D_2}$ porphyrin (see Figure 2.3 in Chapter 2).

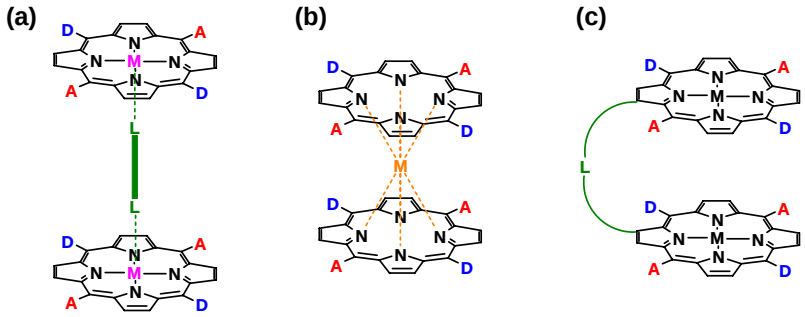

Figure 5.5 Three methods of cofacial dimerization of porphyrins discussed in the text. Method **(c)** brings the two porphyrins in an off-centered manner and the two porphyrin rings are only partly coplanar. Method **(b)** forces the two porphyrin units to a very close proximity; both porphyrin planes are subjected to severe conformational twisting unsuitable for conjugation-dependent TPA and NLO applications. Method **(a)** offers additional modularity in terms of ligand choice and keeps the two porphyrin rings in parallel planes.

5.4 COFACIAL DIMERIZATION

The dimeric assembly of porphyrin molecules, to yield the cubic octupole shown in Figure 5.4b, can be achieved in several ways. We considered the following three procedures (Figure 5.5): (a) in-plane metallation of porphyrins followed by dimerization using linear bidentate ligands;[22] (b) dimerization by direct bonding of inner pyrrolic nitrogen atoms by octacoordinated metal ions (e.g., Os and Ce),[23] and (c) dimerization by covalent bridging of porphyrin units at peripheral position.

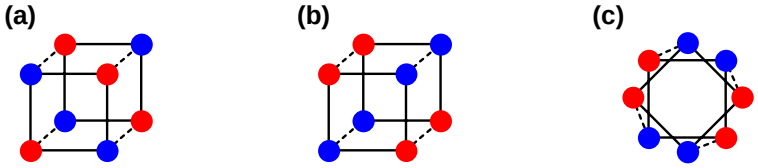

Figure 5.6 Possible conformations of cofacial dimers formed by self-assembly between metal cations embedded in the porphyrin core and linear bidentate ligands.

We initiated our work with the first procedure because it is synthetically the easiest and high yielding, and the product dimers are stable. We note that dimerization by this approach could lead to the three possible conformations shown in Figure 5.6. Of the three conformers, **a** and **c** are noncentrosymmetric and octupolar. Conformer **b**, however, is centrosymmetric and non-octupolar. While the octupolar conformers are useful in NLO applications such as second harmonic generation (SHG), all the conformers are excellent candidates for applications in TPA. The goals of this work are limited to the synthesis and characterization of the dimers and derive some relationships among the constitution of the dimers and their structures.

5.5 PORPHYRIN DIMERS STUDIED

5.5.1 Dimers of Symmetric A_4- or D_4-Porphyrins. Figure 5.7 shows the tetraaryl porphyrins ($\mathbf{A}_4$ or $\mathbf{D}_4$) we have synthesized or purchased. We call these tetraaryl porphyrins symmetric porphyrins to distinguish them from *trans*-$\mathbf{A_2D_2}$ porphyrins. We have used three different procedures to make meso-tetraarylporphyrins;[24-27] detailed synthetic procedures are given in the Experimental Section at the end of the chapter. We begin with these symmetric porphyrins because of their ready availability in large quantity and also because of their potential use in TPA studies. Theoretical and experimental investigations showed that molecules substituted with electron donating or withdrawing groups at the boundaries of a conjugated system can enhance the TPA cross section through the flow of charge from periphery to the center or vice versa.[3] The symmetric porphyrins we considered have some strong electron withdrawing (e.g., PhF_5) and moderate donating (e.g., methoxy) groups.

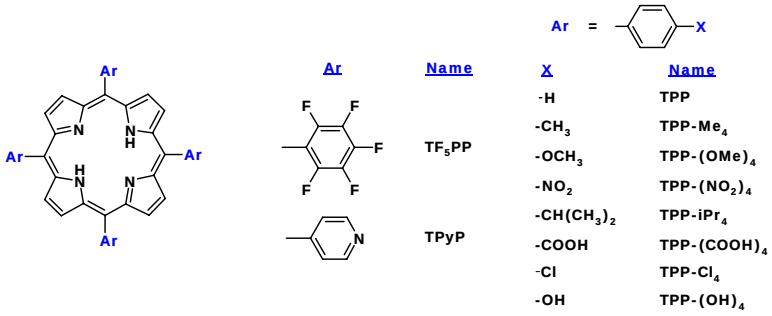

Figure 5.7 Symmetric A_4- and D_4-porphyrins currently studied and their nomenclature.

5.5.2 Dimers of *trans*-A_2D_2-Porphyrins. Synthesis of *trans*-A_2D_2-porphyrins is more involved than symmetric porphyrins. We have used a two-step approach to synthesize *trans* porphyrins as discussed in previous chapters. Figures 5.8 and 5.9 display the different *trans* porphyrins we have synthesized.

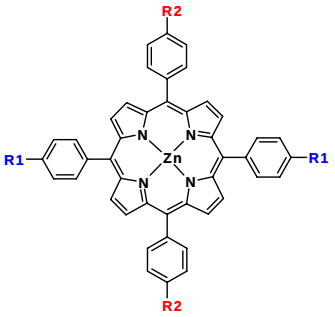

R1	R2	Compound	Code
CH_3	NO_2	Zn-TPP-$Me_2(NO_2)_2$	1-Zn
Cl	NO_2	Zn-TPP-$Cl_2(NO_2)_2$	2-Zn
Br	NO_2	Zn-TPP-$Br_2(NO_2)_2$	3-Zn
H	NO_2	Zn-TPP-$H_2(NO_2)_2$	4-Zn
I	NO_2	Zn-TPP-$I_2(NO_2)_2$	
$CH(CH_3)_2$	NO_2	Zn-TPP-$iPr_2(NO_2)_2$	
$C(CH_3)_3$	NO_2	Zn-TPP-$tBu_2(NO_2)_2$	
OCH_3	NO_2	Zn-TPP-$(OMe)_2(NO_2)_2$	
H	Cl	Zn-TPP-H_2Cl_2	
H	Br	Zn-TPP-H_2Br_2	

Figure 5.8 Metallated *trans*-$\mathbf{A_2D_2}$-porphyrins based on phenyl- and 4-nitrophenyldipyrromethanes.

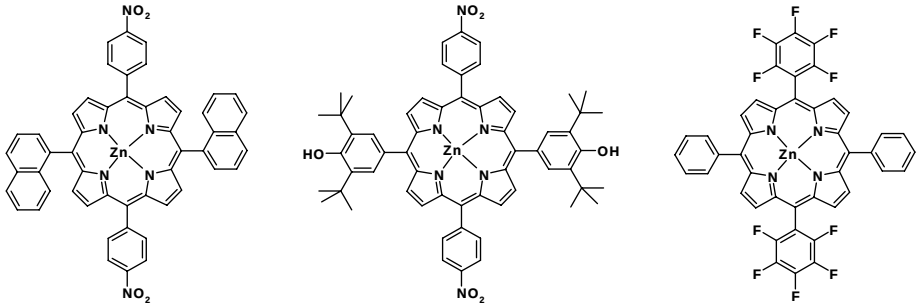

Figure 5.9 *trans*-$\mathbf{A_2D_2}$-porphyrins with bulky groups (**5-Zn** and **6-Zn**) and with perfluorophenyl groups (**7-Zn**).

5.6 METAL SELECTION

A literature survey revealed that the Zn^{2+} ion in the porphyrin center has a marked preference for five-coordinate square-pyramidal geometry.[28] Depending on the porphyrin-ligand ratio, zinc can bind from one or both of the axial positions. It binds to the four inner pyrrole nitrogens of the porphyrin macrocycle and quite often also to another ligand in the axial direction, revealing a particularly high affinity for nitrogen Lewis bases. Also, the distance between the two opposite inner pyrrole nitrogens is about 4 Å, and the zinc ion fits in this void very well, leaving the porphyrin macrocycle in a reasonably flat position. Another metal we considered is cobalt. Cobalt has a similar size as zinc, and cobalt porphyrins exhibit similar binding characteristics as discussed in Chapter 2.

5.7 LIGAND SELECTION

Figure 5.10 displays the ligands we have selected for dimerization. These ligands have the following characteristics that make them suitable candidates for dimerization: (a) they are ditopic, (b) they contain aza donor atoms, (c) their two donor atoms are relatively linearly disposed, and (d) they contain no other competing donor atoms. In addition, these ligands also allow the distance between the two porphyrin rings in a dimer to be varied; a property that can be used in conjunction with the steric bulk of substituents in **A** or **D** aryl rings.

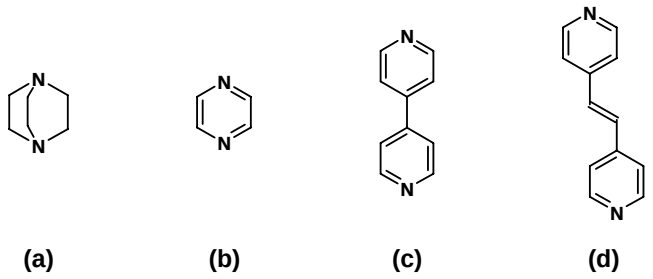

Figure 5.10 Bidentate ligands used in this work: **(a)**1,4-diazabicyclo[2.2.2]octane (**dabco**) **(b)** pyrazine (**pz**); **(c)** 4,4′-bypyridyl (**bpy**) and **(d)** 1,2-di(4-pyridyl)ethylene (**dpe**).

Since symmetric porphyrins ($\mathbf{A}_4$ and $\mathbf{D}_4$) are relatively straight-forward to make, we began our work on dimerization using these compounds as starting materials. Once we optimized the conditions for dimerization in terms of metal and ligand combinations, we extended these conditions to *trans*-$\mathbf{A}_2\mathbf{D}_2$-porphyrins.

5.8 DIMERIZATION OF PORPHYRINS

Cofacial dimerization is achieved through metal-ligand binding of organic bridging ligands with the metal core of the porphyrin molecules. The Zn^{2+} ion inserted into the porphyrin core displays a highest coordination number of six (Chapters 2-4). Thus, zinc metallated porphyrin and aza ligands can give four possible products: (i) sandwich dimer (trimolecular complex, 1:2 ligand-porphyrin ratio), (ii) bimolecular complex (1:1 ligand-

porphyrin ratio), (iii) trimolecular complex with 2:1 ligand-porphyrin ratio and (vi) linear polymer. In most cases, dimers are formed exclusively.

Chloroform is used as a solvent for crystallization, because it dissolves both the porphyrin and the ligand. The addition of a small amount of nitrobenzene to the crystallization solution almost always facilitated the growth of crystalline solids. The molecular structure of porphyrin dimers precludes them from forming close-packed crystal structures; thus growing single crystals of these dimers is usually a difficult task. We and others have found that nitrobenzene molecules fill the cavities in crystals preventing the structural collapse and enabling the formation of crystals.[29]

5.9 ^{1}H-NMR CHARACTERIZATION OF PORPHYRIN DIMERS

Here we give some details on porphyrin-ligand complexes in solution. The primary goal here is to test whether these complexes form in solution through the analysis of ^{1}H-NMR spectra. Typically, when an aza ligand is added to the chloroform solution containing the porphyrins, the color of the solution turns from red to green or dark green. This change in color suggests some sort of association between the porphyrin and ligand molecules. Through ^{1}H-NMR spectral analysis we hoped to glean the structural and stoichiometric details of the porphyrin-ligand complexes. As we show below it is possible to deduce whether a given porphyrin-ligand assembly is a bimolecular or trimolecular complex (sandwich dimer) and so on.

5.9.1 Solvent Inclusion and Upfield Shift of Ligand Protons. As discussed earlier, nitrobenzene is included in the crystals of many porphyrin dimers. When nitrobenzene is included in the crystals of porphyrin-ligand complexes, the peaks corresponding to the protons of nitrobenzene appear at 7.54, 7.68 and 8.20 ppm, without any significant shift, in the ^{1}H-NMR spectra. The ligand in a porphyrin dimer is sandwiched between two porphyrin macrocycles. Thus the C–H protons of the ligand are enclosed within the field of diamagnetic ring current of porphyrins, which causes the proton absorptions to shift upfield (lower ppm values). In addition, these peaks appear broad in the ^{1}H-NMR spectra of complexes because of the fast exchange of unbound and bound ligands. In all spectra shown below, the peak at ~1.5 ppm corresponds to the protons on water, a contaminant in the $CDCl_3$ solvent. In the following figures, the ^{1}H-NMR spectra of some selected porphyrin ligand complexes are shown to assess the following features: (a) identification of included guests; (b) upfield shift of absorptions corresponding to ligand protons; (c) establishment of stoichiometry based on the relative upfield shift of the peaks of ligand protons.

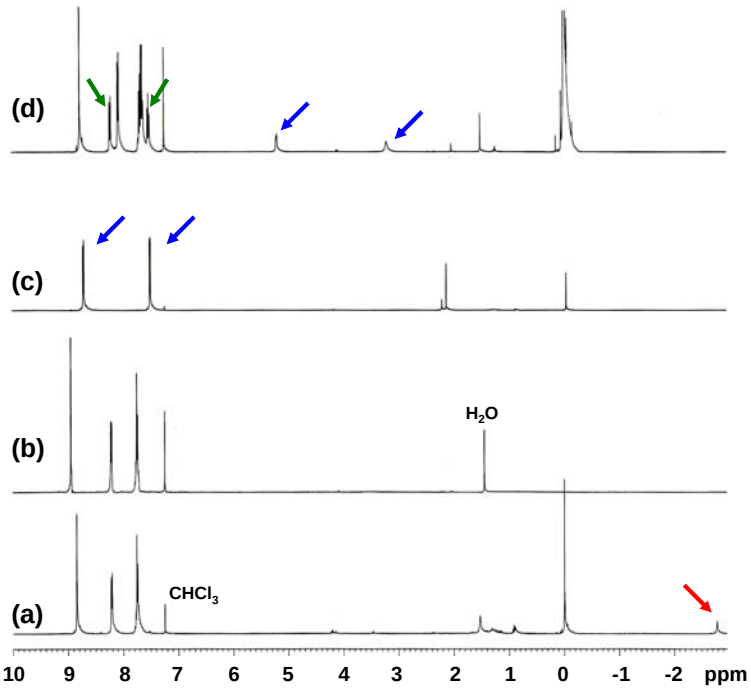

Figure 5.11 ^{1}H-NMR spectra of **(a) TPP**, **(b) Zn-TPP**, **(c) bpy** and **(d) (Zn-TPP)$_2$-bpy**. Notice in **(b)** the disappearance of the peaks corresponding to pyrrolic protons at -3 ppm; red arrow in **(a)**. Compare **(c)** and **(d)** to note the upfield shift of **bpy** protons indicated by blue arrows. Two blue arrows indicate for two different kinds of ligand protons. Compare 7-9 ppm region in **(b)** and **(d)** to note the peaks corresponding to the nitrobenzene guest molecules (green arrows) in the crystals of **(Zn-TPP)$_2$-bpy**.

Figure 5.11 illustrates the process of following the metallation and ligand complexation in unsubstituted symmetric porphyrin **TPP** using the ^{1}H-NMR spectroscopy. Metallation can be followed by focusing in the region of -3 ppm (Figures 5.11a-b) because insertion of Zn^{2+} cation into the porphyrin core eliminates the pyrrolic protons at ~ -3 ppm. Stacked on the spectra of TPP and Zn-TPP are the spectra of pure **bpy** (Figure 5.11c) and the dimer (**Zn-TPP)$_2$-bpy** (Figure 5.11d). The ^{1}H-NMR spectrum of this complex was acquired after the crystals were thoroughly washed with chloroform and dried in air on filter papers. Figure 5.11d indicates that the crystals are solvated with nitrobenzene (peaks 7.54, 7.68 and 8.20 ppm). The H3 and H3′ peaks of 4,4′-**bpy** are shifted upfield to 3.22 ppm (from 8.72 ppm); those of H2 and H2′ are shifted to 5.20 ppm (from 7.50 ppm). Integration of the peak areas show that, for 16 β H-atoms of the **Zn-TPP**, there are four of each type of H-atoms of **bpy**; the complex is a trimolecular species with porphyrin and the ligand in 2:1 ratio. Figure 5.12 shows that similar features (upfield shift and peak broadening of ligand protons) are observed in the case of a sandwich dimer formed from **Zn-TPP-Me$_4$** and **pz**; all the other complexes studied in this work also displayed similar characteristics (spectra not shown here).

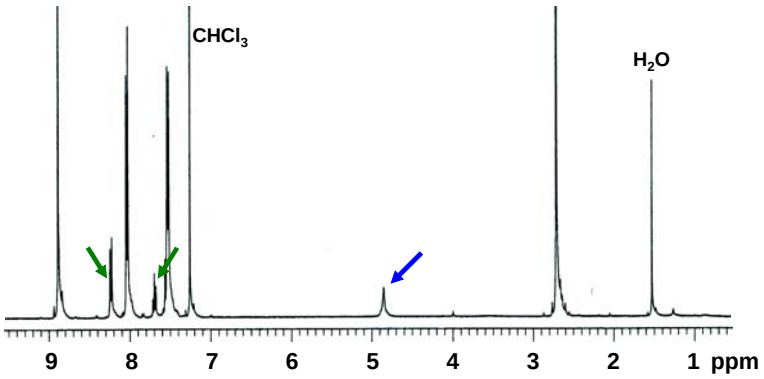

Figure 5.12 ^{1}H-NMR spectrum of **(Zn-TPP-Me$_4$)$_2$-pz**. The peak corresponding to the **pz** protons appears at 4.85 ppm (blue arrow); the same peak appears at 8.52 ppm in pure **pz**. Notice also the peaks (green arrows) corresponding to the nitrobenzene guest molecules.

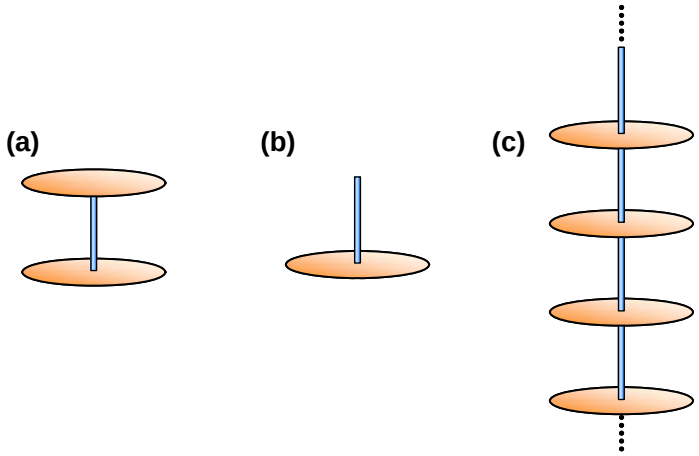

Figure 5.13 Schematic illustration of **(a)** a 2:1 sandwich dimer between porphyrin (orange ellipses) and ligand (blue rectangle) molecules, **(b)** a discrete 1:1 complex and **(c)** an infinite 1:1 coordination polymer.

5.9.2 Effect of Stoichiometry on the Upfield Shift of Ligand Protons. The relative ratio of the porphyrin and ligand influences the structure of the porphyrin-ligand complex. In solution, a 2:1 stoichiometry between porphyrin and ligand most likely leads to the formation of a sandwich dimer (Figure 5.13a). A 1:1 stoichiometry, in principle, can lead to a discrete binary complex (Figure 5.13b) or a linear 1:1 polymer (Figure 5.13c). It is, however, unlikely that linear polymers prevail in solution. Figure 5.14 reveals that the presence of the discrete binary complex can be established from the ^{1}H-NMR spectroscopy. The ligand protons experience a greater shielding effect in a 2:1 dimer compared to the discrete 1:1 complex. In the former, the ring currents of two porphyrin molecules contribute to the shielding effect; in the latter only one porphyrin

ring is involved in the shielding of ligand protons. This is clearly evidenced by the relative peak positions of ligand protons in the 2:1 and 1:1 complexes between **Zn-TPP-Cl$_4$** and **bpy** (Figure 5.14). If the 1:1 complex in Figure 5.14b were to be a linear polymer the ligand protons are expected to show the same level of shielding in the 2:1 complex.

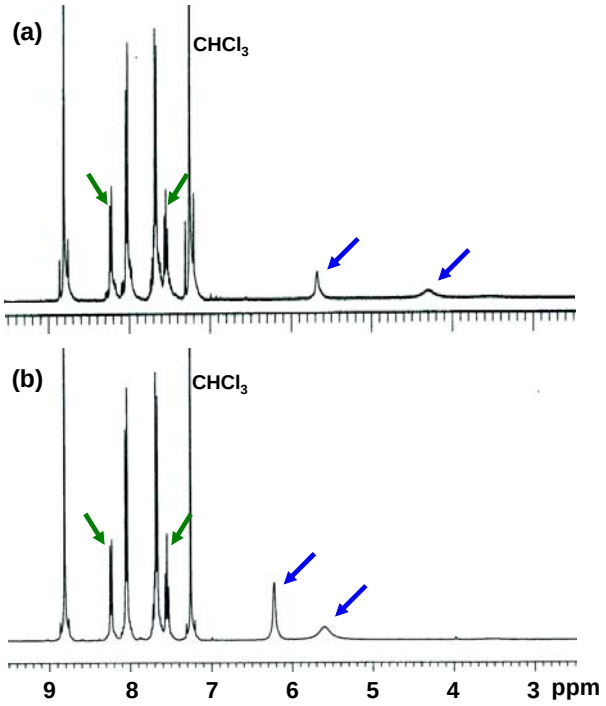

Figure 5.14 ^{1}H-NMR spectrum of **(a)** 2:1 and **(b)** 1:1 complexes between **ZnTPP-Cl$_4$** and **bpy**. Notice the difference between the upfiled shifts of **bpy** protons indicated by blue arrows. Green arrows indicate the protons of nitrobenzene molecules. See text for details.

5.9.3 ^{1}H-NMR Spectra of Dimers of *trans*-A$_2$D$_2$-Porphyrins. The introduction of two different functional groups at the periphery increases the number of unrelated protons in *trans*-A_2D_2-porphyrins; thus, there are more peaks in the 7-9 ppm region in the ^{1}H-NMR spectra of these complexes. Apart from this difference, the ^{1}H-NMR spectra of *trans*-A_2D_2-porphyrins show the same characteristics as the symmetric porphyrins in terms of guest inclusion and upfield shift of ligand peaks (Figure 5.15). We have also monitored the change in relative shift of the ligand peaks as a function of porphyrin-ligand ratio (Figure 5.16). The results from this experiment are consistent with our observations on 2:1 and 1:1 complexes discussed in the previous section.

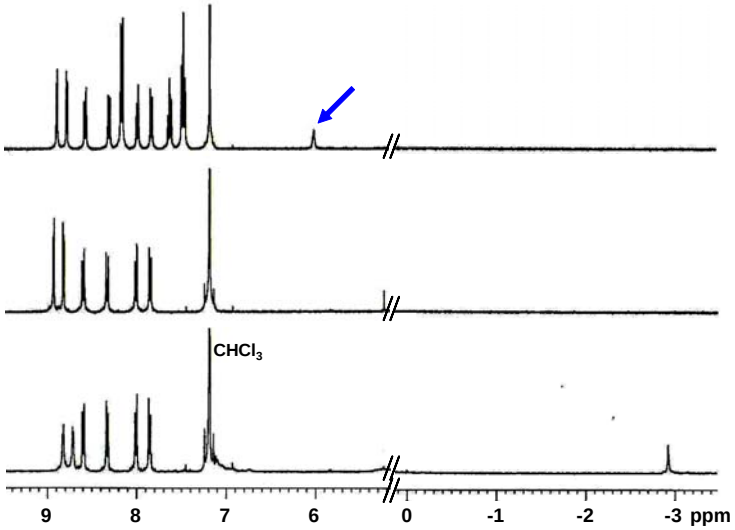

Figure 5.15 ^{1}H-NMR spectra of **(a) 3**, **(b) 3-Zn**, and **(c) (3-Zn)$_2$-pz**. Notice in **(b)** the disappearance of the peaks corresponding to pyrrolic protons at -3 ppm. The **pz** protons appear at 6.12 ppm (blue arrow); the same peak appears at 8.52 ppm in pure **pz**. Compare the 7-9 ppm region in **(b)** and **(c)** to note the peaks corresponding to the nitrobenzene guest molecules in the crystals of **(3-Zn)$_2$-pz**.

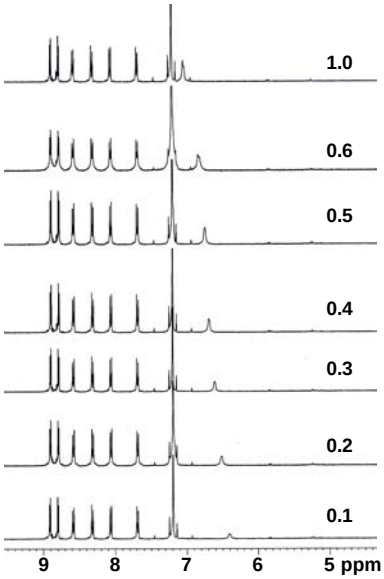

Figure 5.16 Titration of **2-Zn** with **pz** followed by ^{1}H-NMR spectroscopy. The mole fraction of **pz** is indicated on each spectrum. Notice the decrease in the upfield shift of **pz** peaks with increasing mole fraction of the ligand.

5.10 CRYSTAL STRUCTURES OF SOME COMPLEXES OF SYMMETRIC PORPHYRINS

As indicated in the previous chapters, the crystallization of porphyrin complexes often leads to very small and poorly diffracting crystals and X-ray diffraction analysis of these crystals is seldom straight-forward. At the beginning of this work we explored the crystallization of complexes between symmetric porphyrins and various ligands. In this section, we report the crystal structures of some odd and unexpected porphyrin complexes to emphasize the difficulties in obtaining the required dimers in quantitative yields.

5.10.1 A 1:1 Porphyrin-Ligand Complex with 1:2 Porphyrin-Ligand Stoichiometry. Slow evaporation of a chloroform solution containing **Zn-TPP-Me$_4$** and **bpy** in 2:1 proportions led to the growth of small crystalline plates and needles within three days. ^{1}H-NMR analysis of the plate-like crystals showed that the porphyrin and ligand are in 1:2 ratio as opposed to the expected 2:1 ratio. Single crystal X-ray diffraction analysis showed that these crystals belong to the space group $P2_1/c$ with two symmetry independent **bpy** molecules. One of the **bpy** molecules binds to porphyrin from one side only (Zn–N: 2.14 Å) and the other **bpy** molecule acts as a guest occupying the interstitial spaces in the crystals (Figure 5.17). The porphyrin-ligand ratio in this crystal is 1:2.

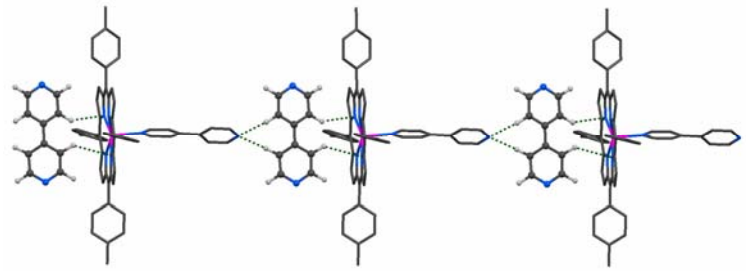

Figure 5.17 Crystal structure of **ZnTPP-Me$_4$-bpy**. The guest **bpy** molecules are drawn in ball-and-stick models. The binary complex and the guest **bpy** form linear arrays along the *b*-axis through C–H···N interactions. These chains further assemble along *a*- and *c*-axes using C–H···N and other interactions to result in the overall crystal structure.

5.10.2 Nitrobenzene Solvate of Zn-TPP-Me$_4$. The needle shaped crystals obtained in the crystallization experiments discussed in Section 5.10.1 turned out to be a 1:1 solvate of **Zn-TPP-Me$_4$** with nitrobenzene. This solvate adopts a layered structure with guest molecules occupying the interlayer spaces (Figure 5.18). These two structures (shown in Figures 5.17 and 5.18) point to the difficulties in preparing the crystals of porphyrin-ligand complexes that have required stoichiometry.

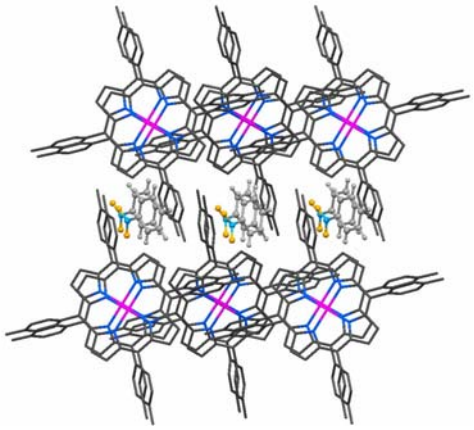

Figure 5.18 Crystal structure of **Zn-TPP-Me$_4$-PhNO$_2$**. The guest molecules are drawn in lighter colors and in ball-and-stick models. Only one of the two disordered orientations of the guest is shown.

5.10.3 Nitrobenzene Solvate of Zn-TPP-Cl$_4$-bpy. Slow evaporation of a chloroform solution containing **Zn-TPP-Cl$_4$** and **bpy** in 2:1 proportions led to the growth of crystalline chunks of a 1:1 porphyrin-ligand complex. This complex belongs to the space group $P\,\bar{1}$ and the Zn–N bond length is 2.12 Å. Unlike in **Zn-TPP-Me$_4$-bpy** the interstitial spaced are filled by nitrobenzene molecules instead of excess ligand molecules. This complex includes three symmetry independent nitrobenzene guests in the crystals and one of these guest molecules is disordered.

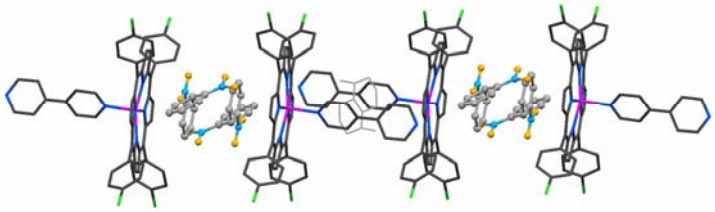

Figure 5.19 Crystal structure of **Zn-TPP-Cl$_4$-bpy**. Guest molecules are drawn in lighter colors. Disordered nitrobenzene is drawn in wireframe model. Notice the difference in the packing pattern in this figure and Figure 5.17.

In the following sections we discuss the structures of some porphyrin complexes formed between different *trans*-A_2D_2-poprhyrins (Figures 5.8 and 5.9) and ligands (Figure 5.10). Using these porphyrins and ligands, we attempted the crystallizations of over 40 dimers; and obtained the crystal structures of eleven complexes. Nine of these complexes are sandwich dimers, one is a 1:2 porphyrin-ligand trimolecular complex and another is a linear polymer. We do not discuss the structures of latter two complexes here. The nine sandwich dimers constitute six different porphyrins and four different ligands. Five of these porphyrins are metallated with zinc and one with cobalt. As shown in Figure 5.10 the four ligands have different lengths. The structures of these complexes can be

categorized in different ways; in the description below the structures are grouped according to the ligand they contain.

5.11 DIMERS CONTAINING 4,4′-BIPYRIDYL

We have been successful at preparing the 2:1 sandwich dimers based on porphyrins **1-Zn**, **2-Zn** and **3-Zn** with the ligand **bpy**. All the complexes adopt the eclipsed sandwich conformation shown in Figure 5.6b, with nitrophenyl groups of the top and bottom porphyrins situated on each other (Figure 5.20). The complexes are thus centrosymmetric. The crystals of **2-Zn** and **3-Zn** are isostructural; their overall structures are nearly identical – but they differ from **1-Zn** in terms of inter-dimer packing. The bridging of the two porphyrin molecules by **bpy**, a fairly long ligand, leaves space between the top and bottom faces of the dimer; neighboring dimers project their aryl groups into this space (Figure 5.21) to facilitate weak interactions such as C–H···O, C–H···N, C–H···π and π stacking. Void spaces that remain after accounting for the closest inter-dimer packing are occupied by nitrobenzene molecules.

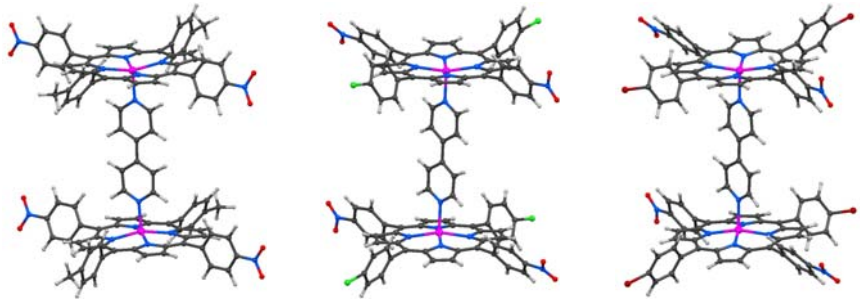

Figure 5.20 Eclipsed centrosymmetric dimers in the crystal structures of 2:1 complexes between porphyrins **1-Zn**, **2-Zn** and **3-Zn**, and **bpy**. Notice the similarity in the sizes of the dimers and relative orientations of aryl groups at the *meso* positions.

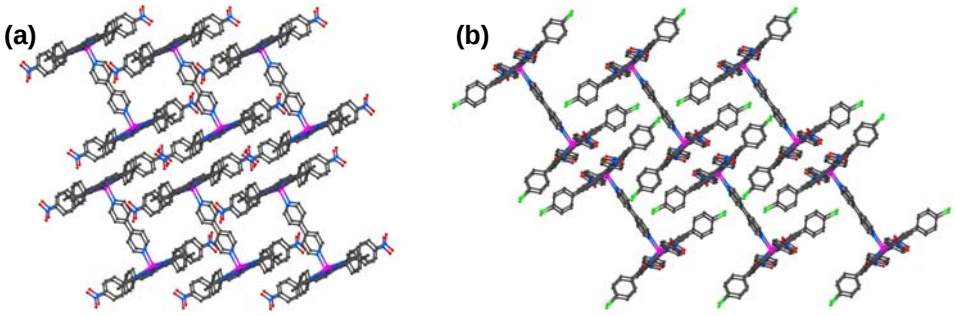

Figure 5.21 Packing of dimers in **(a) (1-Zn)$_2$-bpy** and **(b) (2-Zn)$_2$-bpy**. Notice the difference the dimer packing between the two structures. The packing of dimers in **(3-Zn)$_2$-bpy** is identical to that shown in **(b)**.

5.12 SANDWICH DIMER OF 3-ZN AND 1,2-DI-(4-PYRIDYL)ETHYLENE

Among the four ditopic aza ligands we have used, **dpe** (Figure 5.10d) is the longest ligand with the highest number of conjugated double bonds. Unlike the other three ligands, the lone pairs on the two N-atoms are not directly opposite of each other; they are offset by the intervening double bond between the two pyridyl rings. This shift is expected to impose a slight offset in the top and bottom porphyrin rings in the sandwich dimers. Though we have been able to grow crystals of several dimers with **dpe** as the bridging ligand, only one complex has yielded crystals large enough for X-ray diffraction analysis.

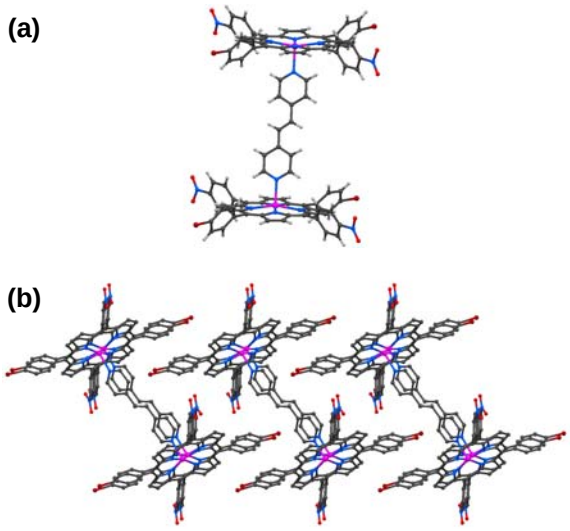

Figure 5.22 (a) Eclipsed centrosymmetric dimer in the crystal structure of **(3-Zn)$_2$-dpe**. The inter-dimer packing is more involved; the view in **(b)** shows the view down *a*-axis.

Crystals of **(3-Zn)$_2$-dpe** belong to the space group $P\bar{1}$ and contain the porphyrin and the ligand in 2:1 ratio (Figure 5.22). The dimer adopts the eclipsed centrosymmetric configuration shown in Figure 5.6b. The two porphyrin rings are parallel to each other and the centers of the rings are slightly offset to accommodate strong bonding between the Zn^{2+} ions and the pyridyl N-atoms. As with **bpy** complexes discussed in the previous section, the space left between the top and bottom porphyrin molecules in this **dpe** dimer is filled by the dovetailing of neighboring complexes.

5.13 DIMERS CONTAINING PYRAZINE

Of the several **pz** dimerizations we have attempted, only **3-Zn** and **5-Zn** produced crystals suitable for X-ray diffraction analysis. Both crystals contained sandwich dimers with the porphyrins and ligand in 2:1 ratio. Length of ligand plays an important role in the inter-dimer packing within the crystal. Due to the shorter length of the **pz** ligand, the packing characteristics of **(3-Zn)$_2$-pz** and **(5-Zn)$_2$-pz** are different from the dimers shown

above. Adjacent dimers can no longer dovetail into each other and are forced to interact with each other through contacts between the peripheral groups. This kind of enforcement is helpful in the design of solids that have overall noncentrosymmetry (Figure 5.4c). The inter-dimer packing in these **pz** based complexes show several strong C–H···O interactions between the nitro groups of the porphyrin and various C–H groups.

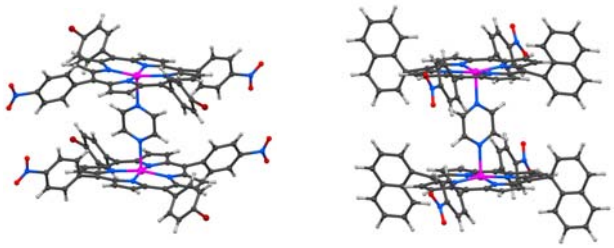

$(3\text{-Zn})_2$-pz $(5\text{-Zn})_2$-pz

Figure 5.23 Eclipsed centrosymmetric dimers in the crystal structures of **$(3\text{-Zn})_2$-pz** and **$(3\text{-Zn})_2$-pz**.

5.14 CENTRIC AND ACENTRIC DIMERS CONTAINING DABCO

The non-conjugated ligand **dabco** has about the same length as the aromatic ligand **pz**. The N-atoms of **dabco** are more basic; they are expected to form stronger bonds with the metal cations in the porphyrin core. To date, we have solved the crystal structures of three different dimers that contain **dabco**. The 2:1 dimer between **4-Zn** and **dabco** (Figure 5.24) is similar to that of the **pz** dimers shown above. The nitrophenyl rings of the top and bottom porphyrin units are situated on top of each other and the dimer adopts the centric, eclipsed conformation. Adjacent dimers are interact through C–H···O and C–H···π contacts laterally and face-to-face contacts vertically to complete the overall structure.

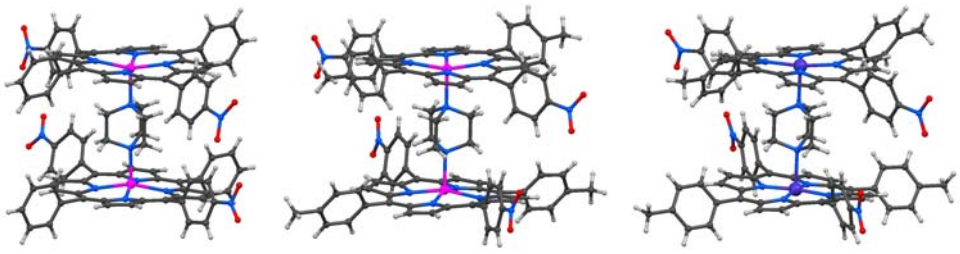

$(4\text{-Zn})_2$-dabco $(1\text{-Zn})_2$-dabco $(1\text{-Co})_2$-dabco

Figure 5.24 Eclipsed centrosymmetric dimers in **$(4\text{-Zn})_2$-dabco** and staggered noncentrosymmetric dimers in **$(1\text{-Zn})_2$-dabco** and **$(1\text{-Co})_2$-dabco**.

Compound **1-Zn** contains *p*-tolyl groups and it is slightly bigger than the porphyrin **4-Zn**, which contains phenyl rings. This slight increase in the size of the porphyrin in **1-Zn** combined with the shorter length of the **dabco** results in a sandwich dimer that adopts *staggered* conformation (Figures 5.24 and 5.25). This is the first dimer ever to adopt the

staggered conformation. Remarkably, this staggered geometry is noncentrosymmetric and is pseudo-octupolar. We extended this dabco dimerization to the porphyrin **1-Co**; and crystals of **$(1\text{-Co})_2$-dabco** are isostructural to **$(1\text{-Zn})_2$-dabco** (Figures 5.24 and 5.25). In both cases, the inter-dimer packing is mediated by short C–H···O hydrogen bonds laterally and face-to-face stacking vertically. At this stage, we conclude the structural description of the complexes between metallo-porphyrins and ditopic ligands. The ability to create multiple related structures in a straight-forward synthetic protocol is useful in the studies of crystal engineering. We emphasize that the modular approach shown here is practical in exploring a large number of dimeric and other related complexes. We believe that through proper modulation of the peripheral groups, metal cations and the ditopic ligands it will be possible to create dimers that have true octupolar geometry.

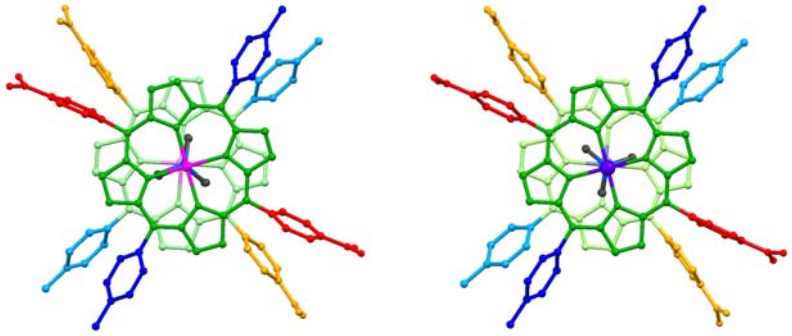

Figure 5.25 Staggered noncentrosymmetric dimers in the crystal structures of **$(1\text{-Zn})_2$-dabco** and **$(1\text{-Co})_2$-dabco**.

5.15 EXPERIMENTAL

All the solvents were purchased from Pharmco and rest of the chemicals were purchased from Alfa Aesar and used as received in the synthesis and crystallization. Dueterated solvents were purchased from Norell. The NMR spectra were recorded on a Bruker 400 MHz or a Bruker 500 MHz spectrometer. The IR spectra were recorded in the ATR (attenuated total reflection) mode on a Perkin Elmer Spectrum One spectrometer. Single crystal X-ray data were collected on either a Bruker SMART diffractometer or a Bruker APEX II diffractometer equipped with CCD detectors and Oxford Cryostream or Oxford Cryostream Plus low-temperature devices. Further details of X-ray data collection are given in Chapter 2 and the space group and unit cell data are given in Appendix 1.

5.15.1 Synthesis of Symmetric Porphyrins. We have synthesized four tetraaryl porphyrins using the Adler procedure (Figure 5.26).[24] In this method, freshly distilled pyrrole (0.2 mmol) and aryl aldehyde (0.2 mmol) were added to 75 ml of refluxing propionic acid. After refluxing for 30 minutes the solution was cooled down to room temperature and stored overnight at 0 ^{o}C. The resulting solution was filtered, and the filter cake was washed thoroughly with methanol and hot water in succession, and air

dried to give a purple product. NMR and UV-Vis spectroscopic details of four porphyrins synthesized according to this method are given below.

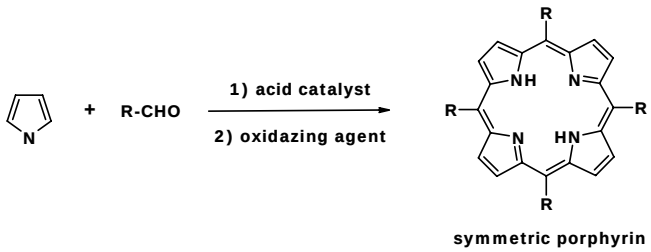

Figure 5.26 Adler procedure for the synthesis of symmetric porphyrins.

TPP-Me$_4$: ^{1}H-NMR ($CDCl_3$): -2.77 (br. s, 2 H, NH); 2.71 (s, 12 H, CH_3); 7.56 (d, 8 H, *m*-Ph); 8.10 (d, 8 H, *o*-Ph); 8.85 (s, 8 H, *β*-pyrrole). UV-Vis (CH_2Cl_2): λ_{max} 417; 515; 551; 590; 648 nm.

TPP-Cl$_4$: ^{1}H-NMR ($CDCl_3$): -2.86 (br. s, 2 H, NH); 7.74 (d, 8 H, *m*-Ph); 8.13 (d, 8 H, *o*-Ph); 8.83 (s, 8 H, *β*-pyrrole). ^{13}C-NMR ($CDCl_3$): 119.0 (C_{meso}); 127.0; 131.3; 132.0; 134.4; 135.5; 140.3. UV-Vis ($CHCl_3$): λ_{max} 418; 482; 514; 548; 589; 646 nm.

TPP-OMe$_4$: ^{1}H-NMR ($CDCl_3$): -2.74 (br. s, 2 H, NH); 4.10 (s, 12 H, OCH_3); 7.3 (d, 8 H, *m*-Ph); 8.12 (d, 8 H, *o*-Ph); 8.86 (s, 8 H, *β*-pyrrole).

TPP-*i*Pr$_4$: ^{1}H-NMR ($CDCl_3$): -2.76 (br. s, 2 H, NH); 1.51 (d, 24 H, CH_3); 3.25 (m, 4 H, CH), 7.60 (d, 8 H, *m*-Ph); 8.13 (d, 8 H, *o*-Ph); 8.86 (s, 8 H, *β*-pyrrole).

5.15.2 Synthesis of TF$_5$PP. Pentafluorobenzaldhyde (2.5 mmol, 0.31 mL) and pyrrole (2.5 mmol, 0.17 mL) were dissolved in 250 mL dichloromethane (CH_2Cl_2) and degassed with nitrogen for 10 minutes.[27] To this solution, the acid catalyst BF_3 etherate (0.1 mL) as a 2.5 M solution in CH_2Cl_2, (0.25 mmol) was added via syringe. The reaction vessel was shielded from light and stirred at room temperature under a purge of nitrogen gas. After 1 hour, *p*-chloranil (1.875 mmol, 0.461 g) was added in powder form and the reaction mixture refluxed for 1h. The reaction mixture was cooled down to room temperature, 1 equiv. of triethylamine (0.825 mmol, 0.115 mL) was added and the solution was evaporated to dryness. The dry product was purified by column chromatography (silica, CH_2Cl_2/hexanes 1:3) to give the title compound (0.19 g; 31%). ^{1}H-NMR ($CDCl_3$): -2.89 (s, 2 H, NH); 8.95 (s, 8 H, *β*-pyrrole). UV-Vis ($CHCl_3$): λ_{max} 410, 504, 582, 634 nm.

5.15.3 Modified Adler Procedure for the Synthesis of TPP-(NO$_2$)$_4$. 4-nitrobenzaldehyde (36.42 mmol, 5.5 g) was dissolved in 150 mL propionic acid and brought to reflux.[26] The refluxing solution was treated first with freshly distilled acetic anhydride (63.59 mmol, 6 mL) and then with freshly distilled pyrrole (36.16 mmol, 2.5 mL) dissolved in 5 mL of propionic acid. The solution was refluxed for 30 minutes with stirring and the resultant tarry product was allowed to cool and stand for 24 hours in a refrigerator. A dark solid was collected by filtration, washed with six portions of 70 mL

water, and dried. The powdery solid was taken up in 40 mL pyridine, refluxed with stirring for 1 hour, cooled to room temperature, and stored at -4 °C overnight. The tarry mixture was filtered and the solid product washed repeatedly with acetone until the rinsing extracts were no longer dark; yield 1.29 g (18 %). The final product has very low solubility in chloroform. A small amount of trifluoro acetic acid (TFA) (~5 %) was added to increase the solubility to collect NMR data. ^{1}H-NMR ($CDCl_3$ + TFA 5%): -0.99 (b. s, 4 H, NH); 8.74 (d, 8 H, *m*-Ph); 8.83 (s, 8 H, *β*-pyrrole); 8.92 (d, 8 H, *o*-Ph). ^{13}C-NMR ($CDCl_3$ + TFA 5%): 121.8 (C_{meso}); 123.9; 129.8; 138.6; 143.9; 145.4; 149.3; (signals for TFA are not listed).

5.15.4 Synthesis of Dipyrromethanes. As shown in Figure 5.27 dipyrromethanes are the critical intermediates in the modular synthesis of *trans*-$\mathbf{A_2D_2}$ porphyrins. Once a dipyrromethane is synthesized from an **A** (or **D**) aldehyde, several *trans*-$\mathbf{A_2D_2}$ porphyrins can be synthesized from it using a number of different **D** (or **A**) aldehydes. The procedure for the synthesis of 5-nitrophenyldipyrromethane is given in Chapter;[30] below we give the procedure for the synthesis of phenyldipyrromethane.[31]

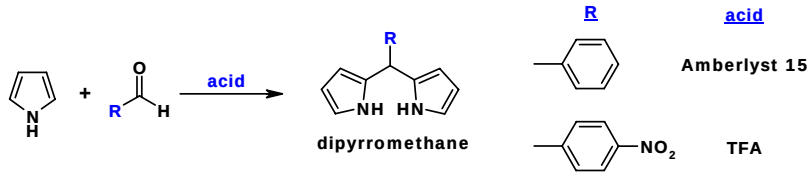

Figure 5.27 Synthesis of phenyl- and 5-nitrophenyldipyrromethanes.

A solution of benzaldehyde (0.2 mol, 20 mL) and pyrrole (4 mol, 280 mL) was degassed with nitrogen for 10 min. Cation exchange resin Amberlist-15 (60 g) was added to this mixture. The solution was stirred for 25 hours at room temperature and diluted with CH_2Cl_2 (200 mL). Triethylamine (2 mL) was added to this mixture to prevent acidolysis of the 5-phenyldipyrromethane and the resulting mixture was filtered. The filtrate was washed with water (3 × 70 mL) and the organic layer was dried over Na_2SO_4. The solvent was removed under reduced pressure and unreacted pyrrole was removed by high vacuum evaporation. The remaining brownish viscous liquid was purified by column chromatography (silica, hexanes/ethylacetate/triethylamine 80:20:1). Further purification by another column chromatographic separation (silica, hexanes-CH_2Cl_2, 3:1) gave grayish-white crystals (12.2 g; 27.5%). ^{1}H-NMR ($CDCl_3$): 5.47 (s, 1 H); 5.92 (s, 2 H); 6.16 (m, 2 H); 6.70 (m, 2 H); 7.20-7.32(m, 5 H); 7.92 (br s, 2 H). ^{13}C-NMR ($CDCl_3$): 43.9; 107.2; 108.4; 117.2; 127.0; 128.4; 128.6; 132.4; 142.0.

5.15.5 General Procedure for the Synthesis of *trans*-$\mathbf{A_2D_2}$ porphyrins. The procedure described below[30] is used to make all but one of the *trans*-$\mathbf{A_2D_2}$ porphyrins (**7**) studied. Section 5.15.6 gives the slightly modified procedure for the synthesis of **7**. The general procedure is given for **Zn-TPP-H_2Br_2**.[32]

5.15.5.1 Synthesis of Zn-TPP-H_2Br_2. Samples of 5-phenyldipyrromethane (4 mmol, 0.888 g) and 4-bromobenzaldehyde (4 mmol, 0.74 g) were dissolved in CH_2Cl_2 (400 mL, distilled) in a 500 mL round-bottomed flask. After degassing the flask for 15 min with

nitrogen, TFA (7.12 mmol, 0.55 mL) was added. The reaction mixture was stirred for 35 min at room temperature, and 2,3-dichloro-5,6-dicyano-1,4-benzoquinone (DDQ) (4 mmol, 0.91 g) was added, and stirred for an additional 1 hour at room temperature. The complete reaction mixture was poured onto a pad of alumina (1L separatory funnel, about half-filled) and eluted with CH_2Cl_2 until the eluting solution was pale brown (~ 1L). The solvent was removed under vacuum, and the remaining purple-black solid was dissolved in toluene (150 mL) and refluxed for 1 hour in the presence of DDQ (4mmol, 0.91g) to oxidize any remaining chlorin. After cooling to room temperature, the entire reaction mixture was passed through a pad of alumina (500 mL separatory funnel, about half-filled) and eluted with CH_2Cl_2 (~600 mL) until purple material had completely eluted. Removal of the solvent under vacuum gave the product as a purple solid (0.44 g, 28.5%). ^{1}H-NMR ($CDCl_3$): -2.83 (br. s, 2 H, NH); 7.75 (m, 6 H, *o*- and *p*-Ph); 7.88 (d, 4 H); 8.08 (d, 4 H, *m*-Ph); 8.20 (d, 4 H, *o*-Ph); 8.83 (dd, 8 H, β-pyrrole)

5.15.5.2 Synthesis of Zn-TPP-H_2Cl_2. Condensation of 5-phenyldipyrromethane (4 mmol, 0.888 g) and 4-chlorobenzaldehyde (4 mmol, 0.56 g) in CH_2Cl_2 (400 mL) with TFA (7.12 mmol, 0.55 mL) gave a purple solid (0.4 g; 29%). ^{1}H-NMR ($CDCl_3$): -2.82 (br. s, 2 H, NH); 7.75 (m, 10H, *o*-, *m*- and *p*-Ph); 8.14 (d, 4 H, *m*-Ph); 8.20 (d, 4 H, *o*-Ph); 8.83 (s, 8 H, β-pyrrole)

5.15.5.3 Synthesis of Zn-TPP-$H_2(NO_2)_2$. Condensation of 5-phenyldipyrromethane (4 mmol, 0.888 g) and 4-nitrobenzaldehyde (4 mmol, 0.604 g) in CH_2Cl_2 (400 mL) with TFA (7.12 mmol, 0.55 mL) gave a purple solid (0.135g; 19%). ^{1}H-NMR ($CDCl_3$): -2.90 (br. s, 2 H, NH); 7.79 (m, 6H, *o*-and *p*-Ph); 8.21 (d, 4 H, *m*-Ph); 8.40 (d, 4 H, *o*-Ph); 8.64 (d, 4 H, *m*-Ph); 8.76 (d, 4 H, β_1-pyrrole); 8.90 (d, 4 H, β_2-pyrrole).

5.15.5.4 Synthesis of Zn-TPP-$iPr_2(NO_2)_2$. Condensation of 5-(4-nitrophenyl)dipyrromethane (3 mmol, 0.8 g) and 4-isopropylbenzaldehyde (3 mmol, 0,446 g; 0.46 mL) in CH_2Cl_2 (300 mL) with TFA (5.34 mmol, 0.41 mL) gave a purple solid (0.25 g; 21%). ^{1}H-NMR ($CDCl_3$): -2.79 (br. s, 2 H, NH); 1.55 (s, 12 H, CH_3); 3.27 (m, 4 H, CH); 7.62 (d, 4 H); 8.12 (d, 4 H); 8.40 (d, 4 H); 8.65 (d, 4 H); 8.74 (d, 4 H, β_1-pyrrole); 8.94 (d, 4 H, β_2-pyrrole).

5.15.5.5 Synthesis of Zn-TPP-$I_2(NO_2)_2$. Condensation of 5-4-nitrophenyldipyrromethane (4 mmol, 1.07 g) and 4-iodobenzaldehyde (4 mmol, 0.93 g) in CH_2Cl_2 (400 mL) with TFA (7.12 mmol,0.55 mL) gave a purple solid (0.17 g; 8.9 %). ^{1}H-NMR ($CDCl_3$): -2.85 (br. s, 2 H, NH); 7.93 (d, 4 H); 8.12 (d, 4 H); 8.39 (d, 4 H); 8.66 (d, 4 H); 8.77 (m, 4 H, β_1-pyrrole); 8.89 (m, 4 H, β_2-pyrrole).

5.15.5.6 Synthesis of Zn-TPP-$(OMe)_2(NO_2)_2$. Condensation of 5-(4-nitrophenyl)dipyrromethane (4 mmol, 1.07 g) and 4-methoxybenzaldehyde (4 mmol, 0,54 g; 0.49 mL) in CH_2Cl_2 (400 mL) with TFA (7.12 mmol, 0.55 mL) gave a purple solid (0.13 g; 8.5 %). ^{1}H-NMR ($CDCl_3$): -2.86 (br. s, 2 H, NH); 4.03 (s, 6 H, OCH_3); 7.23 (d, 4 H); 8.04 (d, 4 H); 8.32 (d, 4 H); 8.56 (d, 4 H); 8.67 (d, 4 H, β_1-pyrrole); 8.86 (d, 4 H, β_2-pyrrole).

5.15.5.7 Synthesis of Zn-TPP-^{t}Bu$_2$(NO$_2$)$_2$. Condensation of 5-(4-nitrophenyl)dipyrromethane (4 mmol, 1.07 g) and 4-*tert*-butylbenzaldehyde (4 mmol, 0,65 g; 0.67 mL) in CH_2Cl_2 (400 mL) with TFA (7.12 mmol, 0.55 mL) gave a purple solid (0.25 g; 15.3%).^{1}H-NMR ($CDCl_3$): -3.00 (br. s, 2 H, NH); 1.47 (s, 18 H, $C(CH_3)_3$); 7.64 (d, 4 H); 7.99 (d, 4 H); 8.26 (d, 4 H); 8.51 (d, 4 H); 8.60 (d, 4 H, β_1-pyrrole); 8.80 (d, 4 H, β_2-pyrrole).

5.15.5.8 Synthesis of Zn-5,15-Bis(3,5-di-^{t}butyl-4-hydroxyphenyl)-10,20-di(4-nitrophenyl) porphyrin. Condensation of 5-(4-nitrophenyl)dipyrromethane (4 mmol, 1.07 gr) and 3,5-di-^{t}butyl-4-hydroxybenzaldehyde (4 mmol, 0.94 gr) in CH_2Cl_2 (400 mL) with TFA (0.55 mL) gave a purple solid (0.11 gr; 2.86 %) which was metallated using zinc acetate. ^{1}H-NMR ($CDCl_3$): 1.64 (s, 18 H, CH_3); 5.58 (s, 2 H, OH); 8.04 (s, 4 H); 8.42 (d, 4 H); 8.64 (d, 4 H); 8.86 (d, 4 H, β_1-pyrrole); 9.10 (d, 4 H, β_2-pyrrole).

5.15.6 Synthesis of 5,15-Bis(pentafluorophenyl)-10,20(diphenyl)porphyrin (7). The synthetic procedure used above led to scrambling in this case. Scrambling refers to the formation of a mixture of porphyrins (that contain *trans*-A_2D_2, *cis*-A_2D_2, A_3D, and AD_3; A = perfluorophenyl; D = phenyl). A modified procedure that uses smaller amounts of acid catalyst provided the pure *trans*A_2D_2 product.[32] A solution of pentafluorobenzaldehyde (0.5 mL, 4 mmol) and 5-phenyldipyrromethane (0.888 g, 4 mmol) in 400 mL of CH_2Cl_2 was degassed with nitrogen for 10 minutes. Acid catalyst TFA (0.3 mL,4 mM) was added with a syringe. The mixture was stirred for 1 hour at room temperature and DDQ (8 mmol, 0.728 g) was added as an oxidizing agent. The reaction mixture was stirred at room temperature for 90 minutes. The solvent was removed under reduced pressure. The remaining dry product was purified by column chromatography (alumina, CH_2Cl_2/hexanes, 1:2) to give 0.132 g (16.6 %) of *trans* product. ^{1}H-NMR ($CDCl_3$): -2.84 (br. s, 2 H, NH); 7.80 (m, 6 H, *m*-Ph and *p*-Ph); 8.21 (dd, 4 H, *o*-Ph); 8.80 (d, 4 H, β_1-pyrrole); 8.95 (d, 4 H, β_2-pyrrole).

5.15.7 Metallation of Porphyrins. Previous sections describe the synthesis of symmetric ($\mathbf{A}_4$ and $\mathbf{D}_4$) and *trans*-$\mathbf{A_2D_2}$ porphyrins. In this section we describe two methods of inserting Zn^{2+} cation into free-base porphyrin.[33-34] During the metallation the two inner pyrrolic protons are removed, leaving the metallated porphyrin as a charge neutral species.

5.15.7.1 Metallation using Chloroform and Methanol. Two separate solutions were prepared as follows: free base porphyrin (1 equiv) was dissolved in chloroform and zinc acetate dihydrate (10-15 equiv) was dissolved in methanol. These two solutions were combined and refluxed for 1 hour and then cooled to room temperature. Excess methanol was added to the reaction mixture to precipitate metallated porphyrin and the resultant solid filtered, washed with methanol, and air dried. This procedure was successful in ~90% of the experiments we attempted. Sometimes, however, significant fraction (5-10%) of the free-base was left in the reaction mixture. In such cases we used the following procedure to obtain pure metallated product.

5.15.7.2 Metallation using Dimethylformamide. Free-base porphyrin (1 eqiv.) and zinc acetate dihydrate (2 eqiv.) were dissolved in dimethylformamide and refluxed for 1 hour. The solution was cooled to room temperature and kept in a deep-freezer for 12 hours. In some instances metallated product was precipitated. This precipitate was filtered, washed and air dried, and used for further experiments. Sometimes, however, precipitation did not occur even after 12 h of cooling; in these cases the product was purified by column chromatography.

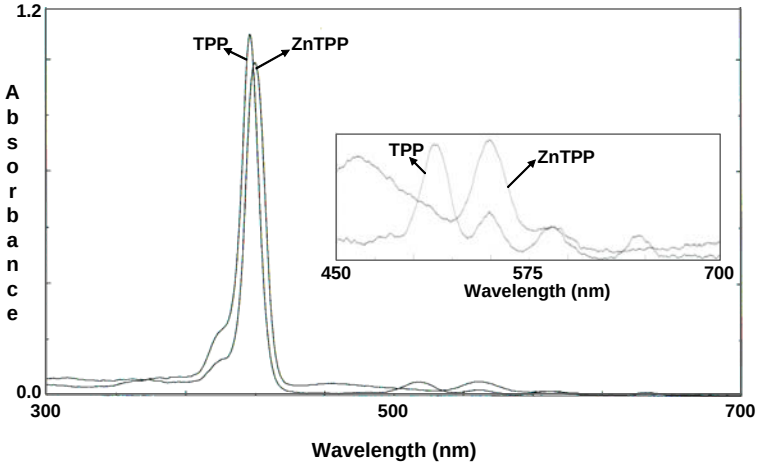

Figure 5.27 Absorption spectra of **TPP** and **Zn-TPP** dissolved in chloroform solution.

5.15.7.3 Monitoring and Characterization of Metallation. In ^{1}H-NMR spectroscopy, the broad singlet from pyrrolic N–H groups at ~ -3 ppm disappears after metallation. In UV-Vis spectroscopy, the free-base porphyrin with two inner pyrrolic N–H groups possesses D_{2h} symmetry, and displays four Q-bands in the 450-700 nm region, in addition to a strong Sorret band at ~420 nm. When metallated, porphyrin molecules adopt a higher symmetry, namely D_{4h}. This change in symmetry is clearly reflected in the region of Q-band absorption.[35] Metallated porphyrins show only two Q-bands, and this change can be readily monitored by recording UV-Vis absorption spectra. Figure 5.28 shows the UV-Vis spectra of **TPP** and **Zn-TPP** to accentuate the changes that occur after metallation. Other porphyrins studied in this work showed similar characteristics in their UV-Vis absorption spectra.

5.16 SUMMARY AND CONCLUSION

Porphyrin assemblies are important targets in applications such as multi-photon absorption, light harvesting and second order NLO. We envisaged *cubes* as *dimers of squares* and developed a modular procedure for the synthesis of multiple porphyrin coordination assemblies with a diverse array of functional groups. These dimeric assemblies have at least twice the conjugation density compared to the corresponding monomers. The synthetic approach we used is modular at many levels: one dipyrromethane can react with different aldehydes to produce multiple porphyrins; each

porphyrin can be metallated with a range of metal cations; and each metallo-porphyrin can be bridged with a variety of ditopic ligands to yield a large number of dimeric assemblies. We analyzed the dimers of symmetric A_4- or D_4-porphyrins with ^{1}H-NMR spectroscopy to establish that (a) the protons of the bridged ligand experience the aromatic ring current of porphyrin core and shift upfield, (b) the extent of upfield shift can be used as a measure to verify the stoichiometry of the coordination assembly, and (c) guest (nitrobenzene) molecules occupy the voids left after inter-dimer association in the crystals. Formation of dimers can be hampered by possible side products such as 1:1 porphyrin-ligand complexes or linear polymers and conditions must be explored for the preparation of required end products. The dimers of *trans*-A_2D_2-porphyrins can take up three types of conformations; two of these are acentric and possess octupolar nonlinear character. Preparation of over forty assemblies of *trans*-A_2D_2-porphyrins is attempted and crystal structures of nine different dimers are reported. These dimers contain six different porphyrins, two metal cations, and four different ligands. We showed the relation between the length of the bridging ligand and the type of inter-dimer association. Shorter ligand can in principle facilitate the octupolar dimerization; two porphyrin dimers bridged by the ligand **dabco** adopt the acentric, staggered and octupolar conformation in the solid state.

5.17 REFERENCES

1. Lehn, J. M., *Supramolecular Chemistry: Concepts and Perspectives*. Wiley: New York, 1995.
2. Dunitz, J. D., Phase transitions in molecular crystals from a chemical viewpoint. *Pure. Appl. Chem.* **1991,** *63*, 177-85.
3. Albota, M.; Beljonne, D.; Bredas, J.-L.; Ehrlich, J. E.; Fu, J.-Y.; Heikal, A. A.; Hess, S. E.; Kogej, T.; Levin, M. D.; Marder, S. R.; McCord-Maughon, D.; Perry, J. W.; Rockel, H.; Rumi, M.; Subramaniam, G.; Webb, W. W.; Wu, X.-L.; Xu, C., Design of organic molecules with large two-photon absorption cross sections. *Science* **1998,** *281*, 1653-1656.
4. Chemla, D. S.; Zyss, J.; Editors, *Nonlinear Optical Properties of Organic Molecules and Crystals, Vol. 1*. 1987.
5. Chemla, D. S.; Zyss, J.; Editors, *Nonlinear Optical Properties of Organic Molecules and Crystals, Vol. 2*. 1987.
6. Cumpston, B. H.; Ananthavel, S. P.; Barlow, S.; Dyer, D. L.; Ehrlich, J. E.; Erskine, L. L.; Heikal, A. A.; Kuebler, S. M.; Lee, I. Y. S.; McCord-Maughon, D.; Qin, J.; Rockel, H.; Rumi, M.; Wu, X.-L.; Marder, S. R.; Perry, J. W., Two-photon polymerization initiators for three-dimensional optical data storage and microfabrication. *Nature* **1999,** *398*, 51-54.
7. Zhou, W.; Kuebler, S. M.; Braun, K. L.; Yu, T.; Cammack, J. K.; Ober, C. K.; Perry, J. W.; Marder, S. R., An efficient two-photon-generated photoacid applied to positive-tone 3D microfabrication. *Science* **2002,** *296*, 1106-1109.
8. Ogawa, K.; Ohashi, A.; Kobuke, Y.; Kamada, K.; Ohta, K., Strong Two-Photon Absorption of Self-Assembled Butadiyne-Linked Bisporphyrin. *J. Am. Chem. Soc.* **2003,** *125*, 13356-13357.

9. Collini, E.; Ferrante, C.; Bozio, R., Strong enhancement of the two photon absorption cross section of porphyrin J-aggregates in water. *Mater. Res. Soc. Symp. Proc.* **2005,** *846*, 39-44.
10. Drobizhev, M.; Stepanenko, Y.; Rebane, A.; Wilson, C. J.; Screen, T. E. O.; Anderson, H. L., Strong cooperative enhancement of two-poton absorption in double-strand conjugated porphyrin ladder arrays. *J. Am. Chem. Soc.* **2006,** *128*, 12432-12433.
11. Fejer, M. M., Nonlinear optical frequency conversion. *Physics Today* **1994,** *47*, 25-32.
12. Eaton, D. F., Nonlinear optical materials. *Science* **1991,** *253*, 281-7.
13. Zhang, X. C.; Ma, X. F.; Jin, Y.; Lu, T. M.; Boden, E. P.; Phelps, P. D.; Stewart, K. R.; Yakymyshyn, C. P., Terahertz optical rectification from a nonlinear organic crystal. *Appl. Phys. Lett.* **1992,** *61*, 3080-2.
14. Zyss, J., Molecular engineering implications of rotational invariance in quadratic nonlinear optics: from dipolar to octupolar molecules and materials. *J. Chem. Phys.* **1993,** *98*, 6583-99.
15. Zyss, J.; Ledoux, I., Nonlinear optics in multipolar media: theory and experiments. *Chem. Rev.* **1994,** *94*, 77-105.
16. Bartholomew, G. P.; Ledoux, I.; Mukamel, S.; Bazan, G. C.; Zyss, J., Three-Dimensional Nonlinear Optical Chromophores Based on Through-Space Delocalization. *J. Am. Chem. Soc.* **2002,** *124*, 13480-13485.
17. Zyss, J., Octupolar organic systems in quadratic nonlinear optics: molecules and materials. *Nonlinear Opt.* **1991,** *1*, 3-18.
18. Joffre, M.; Yaron, D.; Silbey, R. J.; Zyss, J., Second-order optical nonlinearity in octupolar aromatic systems. *J. Chem. Phys.* **1992,** *97*, 5607-15.
19. Dhenaut, C.; Ledoux, I.; Samuel, I. D. W.; Zyss, J.; Bourgault, M.; Le Bozec, H., Chiral metal complexes with large octupolar optical nonlinearities. *Nature* **1995,** *374*, 339-42.
20. Lindsey, J. S., Synthesis of meso-substituted porphyrins. In *Porphyrin Handbook*, Kadish, K. M.; Smith, K. M.; Guilard, R., Eds. Academic Press: San Diego, 2000; Vol. 1, pp 45-118.
21. Suslick, K. S.; Chen, C. T.; Meredith, G. R.; Cheng, L. T., Push-pull porphyrins as nonlinear optical materials. *J. Am. Chem. Soc.* **1992,** *114*, 6928-30.
22. Goldberg, I., Crystal engineering of porphyrin framework solids. *Chem. Commun.* **2005**, 1243-1254.
23. Buchler, J. W.; Ng, D. K. P., Metal tetrapyrrole double- and triple-deckers with special emphasis on porphyrin systems. In *Porphyrin Handbook*, Kadish, K. M. S., Kevin M.; Guilard, Roger. , Ed. Academic Press: San Diego, 2000; Vol. 3, pp 245-294.
24. Adler, A. D.; Longo, F. R.; Finarelli, J. D.; Goldmacher, J.; Assour, J.; Korsakoff, L., A simplified synthesis for meso-tetraphenylporphine. *J. Org. Chem.* **1967,** *32*, 476.
25. Bettelheim, A.; White, B. A.; Raybuck, S. A.; Murray, R. W., Electrochemical polymerization of amino-, pyrrole-, and hydroxy-substituted tetraphenylporphyrins. *Inorg. Chem.* **1987,** *26*, 1009-17.

26. Lindsey, J. S.; Schreiman, I. C.; Hsu, H. C.; Kearney, P. C.; Marguerettaz, A. M., Rothemund and Adler-Longo reactions revisited: synthesis of tetraphenylporphyrins under equilibrium conditions. *J. Org. Chem.* **1987,** *52*, 827-36.
27. Lindsey, J. S.; Wagner, R. W., Investigation of the synthesis of ortho-substituted tetraphenylporphyrins. *J. Org. Chem.* **1989,** *54*, 828-36.
28. Diskin-Posner, Y.; Patra, G. K.; Goldberg, I., Supramolecular assembly of metalloporphyrins in crystals by axial coordination through amine ligands. *J. Chem. Soc., Dalton Trans.* **2001**, 2775-2782.
29. Byrn, M. P.; Curtis, C. J.; Goldberg, I.; Hsiou, Y.; Khan, S. I.; Sawin, P. A.; Tendick, S. K.; Strouse, C. E., Porphyrin sponges: structural systematics of the host lattice. *J. Am. Chem. Soc.* **1991,** *113*, 6549-6557.
30. Littler, B. J.; Miller, M. A.; Hung, C.-H.; Wagner, R. W.; O'Shea, D. F.; Boyle, P. D.; Lindsey, J. S., Refined Synthesis of 5-Substituted Dipyrromethanes. *J. Org. Chem.* **1999,** *64*, 1391-1396.
31. Naik, R.; Joshi, P.; Kaiwar, S. P.; Deshpande, R. K., Facile synthesis of meso-substituted dipyrromethanes and porphyrins using cation exchange resins. *Tetrahedron* **2003,** *59*, 2207-2213.
32. Lee, C.-H.; Lindsey, J. S., One-flask synthesis of meso-substituted dipyrromethanes and their application in the synthesis of trans-substituted porphyrin building blocks. *Tetrahedron* **1994,** *50*, 11427-40.
33. Fleischer, E. B.; Shachter, A. M., Coordination oligomers and a coordination polymer of zinc tetraarylporphyrins. *Inorg. Chem.* **1991,** *30*, 3763-9.
34. Anderson, H. L.; Wylie, A. P.; Prout, K., meso-Tetraalkynylporphyrins. *J. Chem. Soc., Perkin Trans. 1* **1998**, 1607-1611.
35. Dolphin, D.; Editor, Ed. *The Porphyrins, Vol. 3: Physical Chemistry, Pt. A*. Academic Press: New York, 1978.